

Review Article

Depinning and nonequilibrium dynamic phases of particle assemblies driven over random and ordered substrates: a review

C Reichhardt and C J Olson Reichhardt

Theoretical Division, Los Alamos National Laboratory, Los Alamos, New Mexico 87545, USA

E-mail: reichhardt@lanl.gov, cjr@lanl.gov

Abstract. We review the depinning and nonequilibrium phases of collectively interacting particle systems driven over random or periodic substrates. This type of system is relevant to vortices in type-II superconductors, sliding charge density waves, electron crystals, colloids, stripe and pattern forming systems, and skyrmions, and could also have connections to jamming, glassy behaviors, and active matter. These systems are also ideal for exploring the broader issues of characterizing transient and steady state nonequilibrium flow phases as well as nonequilibrium phase transitions between distinct dynamical phases, analogous to phase transitions between different equilibrium states. We discuss the differences between elastic and plastic depinning on random substrates and the different types of nonequilibrium phases which are associated with specific features in the velocity-force curves, fluctuation spectra, scaling relations, and local or global particle ordering. We describe how these quantities can change depending on the dimension, anisotropy, disorder strength, and the presence of hysteresis. Within the moving phase we discuss how there can be a transition from a liquid-like state to dynamically ordered moving crystal, smectic, or nematic states. Systems with periodic or quasiperiodic substrates can have multiple nonequilibrium second or first order transitions in the moving state between chaotic and coherent phases, and can exhibit hysteresis. We also discuss systems with competing repulsive and attractive interactions, which undergo dynamical transitions into stripes and other complex morphologies when driven over random substrates. Throughout this work we highlight open issues and future directions such as absorbing phase transitions, nonequilibrium work relations, inertia, the role of non-dissipative dynamics such as Magnus effects, and how these results could be extended to the broader issues of plasticity in crystals, amorphous solids, and jamming phenomena.

Submitted to: *Rep. Prog. Phys.*

1. Introduction

A wide class of systems can be effectively described as a collection of interacting point particles that are driven over disordered or ordered substrates. In equilibrium and in the absence of a substrate, the interactions between the particles may favor a certain type of symmetry, such as a triangular lattice for repulsively interacting particles in two dimensions. Other types of crystalline phases are possible, however, and in some cases the ground states are frustrated or disordered. When the particles also interact with a substrate, a wealth of new types of phases are possible that depend on whether the substrate is random, quasiperiodic, or periodic, as well as the strength of the coupling between the particles and the substrate. Individual potential minima in the substrate, which we call pinning sites, exert a maximum force on individual particles that we call a pinning strength. For random or disordered substrates, as the substrate coupling strength increases a transition can occur from a crystalline to a disordered or partially disordered state containing grain boundaries or topological defects such as dislocations, with a defect density that increases as a function of the disorder strength. For periodic substrates, various types of commensurate and incommensurate phases can arise depending on the ratio of the number of particles to the number of substrate minima as well as on the pinning strength. For any type of substrate, if a driving force is applied, a depinning transition occurs at a critical driving threshold; below this force, the particles remain stationary, while above this force, some or all of the particles move over the substrate. Examples of systems in which such effects occur include vortices in type-II superconductors interacting with randomly placed pinning sites [1] or periodic arrays of nanostructured pinning sites [2], disordered electron crystals [3], sliding charge density waves under conditions where plasticity can occur [4], charge transport in metallic dot arrays [5], colloidal systems and soft matter assemblies on random substrates [6] or optically created periodic [7] or quasiperiodic substrates [8], driven stripe and pattern forming systems [9], and atoms and molecules moving over two-dimensional (2D) substrates [10]. There are also other examples of the depinning of strictly elastic objects in which the system can be described as an assembly of elastically coupled elements or particles that maintain the same neighbors

over time, including magnetic domain walls [11, 12], individual superconducting vortex lines [13, 14], elastic strings [15, 16], interfaces [17], certain models of charge density waves [4], contact line depinning [18], and slider block models for earthquakes [19].

In this review we focus on particle-based systems which allow the possibility of some form of plastic deformation in which the particles can exchange neighbors. Under certain conditions such as weak disorder, however, these systems can still display elastic behavior. For example, in the case of superconducting vortices or colloids interacting with a random substrate, when the coupling between the particles and the substrate is weak, the depinning transition is elastic and the particles keep the same neighbors as they move, as highlighted in figure 1(b) for a 2D assembly of particles with repulsive Yukawa interactions moving over a weak random substrate. The image shows that motion just above the depinning threshold is coherent, and the particles maintain their triangular ordering. For sufficiently strong particle-substrate coupling, the nature of the depinning changes and plastic motion emerges in which a portion of the particles remain immobile while the other particles can flow around them, permitting the particles to change neighbors over time. This is illustrated in figure 1(a) just above the depinning threshold for the same system in figure 1(b) but with a pinning strength that is twice as large [20]. There can also be a dynamical transition at higher drives between a liquid-like plastic flow state to a coherently moving or dynamically ordered state [21]. Sliding friction or tribology is a related phenomenon, and various frictional models have been proposed that take the form of a collection of particles sliding over an ordered substrate with either fully elastic motion or with plasticity [10, 22]. Other descriptions of atomic friction involve realistic three-dimensional all-atom simulations that allow phonon propagation and even electronic degrees of freedom to be taken into account [10, 23]. The field of tribology is very large and is not the focus of this review; we refer the interested reader to several excellent reviews of this field [10, 22].

One of the reasons why the driven dynamics of particles on ordered and disordered substrates is such a fascinating field is that it has implications well beyond the specific systems that have been studied. It provides an ideal testing ground for understanding general issues of nonequilibrium phases and nonequilibrium phase transitions; thus,

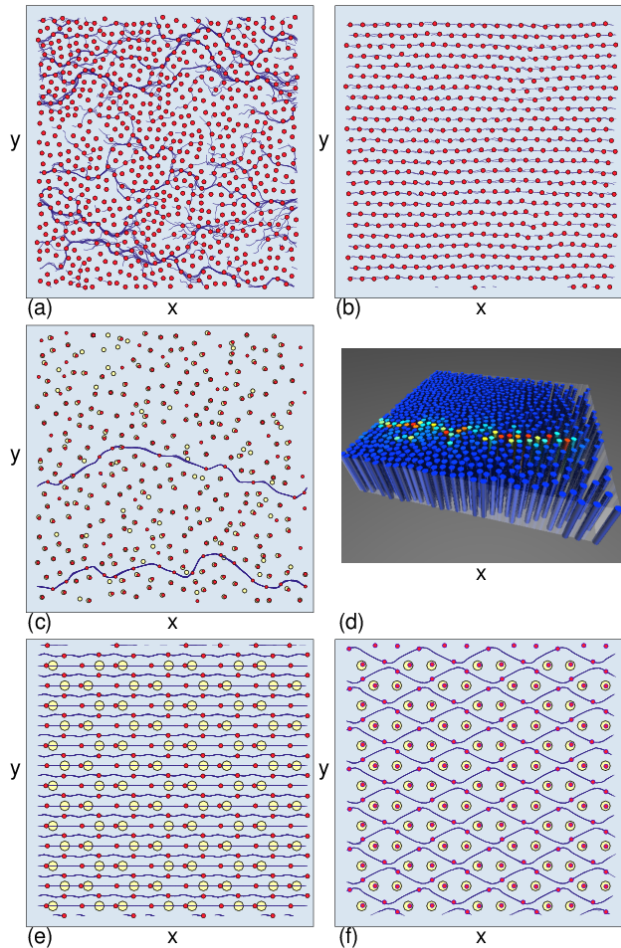


Figure 1. Different varieties of plastic and elastic flow for particles driven in the positive x -direction over substrates with different pinning strengths. Red dots: particle positions; lines: particle trajectories; yellow circles: pinning sites. (a,b) Yukawa interacting colloidal particles on a substrate composed of randomly placed pinning sites (not shown) just above the depinning threshold. (a) For strong coupling to the substrate, given by a pinning strength of $F_p = 0.25$, the depinning transition is plastic and the particles change neighbors as they move. (b) For a weaker pinning strength of $F_p = 0.12$, the depinning is elastic and the colloids maintain the same neighbors as they move. (c-f) Particles representing superconducting vortices. (c) An example of finite size plastic flow in which the particles move in steady state winding channels determined by the substrate disorder. (d) A transient plastic avalanche event in a gradient-driven vortex system, with the vortices represented as columns. Colors indicate speed of motion, from stationary blue particles to rapidly moving red particles. (e) A moving crystal in a periodic honeycomb substrate. (f) An ordered plastic flow phase in a periodic honeycomb substrate. Adapted with permission from: (a,b) C. Reichhardt and C.J. Olson, *Phys. Rev. Lett.* **89**, 078301 (2002). Copyright 2002 by the American Physical Society; (c) C. Reichhardt, C.J. Olson, and F. Nori, *Phys. Rev. B* **58**, 6534 (1998). Copyright 1998 by the American Physical Society; (e,f) C. Reichhardt and C.J. Olson Reichhardt, *Phys. Rev. B* **78**, 224511 (2008). Copyright 2008 by the American Physical Society.

a review unifying various aspects of the field is particularly useful. In equilibrium systems, numerous well-developed concepts and procedures exist for characterizing equilibrium states of matter and the transitions between these states [24, 25]. The different states can be identified by symmetries in the system, while transitions between these states can be characterized by the breaking of these symmetries or the measurement of an order parameter that becomes finite or goes to zero at the transition point. Such transitions can be discontinuous or first order, with hysteresis across the transition, or they can be second order, where the transition is continuous. It is also possible to have various mixed first order and second order transitions, weak first order transitions, or simply crossover behaviors. Continuous transitions can fall into different universality classes which have different scaling behaviors near the transition point. A particularly powerful result of universality is that even if different systems have very different microscopic details, the essential behavior at the transition remains the same if they are in the same universality class. One of the most outstanding open questions in physics and materials science is whether systems that are out of equilibrium can also exhibit specific types of nonequilibrium phase transitions between such states, and whether there are universal properties of these transitions that remain the same between different systems [26, 27]. If a unifying framework can be established for understanding nonequilibrium systems, it would have profound implications for statistical physics, condensed matter, materials science, biological science, information science, and even the social sciences.

There are many difficulties in understanding nonequilibrium phases, such as which measurable properties of the system could play the role of an order parameter, what quantities would be diverging, and where exactly the transition occurs. Only recently have some systems been experimentally realized which clearly exhibit nonequilibrium phase transitions, such as transitions between different turbulent states in a liquid crystal [28] and reversible to irreversible transitions in periodically sheared dilute colloidal suspensions [29]. It would be highly desirable to identify additional model systems where such questions could be readily addressed or in which the system parameters could be easily controlled. Systems that can be represented as individual particles moving over random and periodic substrates have both of these properties, making them ideally suited for testing the concepts of nonequilibrium phases. As advances in microfabrication, nanotechnology, optics, and synthesis techniques continue, more precise control

over many aspects of these systems such as the strength and type of substrate and the nature of the particle-particle interactions becomes feasible. For example, in superconducting systems it is now possible to create tailored substrates with specific geometries, to control the ratio of the number of vortices to the number of pinning sites with an applied magnetic field, and to control the driving force with an applied current [2]. In colloidal systems, optical traps can be used to create a periodic substrate in which the depth of the traps can be readily controlled, and in many cases the interactions between the colloids can also be tuned [7].

In this review, we specifically highlight several different systems in which depinning and nonequilibrium phases have been studied, including vortices in superconductors interacting with random and periodic substrates in two and three dimensions, colloids driven over ordered and disordered substrates, sliding Wigner crystals, and charge hopping in dot arrays. We show how the different dynamical phases have been identified, describe the possible order parameters, and examine the roles of dimensionality, ergodicity breaking, transient behaviors, and transport properties. We also discuss pattern forming systems in which the interactions between the particles have both attractive and repulsive components, so that when driven over a substrate the particles form stripe, bubble, glassy, and emulsion states. We examine the recent developments in nonequilibrium phases in skyrmion systems where the non-dissipative effects from the Magnus term can dominate the dynamics. Finally, we briefly discuss other systems which could potentially be driven over random and periodic substrates, such as active matter or self-driven particles, and mention possible connections to jamming phenomena and quantum effects.

This review is organized as follows. In Section 2 we provide an overview of depinning transitions and dynamic phase transitions, as well as the classes of systems that exhibit such phenomena. In Section 3 we describe experimental, theoretical, and 2D simulation studies of plastic and elastic depinning and dynamical ordering transitions for vortices in type-II superconductors. In Section 4 we discuss depinning and first order dynamical phase transitions in 3D models of superconducting vortex systems, as well as phase locking effects that occur when an ac drive is added to the dc driving force. In Section 5 we describe depinning and first order dynamical phase transitions in other layered systems with many or few layers, including charge density waves (CDWs), mean field models, and coupled 1D channels. In Section 6 we cover depinning and dynamic phases for superconducting vortices and colloids moving over periodic substrates, including both egg carton and muffin tin substrate types. In Section 7 we discuss

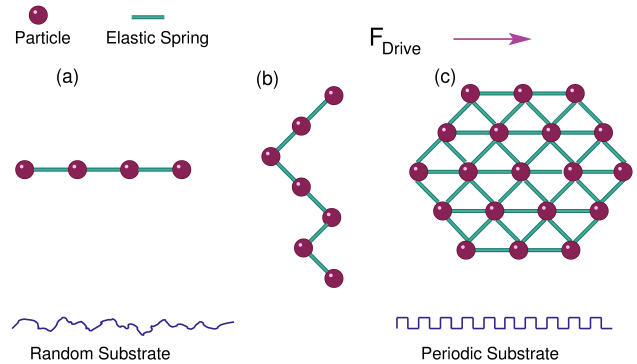


Figure 2. Schematic representations of elastic systems. Lines represent unbreakable elastic springs, circles are particles, and an external driving force F_{Drive} is applied to the particles in the positive x -direction. In the remainder of this review we write F_{Drive} as F_D . The particles can interact with a random or disordered substrate (lower left) or a periodic substrate (lower right). (a) A 1D system with a 1D chain of particles. (b) A 2D system with a 1D string driven perpendicularly to its length to model a domain wall or interface. (c) A 2D system with a 2D elastic lattice. Generalizations can also be made to higher dimensions. These systems exhibit an elastic depinning transition from a pinned state to a moving state in which the particles maintain their same nearest neighbors.

dynamic phases that arise for particles driven over quasiperiodic substrates. Section 8 covers depinning and dynamics in charge transport for 2D Wigner crystal systems and Coulomb-coupled metallic dot arrays. In Section 9 we describe the depinning and dynamics of magnetic skyrmions, where Magnus effects play an important role in the behavior. In Section 10 we connect depinning phenomena with jamming transitions observed in 2D packings of hard disks. Section 11 describes the depinning and dynamics in systems with competing attractive and repulsive particle-particle interactions, where pattern formation occurs, including pairwise and non-pairwise competing interactions, phase field models, and driven binary systems. In Section 12 we discuss the connection between depinning transitions and nonequilibrium absorbing phase transitions. In Section 13 we briefly describe other systems in which depinning and dynamical phases have been studied, and indicate some future directions for study. There is no uniform terminology in the literature for driven systems and depinning phenomena. Throughout this review we use the symbol F_D to represent a driving force, V to represent the average velocity of the particles, F_p to represent the pinning strength, and F_c to represent the critical depinning threshold. In each section and figure caption we indicate how these symbols map onto the physical driving forces and velocities in a given system, and to the symbols used in a given figure.

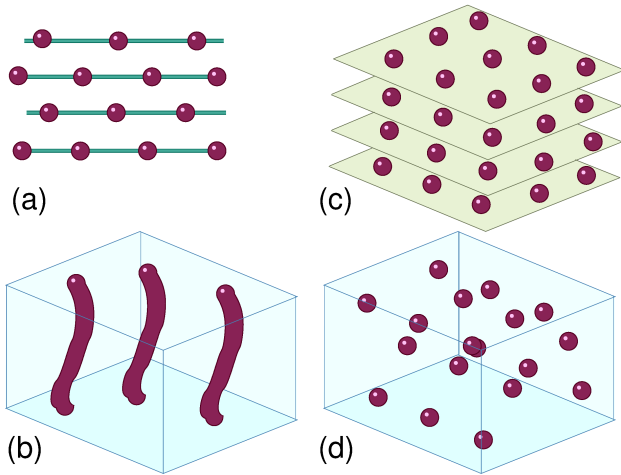


Figure 3. Schematic representations of systems that allow for plasticity or exchange of particle neighbors. Lines represent unbreakable elastic springs and circles are particles. (a) A 2D system of 1D layers. The particles keep the same neighbors in each layer but adjacent layers can decouple. A 2D system in which the particles can exchange all their neighbors is illustrated in figure 1(a). (b) A 3D system of elastic lines with endpoints in a pair of parallel planes. Plastic motion with exchange of neighbors can occur parallel to the planes, but the lines remain elastic along their length. (c) A layered 3D system of particles, in which particles can exchange neighbors within a given plane but remain confined by that plane. (d) An isotropic 3D system where particles can exchange neighbors in all directions.

2. Types of Systems and Depinning Phenomena

2.1. Elastic depinning

At a depinning transition, a system changes from a state in which all of the particles are stationary to one in which some or all of the particles are moving under the influence of a driving force. Depending on the nature of the coupling between the particles, their geometry, and the nature of the substrate, as illustrated in figures 2 and 3, different types of depinning transitions can occur. We first consider elastic depinning, where the moving state above the depinning transition is perfectly elastic, with all the particles moving and no plastic flow so that all particles maintain the same neighbors as a function of time. Figures 1(b) and (e) illustrate systems that have depinned elastically. For models of harmonically coupled particles driven over random or periodic substrates, which could be in one, two, or three dimensions, plasticity does not occur, and the depinning transition is elastic. In figure 2 we show schematic examples of elastically coupled systems in which the particles interact via unbreakable elastic springs and are driven by a force F_{Drive} over some form of substrate. We call the driving force F_D in the remainder of this review. Individual potential minima

in the substrate, which we call pinning sites, exert a maximum force on individual particles that we refer to as a pinning strength F_p . Figure 2(a) illustrates a one-dimensional (1D) system with a chain of coupled particles, figure 2(b) shows a 2D system containing a 1D string driven perpendicular to its length to model a domain wall or moving interface, and figure 2(c) shows a 2D system with a 2D array of elastically coupled particles. Similar features appear in three-dimensional (3D) systems (not shown), which can contain 1D strings, 2D membrane-like arrays, or 3D lattices of elastically coupled particles. Inclusion of a random or periodic substrate introduces a depinning threshold F_c ; for drives $F_D < F_c$ the particles exhibit no steady state motion. As the driving force is increased from zero, the string, membrane, or lattice becomes increasingly rough as the depinning threshold is approached. At F_c , depinning occurs and there is a transition to an elastic sliding phase. In most cases, the roughness of the sliding particle structure decreases for sufficiently high drives when the perturbations from the pinning sites become negligible. Since the particles are elastically coupled, they keep their same neighbors over time, so that the system can be viewed as an unbreakable rubber sheet pulled over a carpet.

The velocity V at a given value of F_D is taken to be the steady state time-averaged velocity of all particles in the system, $V = \langle N^{-1} \sum_i^N (\mathbf{v}_i \cdot \hat{\mathbf{x}}) \rangle$ for a sample containing N particles which each have velocity \mathbf{v}_i that are subjected to a driving force applied along the x direction. The curve V versus F_D is referred to as a velocity-force curve. The velocity-force curves for elastic depinning transitions typically exhibit features similar to those shown schematically in figure 4(a). There is a critical value F_c of the driving force corresponding to the highest drive that can be applied for which the system remains pinned with no steady-state motion. This is termed the critical depinning threshold. For overdamped systems, the average particle velocity V in the absence of a substrate increases linearly with F_D according to $V = F_D/\eta$, where η is the damping term. In the presence of a substrate, once the particles are moving for drives above depinning $F_D > F_c$, V is normally smaller than the clean limit value, particularly near the depinning threshold F_c . In figure 4(a) the dashed line indicates the clean or substrate-free velocity-force curve for a system with $\eta = 1.0$. As F_D increases, the value of V for a system with a substrate gradually approaches the clean limit value.

Fisher [30] was one of the first to show that the pinned to sliding transition in an elastic system has similarities to a second order equilibrium phase transition, and exhibits critical phenomena in which certain quantities obey power law scaling close to the

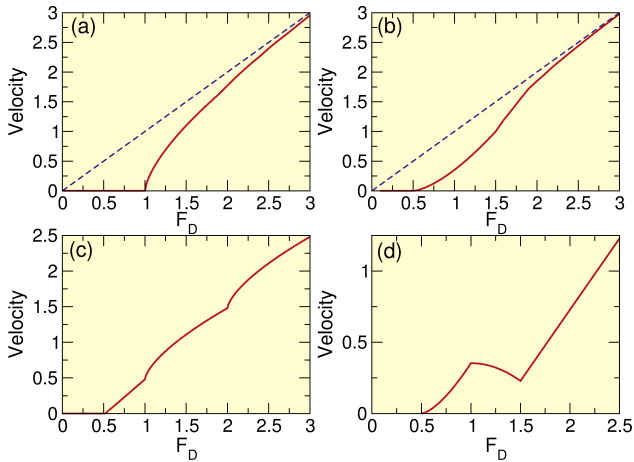


Figure 4. Schematics of typical velocity-force curve behaviors for particle assemblies driven over random or periodic substrates. V , written as Velocity on the figure panels, is the average velocity of the particles, F_D is the driving force, and F_c is the depinning threshold. (a) For elastic depinning, near the depinning threshold $V \propto (F_D - F_c)^\beta$ with $\beta = 2/3$. The dashed line indicates the substrate-free velocity-force response with $V \propto F_D$. (b) For a system similar to that shown in figure 1(a), where plastic depinning occurs, near the depinning threshold $V \propto (F_D - F_c)^\beta$ with $\beta = 1.5$. The velocity-force curve has an overall S-shape, with a transition to a dynamically reordered state at high drives. (c) A system with multiple dynamical transitions, marked by the kinks in the velocity-force curve. (d) A system in which a change in the dynamical flow occurs that causes the average particle velocity to decrease with increasing F_D over a certain range of F_D , producing negative differential conductivity.

critical point F_c . Here, the velocity-force curve takes the form

$$V \propto (F_D - F_c)^\beta \quad (1)$$

where β is a critical exponent [30], while at high drives,

$$V \propto F_D. \quad (2)$$

The power of the approach introduced by Fisher is that it suggests that the class of nonequilibrium systems that exhibit elastic depinning can be understood using an approach similar to that applied to equilibrium critical phenomena, and that if critical exponents and universality classes can be identified, the same critical exponents could arise in many different types of systems even though the microscopic details and size scales of these systems could be vastly different. If F_c is a critical point, other quantities such as a correlation length ξ would also diverge near depinning, $\xi \propto (F_D - F_c)^{-\nu}$, with critical exponent ν . Since this initial proposal, there has been extensive work in identifying the critical exponents for depinning in CDW models, such as the thorough study by Myers and Sethna who find $\beta = 0.45$ in dimension $d = 1$, $\beta = 0.65$ and $\nu = 0.5$ in $d = 2$, and $\beta = 0.8$ in $d = 3$ [31]. In addition to the motion in the sliding phase, transient particle rearrangements can occur below the

depinning threshold if the external drive is increased by some increment and the particles adjust their positions in order to balance the driving and pinning forces. The transient time over which this motion occurs also diverges as the depinning threshold is approached. The rearrangements below F_c can be viewed as avalanches of motion in which correlated groups of particles move for a time before becoming repinned, and the spatial size of the jumps of these particles can provide a measure of the correlation length [31].

There are many complications to understanding critical behavior in driven particle systems. One example is the identification of the critical depinning threshold F_c . In experiments, the driving force is increased at a certain rate; however, if there are transient times associated with criticality at depinning, then at some point these transient times become larger than the inverse rate at which the driving force is being swept, so the system no longer has enough time to settle back into the pinned phase and appears to depin at a drive lower than the true critical point. Additionally, if inertial effects are included in the dynamics of the system, the driving rate dependence may be even stronger, or new types of dynamics could appear that change the criticality of the system or eliminate it altogether. Other possible effects include retardation in modes of dissipation, which could cause local buildups of heat or strain, as well as nonuniformity in the substrate potential itself. Many real materials can have large inhomogeneities in the effective pinning strength and in the spatial distribution of the pinning sites, which means that as the depinning threshold is approached, one part of the sample may reach the critical threshold before the rest of the sample, thus making a scaling analysis difficult to perform. Instead of approaching the depinning threshold from below, it is possible to decrease the driving force from high values in order to approach the threshold from above; however, it is possible that the scaling exponents could be different on each side of the transition [31]. Many models for elastic depinning are in the strongly overdamped limit and include the assumption that the damping constant is fixed; however, in experiments it is possible for the damping constant itself to have a drive dependence if additional damping modes become excited in the sliding state.

There are still many open questions in elastic depinning, particularly regarding the role of inertia and hysteresis effects. There are a growing number of biological systems such as membranes and networks that exhibit highly nonlinear elasticity, and in many cases these biological objects are moving over some type of substrate, so another direction for future research is to study depinning in systems with nonlinear elasticity [32, 33]. Recent studies considered

wrinkling transitions and crumpling in elastic sheets [34], and it would be interesting to see whether the ideas of wrinkling transitions could be applied to depinning of elastic sheets and membranes or to elastic depinning in curved geometries.

2.2. Plastic depinning

This brings us to the next level in complexity in depinning, where some form of plasticity can occur either by the breaking and reforming of physical bonds between neighboring particles or by a change of neighbors for particles without explicit bonds. In the elastic models illustrated in figure 2, if the pinning is very strong, it can induce such large elastic distortions in the particle assembly that a portion of the particles can move past one another a distance larger than the equilibrium lattice constant a , so that the elastic springs connecting the particles would likely break at one or more locations. In experimental systems, where the number of particles can be very large, it is likely that even for weak random pinning there can be rare regions of strong disorder that can produce some plasticity. Thus, it is of paramount importance to understand plastic deformation at depinning, and it has even been argued that plasticity is relevant in most CDW systems [35].

In 2D, the simplest model in which it is realistic to include plastic effects consists of unbreakable 1D elastic chains aligned parallel to each other and coupled by breakable bonds, as illustrated in figure 3(a). Here different depinning processes as well as a variety of dynamical phases can occur. If the pinning is weak, local variations in pinning strength are unimportant and the entire system can behave elastically and depin in a single step, as shown schematically in figure 4(a). For strong pinning, local variations in pinning strength cause individual 1D chains to have different depinning thresholds F_c^i so that the depinning is now plastic, and only the subset of chains for which $F_D > F_c^i$ are able to move. The moving chains slide past the remaining pinned chains, resulting in a coexistence of pinned and flowing chains. The depinning threshold of the entire system is equal to the smallest F_c^i in the system, making plastic depinning an example of an extreme value event. As the driving force is increased, more and more chains begin to move. When $F_D > \max(F_c^i)$ and the depinning threshold of every chain has been exceeded, the sample enters a state in which all the 1D chains are in motion but travel with different average velocities, so that they continue to slide past one another. The difference in velocities arises since at a given F_D , different chains are different distances $F_D - F_c^i$ above their depinning threshold. At high enough drives, $F_D - F_c^i$ is large for all chains and the effective pinning forces experienced by the

moving chains become weak enough that the chains can dynamically recouple and form a moving elastic solid.

The existence of different dynamical phases in the unbreakable 1D elastic chain system can produce signatures in the velocity-force curves as shown schematically in figure 4(c), where only a portion of the particles are moving just above the depinning threshold, and cusps appear as additional chains of particles begin to move or as neighboring chains dynamically recouple. The individual particle velocity distribution function $P(v_i)$ just above the onset of sliding can be bimodal if there is a coexistence of pinned and moving channels or if the channels form distinct groups that slide past each other, while $P(v_i)$ becomes sharply peaked above the dynamical recoupling transition when the motion throughout the sample becomes coherent. The features in the velocity-force curves and velocity distribution functions can depend strongly on dimension, disorder, pinning strength, and inter-particle coupling. The system size is also important. For example, if plastic events occur at a specific size scale, then in systems of infinite size, the elastic response at small scales is washed out, while in small systems the behavior might appear purely elastic, and in intermediate sized systems, elastic and plastic behaviors can compete but the plastic events would be a dominant feature, so that obtaining a meaningful average velocity would be very problematic. Additionally, as a function of driving force, the length scales at which plastic events occur can change.

At the next level of complexity in 2D, the particles are free to plastically deform in any direction, such as in the samples illustrated in figure 1. A system of this type could have isotropic or anisotropic coupling between the particles. Figure 3(b) shows that another class of systems that allow 2D plastic deformation is an assembly of elastic line objects with their endpoints confined to two parallel planes. Plastic motion with exchange of neighbors can occur parallel to the planes, but the lines remain elastic along their length. In figure 3(c) we illustrate a 3D layered system where the particles are confined within a given layer but can exchange neighbors within that layer. Finally, figure 3(d) illustrates an isotropic system of point particles where plasticity can occur in all directions equally. In addition to the different geometries for the particle arrangements, the substrate disorder can also have different spatial features which depend on dimensionality, such as 3D columnar, splayed, or planar defects.

Although all the systems highlighted in figures 1 and 3 exhibit plasticity, it is an open question whether there are distinct types of plastic flow phases, whether

transitions between different types of plastic flow can occur, and how such phases could be characterized. For example, figure 1(a) illustrates a strongly fluctuating plastic flow, figure 1(c) shows a steady state plastic flow through fixed winding channels, figure 1(d) shows transient plastic flow in an avalanche event for a very slowly driven system, and figure 1(f) illustrates an ordered plastic flow state. All of these flows are plastic, but they may have features that would allow them to be subdivided into separate types of plastic flow. The problem of plasticity is generally considered one of the most outstanding problems in materials science, in part because systems that exhibit plasticity can have both solidlike and liquidlike properties at the same time.

One well-defined question in systems with pinning is whether, under certain conditions, plastic depinning is associated with dynamical critical phenomena similar to that found for elastic depinning. For example, in the strong pinning limit where the particles are highly disordered in the pinned state, the flow just above depinning follows channels or riverlike features of the type illustrated in figure 1(a). Such plastic channel flow behavior has been observed in vortex systems [20, 36, 37, 38, 39], Wigner crystals [40, 41], and colloidal systems [6, 20]. For plastic depinning in 2D systems in the strongly amorphous limit, the velocity-force curves also appear to exhibit a scaling of the form $V = (F_D - F_c)^\beta$ with $\beta > 1.0$. This is in contrast to elastic systems in 2D and higher dimensions where $\beta < 1.0$. As a result, velocity-force curves associated with plastic depinning have a concavity opposite to that found for elastic depinning, as shown schematically in figure 4(a,b) which contrasts a representative example of a typical velocity-force curve for elastic depinning with $\beta = 2/3$ with a plastic depinning velocity-force curve with $\beta = 1.5$. These results suggest that if plastic depinning has critical properties, it falls into a different universality class than elastic depinning; however, the existence of such criticality and its exact nature has not been verified, as measured exponents span a wide range of values from $\beta = 1.25$ to $\beta = 2.5$ [20, 21, 37, 41, 42, 43, 44]. The variation in the exponents could result from strong finite size effects, transient effects, or differences in the nature of the particle-particle interactions, or it could indicate that multiple types of criticality occur at plastic depinning due to the different dominant degrees of freedom, such as glide and climb of dislocations, kinetic barriers, and the distinction between long range interactions of the particles and long range interactions between the emergent topological defects. This also suggests that new approaches to understanding plastic depinning will be useful to understand whether plastic depinning possesses truly universal features.

Many of the same challenges that are faced

in general studies of plasticity in crystalline and amorphous solids also arise in the plastic depinning context. Just one example of a challenge in materials plasticity is the fact that stress-strain curves in amorphous systems often have different properties depending on how the material is prepared, such as a deep quench compared to a slow quench. It is likely that similar effects occur for plastic depinning; however, little is known about how this would arise. Another challenge in plastic depinning is that there can be differences between the response of systems with intermediate-range order and those in the strongly amorphous limit. In materials science, crystalline materials can exhibit plastic behavior called crystal plasticity where a well defined number of topological defects such as dislocations or grain boundaries are present and where critical behavior appears near yield that is similar to the behavior observed near depinning [45, 46]. This crystal plasticity is distinct from the plasticity that arises in amorphous systems where topological defects are not well defined. For the case of systems that exhibit plastic depinning transitions, it is not known whether a similar distinction can be drawn between depinning that has properties similar to those associated with crystal plasticity and depinning that is amorphous in nature.

2.3. Dynamical transitions

Despite the challenges in studying plasticity, it appears that plastic depinning of particle systems in the strongly amorphous limit produces some generic features in the transport and dynamics even for very different types of interactions between the particles. Figure 4(b) shows a schematic of a typical velocity-force curve illustrating a pinned phase at low F_D , plastic depinning with $V \propto (F_D - F_c)^\beta$ and $\beta = 1.5$, and an overall S-shape produced by the transition to Ohmic or linear velocity at high drive when the substrate becomes ineffective, associated with a peak in dV/dF_D just below the Ohmic regime. The presence of a peak in dV/dF_D often indicates that there is a transition within the moving phase from a plastic or liquid state into a moving solid where the particles are moving so rapidly over the underlying pinning landscape that the particle-particle interactions dominate over the particle-pinning interactions, causing the particles to adopt a structure similar to that found in the substrate-free limit, which could be a triangular lattice in 2D. This suggests that there can be two generic transitions associated with plastic depinning: the depinning transition itself, and the dynamical ordering transition at higher drive. Such pairs of transitions have been observed in experiments and simulations of vortices in type-II superconductors [21, 38, 43, 47], driven Wigner

crystals [41], colloids [48], frictional studies [49], skyrmions [50], and pattern forming systems driven over random substrates [9]. The dynamically ordered moving state can still be affected by the pinning even in the high drive limit so that the reordered structure is generally not an isotropic crystal but rather an anisotropic moving crystal [51], moving smectic [52, 53, 54, 55], or even anisotropic liquid state [56] depending on the strength of the disorder, the drive, and the dimensionality. An open issue is whether the dynamical ordering transition can be viewed as a nonequilibrium phase transition and, if so, whether the type of nonequilibrium transition can be identified. For example, the ordering transition might have the same properties as the criticality observed for elastic depinning [30] or an absorbing phase transition such as directed percolation [26], or it might be possible to effectively map it to some class of equilibrium phase transition by replacing the dynamical fluctuations with an effective temperature [24, 25].

Plastic depinning can also occur for particles driven over periodic substrates, as illustrated in figure 1(f), and the type of dynamics that occur depend on whether the particle arrangement is commensurate or incommensurate with the substrate [2, 7, 57, 58, 59, 60]. There are number of examples of periodic substrate systems in which the depinning and sliding dynamics appear to exhibit very well-defined transitions between distinct plastic flow phases, suggesting that such systems could be ideal for testing methods for characterizing different nonequilibrium flow states [60, 61, 62, 63, 64]. Figure 4(c) shows an example schematic velocity-force curve for a system that depins plastically and then exhibits transitions between different flow states at higher drives, which are marked by kinks in the curve. The jump up in V at the transitions can arise either because more particles have become mobile or because there has been a change from disordered flow to a more coherent flow. Figure 4(d) shows schematically that in some cases the average particle velocity can actually decrease with increasing drive due to a change in the flow pattern from a more coherently moving state to one with stronger fluctuations, or to a state in which more particles are pinned.

An example of some of the complications in analyzing plastic depinning and the possibility of different kinds of plastic flow states appears in the work of Fily *et al.* [43] who study the depinning of 2D superconducting vortices from a random substrate. They observe combinations of elastic non-chaotic flow and plastic chaotic flow, making it difficult to establish the true value of the critical depinning threshold F_c . Figure 5 shows the vortex trajectories in this system. The depinning transition is associated with the opening

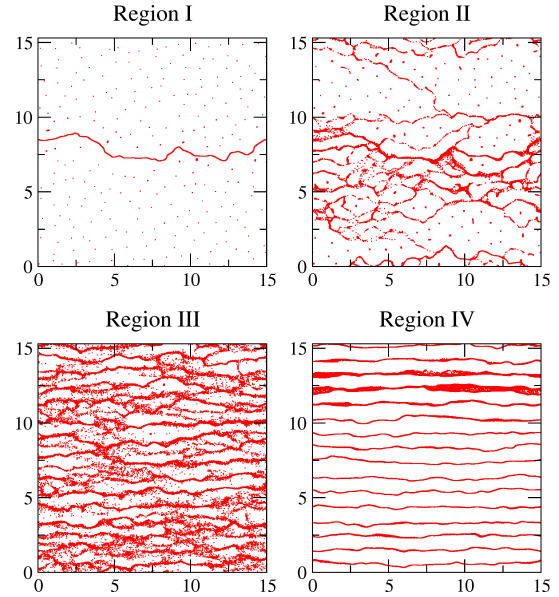


Figure 5. Trajectories of moving superconducting vortices from a 2D simulation in which there is a random substrate and a driving force is applied in the positive x direction, to the right in the figure. (a) Region I just above depinning. (b) Region II at high drives where disordered channels form. (c) Region III, where there is some additional nematic or smectic type ordering of the trajectories. (d) Region IV, where the system is in a dynamically reordered state. Reprinted with permission from Y. Fily, E. Olive, N. Di Scala, and J.C. Soret, *Phys. Rev. B* **82**, 134519 (2010). Copyright 2010 by the American Physical Society.

of isolated channels of motion, labeled Region I in figure 5(a). At higher drives, as shown in figure 5(b) and labeled Region II, multiple channels appear that change as a function of time. Although both Region I and Region II are plastic flows since they both exhibit a coexistence of moving and pinned particles, the two regions have very different dynamics in phase space, as illustrated in figure 6 which shows the value of

$$d(t) = \sqrt{\sum_{i=1}^N |\mathbf{r}_i^1(t) - \mathbf{r}_i^2(t)|^2}. \quad (3)$$

This quantity measures the difference in phase space of two neighboring trajectories $[\mathbf{r}_1^1(t), \dots, \mathbf{r}_N^1(t)]$ and $[\mathbf{r}_1^2(t), \dots, \mathbf{r}_N^2(t)]$. In Region I, figure 6(a) shows that d rapidly drops to a small constant value, indicating that the system has entered a closed orbit in phase space and is non-chaotic, while for Region II in figure 6(b), d increases exponentially with time, indicating chaotic behavior with a positive Lyapunov exponent and diverging trajectories. The saturation in d in the chaotic region occurs at the point at which $d(t)$ becomes of the same order as the size of the chaotic attractor. This result indicates that the flowing state above depinning can have characteristics

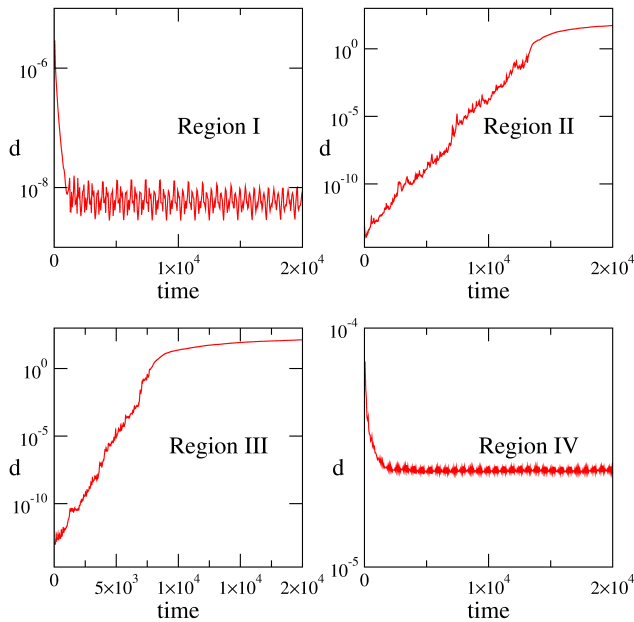


Figure 6. For the superconducting vortex system in figure 5, the distance d between two neighboring particle flow trajectories as a function of time in Region I, which is non-chaotic, Regions II and III, which are chaotic, and Region IV, which is non-chaotic. Reprinted with permission from Y. Fily, E. Olive, N. Di Scala, and J.C. Soret, Phys. Rev. B **82**, 134519 (2010). Copyright 2010 by the American Physical Society.

of both chaotic plasticity and non-chaotic plasticity. In Region I the vortices move in an isolated channel, so this region can also be described as an effectively 1D system of elastically coupled particles that undergoes an elastic depinning transition while the rest of the system remains frozen. As more channels begin to flow with increasing drive, they initially also behave elastically, but at some point the channels begin to intermingle, producing a transition to a chaotic or plastic flow phase. This raises the question of how to accurately determine the critical depinning threshold value F_c since there are now two effective depinning transitions, one at F_{c1} for the non-chaotic Region I flow, and one at F_{c2} for the onset of chaotic plastic flow. Another issue is whether the difference between F_{c1} and F_{c2} changes with system size and if, in the infinite size limit, there is only a single transition with a unique value of F_c . Figure 5(c) shows the trajectories at even higher drives in Region III, where there are more channels and the flow has a more nematic or smectic type character. Although this flow differs in appearance from the Region II flow, figure 6(c) shows that $d(t)$ grows exponentially, indicating that the flow is still chaotic. It is not clear whether Region III is truly a separate flow phase or just a crossover from the Region II flow. At higher drives, the flow transitions into the static 1D flow channels of Region IV, illustrated in figure 5(d), and $d(t)$ saturates at a low

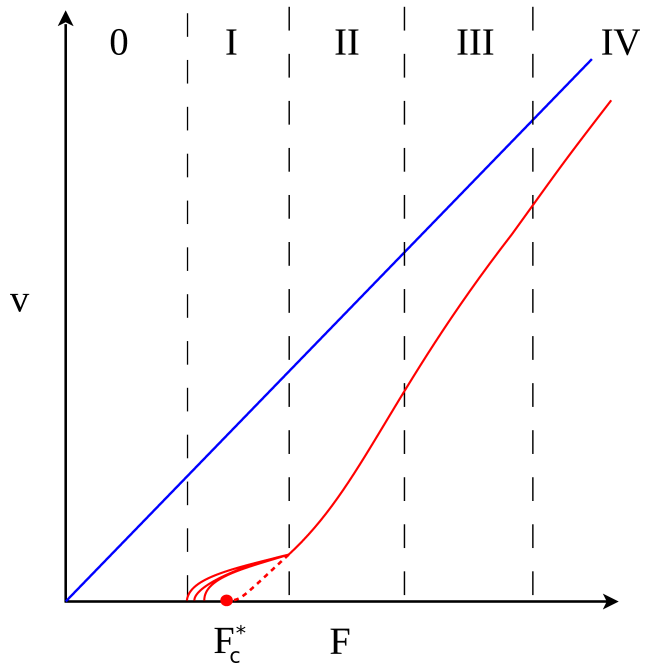


Figure 7. A schematic of velocity-force curves (red lines) from the superconducting vortex system in figures 5 and 6 highlighting where the transitions from Regions 0 through IV occur, where Region 0 is the pinned phase. The blue line is the substrate-free velocity-force response. Here V is velocity and F corresponds to the driving force F_D , while F_c^* denotes the point at which the extrapolated onset of the chaotic flow phase would occur. The actual onset of Region I occurs below F_c^* , indicating that there is a regime in which the velocity-force curves have elastic rather than plastic features. Reprinted with permission from Y. Fily, E. Olive, N. Di Scala, and J.C. Soret, Phys. Rev. B **82**, 134519 (2010). Copyright 2010 by the American Physical Society.

value as shown in figure 6(d), indicating that Region IV is non-chaotic.

Figure 7 shows a schematic of the velocity-force curve for this system, where the upper line denotes the velocity-force response in a clean system without pinning and where the locations of the different regions are indicated. Region 0 corresponds to the pinned phase. The dashed line shows the point F_c^* at which the onset of the chaotic plastic flow phase would be expected to occur based on an extrapolation of the velocity-force curve; however, the true depinning threshold $F_c < F_c^*$, and since the motion in Region I is effectively elastic, the velocity-force curve initially exhibits an elastic scaling exponent of $\beta < 1.0$ before crossing over to a shape consistent with $\beta > 1.0$ at the transition to the chaotic plastic flow regime. Using various scaling techniques, Fily *et al.* determined that $\beta = 1.3$ at the onset of the chaotic plastic flow region. Some questions that remain is whether the transition between Region I and Region II is a dynamical phase transition, or if it instead obeys the period-doubling behavior expected for a transition to chaos in low dimensional systems [65]. Also unknown is the nature

of the transitions between the other regions, and how general the behavior at these transitions is to other systems.

Although this review concentrates on depinning phenomena, we note that there may be deeper connections between depinning and the onset of yield and plasticity in pin-free materials. In recent work on non-chaotic to chaotic transitions near yield in amorphous systems, similar effects arise where reversible or non-chaotic plastic flow appears below yield, followed by a transition to irreversible plastic flow. This would imply that yielding could be understood as a transition to a chaotic state, similar to the transition to chaotic plastic depinning, and raises the question of whether these two different systems fall in the same universality class [66, 67, 68, 69]. Figure 8 shows two examples of stress-strain curves from simulations of sheared amorphous materials, where the solid vertical line represents the yield point above which the system starts to flow. Below yield, the stress increases with strain in what could be considered a pinned regime, while the yielding point could be associated with a depinning transition, and the higher strain regime could be similar to a flowing regime. Recent work has shown that below yield, there can be plastic rearrangements of the particles similar to the rearrangements that occur in pinned systems subjected to drives that are below the depinning threshold. The yellow line in figure 8 indicates that the transient time required for these plastic rearrangements to die out diverges as a power law as the yielding transition is approached, suggesting that yield has critical properties [67] similar to those observed at critical depinning transitions. In Section 12 we discuss how plastic depinning and the onset of irreversible plastic deformations in materials may be governed by the same type of critical behavior.

3. Depinning and Dynamic Phases in Superconducting Vortex Systems

One of the best examples of a system that exhibits different kinds of depinning and dynamical sliding behavior is vortices in type-II superconductors [1]. Under application of a magnetic field, the flux does not enter a type-II superconducting sample in a uniform manner, but rather forms quantized vortices that each carry an elemental unit of magnetic flux $\phi_0 = h/2e$. The field is most intense at the non-superconducting core of the vortex and then falls off at further distances. The existence of a gradient in this field indicates that there is a supercurrent $\mathbf{J} \propto \nabla \mathbf{B}$ circulating around the core, in analogy with the fluid circulating around the core of a superfluid vortex. The superconducting vortices interact repulsively with each

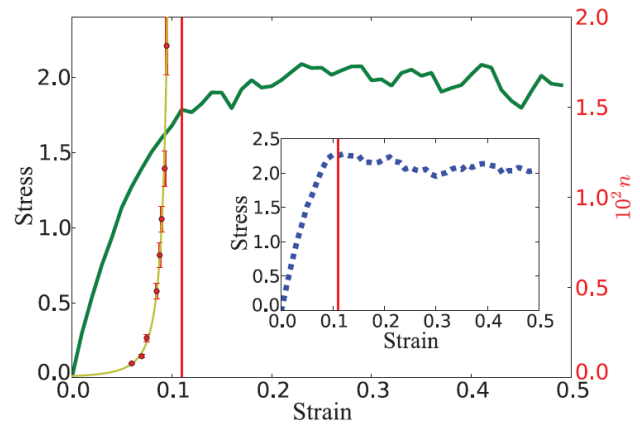


Figure 8. Stress-strain curve (green) from molecular dynamics simulations of 16384 particles under quasistatic shear. Red dots represent the number of shear cycles n required to reach periodic behavior under oscillatory shear (the scale is on the right side of the figure in red). The vertical red line is the strain amplitude at which the time to reach reversible behavior diverges. Inset: stress-strain behavior for the same parameters as the solid green curve but with different initial particle configurations. The vertical red line is the same as in the main figure. Reprinted with permission from I. Regev, T. Lookman, and C. Reichhardt, Phys. Rev. E **88**, 062401 (2013). Copyright 2013 by the American Physical Society.

other through a potential that has the form of a Bessel function $K_1(r_{ij}/\lambda)$ in a superconducting slab, where λ is the London penetration depth of the magnetic field away from the core. This interaction behaves as $\ln(r)$ at short range and falls off exponentially at larger distances. The Bessel function vortex-vortex interaction can be used for 3D systems in which the vortices behave as stiff lines that form a 2D triangular lattice in the plane perpendicular to the magnetic field, and the overall dynamics can be modeled as effectively 2D. Models for vortex lines that are not stiff are described in Section 4. In thin film samples the vortices have a longer range interaction of the form $\ln(r)$ or $1/r$ depending on the sample thickness and the behavior of the magnetic field at the surface. An externally applied current \mathbf{J} interacts with the magnetic field of each vortex and induces a Lorentz driving force $F_D \propto \mathbf{B} \times \mathbf{J}$ that causes the vortex to move. Since the core of the vortex is non-superconducting, the electrons located in the core behave dissipatively, resulting in overdamped vortex motion with a damping term η . The vortex velocity V can be measured as a finite voltage response in the sample produced by the dissipation.

In the absence of pinning produced by a substrate or by intrinsic inhomogeneities in the sample, the vortex velocity increases linearly with the driving force, $V = F_D/\eta$. Most samples, however, contain intrinsic disorder in the form of sites where the order parameter of the superconducting condensate is suppressed. These locations act as pinning sites for

the vortices, and allow the vortex lattice to remain immobile even when a driving current is applied to the sample. The critical current can be defined as the applied current at which a finite voltage response first appears, and corresponds to a depinning threshold F_c . Under a driving current, the vortex velocity-force curves are directly proportional to the voltage-current curves, so that features in the voltage-current curves or the time dependent fluctuations of the voltage reflect how the vortices are moving and their velocity fluctuations. In the interest of generality, we refer to voltage-current curves as velocity-force curves in our discussion. Many applications of type-II superconductors require the material to remain superconducting while transporting high currents, so there has been extensive work on understanding how to optimize the pinning and maximize the critical current in these systems using techniques such as ion irradiation, chemical synthesis [1], and nanostructuring of artificial pinning arrays [2].

At magnetic fields H well below the critical magnetic field H_{c2} at which the sample ceases to superconduct, the vortex core undergoes only small distortions when the vortex moves or interacts with other vortices or pinning sites, so the vortex dynamics can be described by a particle-based equation of motion which for a single vortex i can be written as

$$\eta \frac{d\mathbf{R}_i}{dt} = \mathbf{F}_i^{vv} + \mathbf{F}_i^p + \mathbf{F}_D + \mathbf{F}^T. \quad (4)$$

Here \mathbf{R}_i is the position of vortex i and the vortex-vortex interaction force is $\mathbf{F}_i^{vv} = \sum_{j=1}^{N_v} F_0 K_1(R_i/\lambda) \hat{\mathbf{R}}_{ij}$, where $F_0 = \phi_0^2/2\pi\mu_0\lambda^3$, ϕ_0 is the elementary flux quantum, μ_0 is the permittivity of free space, K_1 is the modified Bessel function, $R_{ij} = |\mathbf{R}_i - \mathbf{R}_j|$, and $\hat{\mathbf{R}}_{ij} = (\mathbf{R}_i - \mathbf{R}_j)/R_{ij}$. The density of vortices in the system is proportional to the applied magnetic field. The interaction with the pinning sites is represented by \mathbf{F}_i^p , which can be modeled in various ways. For example, parabolic traps cut off at a radius R_p or localized Gaussian-shaped traps can be used to represent pointlike pinning sites, while different potentials can represent smoother substrate landscapes or line-like defects such as twin boundaries. In general, a single pinning site or substrate feature exerts a maximum pinning force of F_p on an individual vortex. The external driving force is given by \mathbf{F}_D , and represents a dc and/or ac applied current which generates a force of magnitude F_D . On periodic substrates the drive can be oriented along different angles to the substrate symmetry directions. In typical velocity-force simulations, F_D is increased in small increments δF_D and the velocity of the vortices is measured during a fixed simulation time period to obtain an average value of V for each value of F_D . It is important to wait long enough for the system to settle into a steady state, particularly near the

depinning threshold. The thermal fluctuations \mathbf{F}^T are modeled as random Langevin kicks with the properties $\langle F^T(t) \rangle = 0$ and $\langle F_i^T(t) F_j^T(t') \rangle = 2\eta k_B T \delta_{ij} \delta(t - t')$, where k_B is the Boltzmann constant. In many superconducting vortex systems, thermal forces are not relevant; however, high-temperature superconducting materials can exhibit regimes in which the thermal effects are strong enough to produce liquid-like behavior of the vortices, resulting in strong creep effects in the velocity-force curves. In this review we focus on regimes where thermal fluctuations do not dominate the behavior. In simulations, the vortex ground states can be obtained using various energy minimization schemes or by simulated annealing where the system is started at a high temperature and gradually cooled to $T = 0$. For systems with a Bessel function vortex-vortex interaction, the mutual repulsion of the vortices causes them to naturally avoid the short-distance divergence of the interaction force provided that the vortex density does not become too large, while the interaction can be truncated at sufficiently large distances where it becomes negligible without affecting the results. For $\ln(r)$ or $1/r$ vortex interactions, no long-range cutoff is possible and techniques such as Euler or Lekner summations must be employed in dynamical simulations.

The equation of motion for superconducting vortices can also contain additional non-dissipative terms, such as a Magnus force [70, 71] generated by the interaction of the driving current with the circulating vortex supercurrent. This produces an additional force on the vortex that is transverse to the Lorentz force. In superconductors, Magnus force effects are usually very small [1], but in skyrmion systems, the Magnus term is large and affects the particle dynamics, as we discuss in section 9. In principle the vortex motion can also include an inertial contribution $M\dot{\mathbf{R}}_i$, but the mass M of a vortex is very small so such effects can normally be ignored.

Features of the vortex system that make it ideally suited for studying depinning include the numerous readily experimentally tunable parameters, such as magnetic field which can be used to sweep the system from the single vortex limit at low magnetic fields to the strongly interacting vortex limit at high magnetic fields, as well as the applied current, which can sweep the system from low to high driving forces. Due to the small size of an individual vortex, experimental studies can readily access the long-time dynamics of large assemblies of vortices, so that statistically averaged measures of dynamical steady states can be obtained. It is also possible to tune the vortex-vortex interactions using temperature since λ diverges near T_c and H_{c2} , which denote the temperature and magnetic field at which superconductivity is destroyed. By operating close to T_c , the vortex-vortex interactions can be

weakened relative to other energy scales in the system.

3.1. Elastic and plastic depinning transitions

Ideally, the best samples for studying depinning and dynamic flows have low intrinsic pinning strength, permitting access to the flux flow regime over a wide range of currents without significant generation of local heating effects by the moving normal vortex cores. In such samples, the basic assumptions used in constructing a particle-based vortex equation of motion remain valid. Many weak pinning samples exhibit what is called a “peak effect” in which the critical depinning threshold F_c initially decreases with increasing magnetic field before suddenly increasing to a peak value and then dropping to zero at the superconducting-to-normal transition [21, 72]. The initial decrease in F_c with increasing magnetic field is expected since the vortex-vortex interactions become stronger as the vortices get closer together, reducing the effectiveness of the intrinsic pinning, but the peak in F_c has not been satisfactorily explained. The peak coincides with pronounced changes in the current-voltage curves [21, 73] and noise fluctuations [74, 75], suggesting that the peak effect is associated with changes in the vortex lattice structure in the pinned phase as well as changes in the depinning transition and the vortex motion above depinning.

Higgins and Bhattacharya experimentally measured the effective vortex velocity-force curves across the peak effect in a low pinning sample of 2H-NbSe₂ [21, 73]. Based on the features of these curves, they deduced that below the peak effect the vortices depin elastically, while at and above the peak effect the vortices depin plastically and undergo a transition at higher drives to a dynamically ordered moving vortex state. Figure 9(a) shows the measured effective pinning strength F_p , determined using the relation $F_p = |\mathbf{J}_c \times \mathbf{B}|$, vs H , indicating that there is a peak in the pinning force near $H = 6$ Tesla. Here J_c corresponds to the critical depinning threshold F_c , while the vortex density increases with increasing H . The velocity-force curves in figure 9(b) show changes in concavity when measured at different magnetic field values across the peak effect, and close to the peak effect the curves are S-shaped. The changes in the curves are more clearly visible in the dV/dF_D plots in figure 9(c). At fields below the peak effect regime, as shown in the inset of figure 9(c), there is only a plateau in dV/dF_D , while near the peak effect dV/dF_D develops a spike feature, shown in the main panel of figure 9(c), that reflects the S-shape of the velocity-force curves. For fields above the peak effect, the spike in the dV/dF_D curves diminishes and disappears.

The velocity-force curves in figure 9(b) can be scaled to fit $V \propto (F_D - F_c)^\beta$, with $\beta = 1.75$ above the

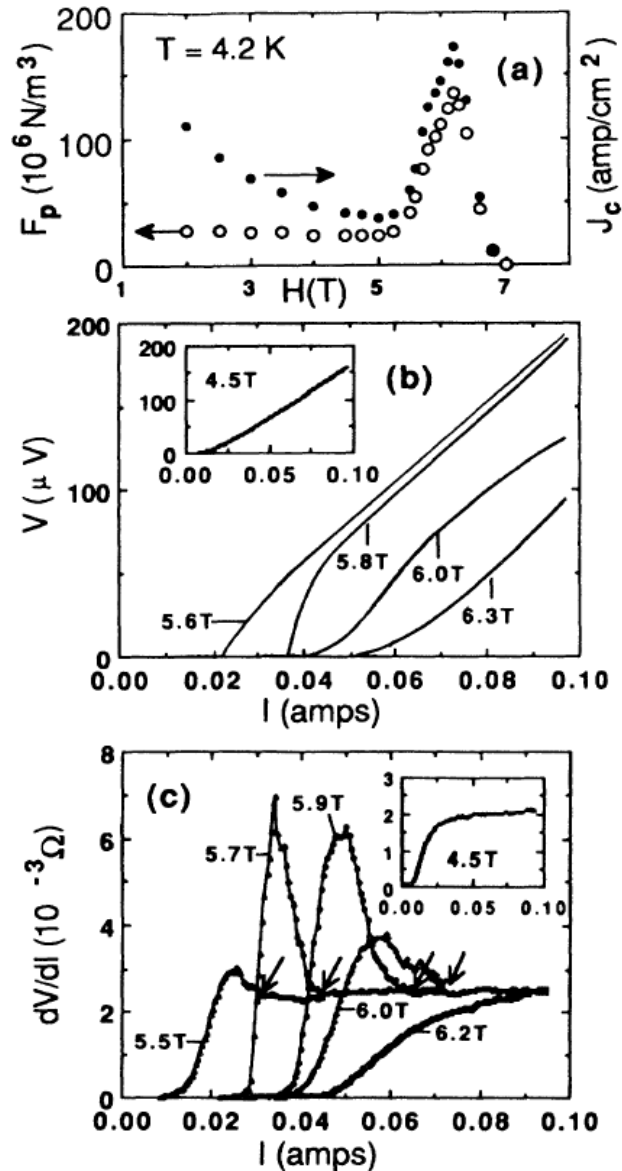


Figure 9. (a) The experimentally measured depinning force F_p (open circles) and critical current J_c (filled circles) versus magnetic field H for vortices in a superconducting sample of 2H-NbSe₂. There is a peak in the pinning force as a function of field. Here J_c corresponds to the critical depinning threshold F_c , while the vortex density increases with increasing H . (b) Voltage V vs current I curves obtained at different magnetic field values (labeled) show a change in the shape of the curves across the peak effect. The voltage corresponds to the vortex velocity V , while the current corresponds to the driving force F_D . (c) The corresponding dV/dI curves, which are proportional to dV/dF_D curves, obtained at different magnetic field values (labeled) each exhibit a spike due to the S-shape of the velocity-force curves. This spike reaches its largest magnitude near the apex of the peak effect. The inset shows that at lower fields below the peak effect, the dV/dI curve does not contain a spike. Reprinted with permission from S. Bhattacharya and M.J. Higgins, Phys. Rev. Lett. **70**, 2617 (1993). Copyright 1993 by the American Physical Society.

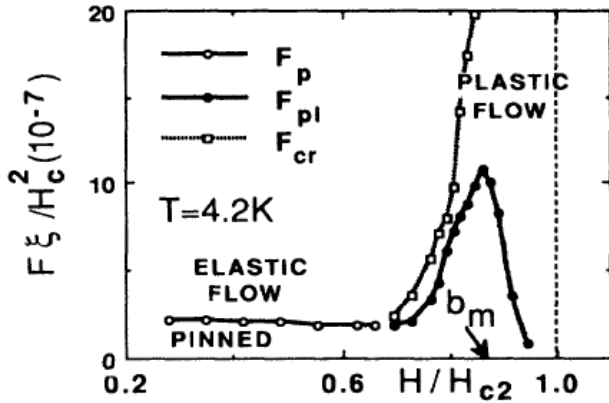


Figure 10. Experimentally measured dynamic phase diagram as a function of the effective applied driving force $F\xi/H_{c2}^2$, which corresponds to F_D , vs magnetic field H/H_{c2} , which corresponds to the vortex density, from the 2H-NbSe₂ sample in figure 9. Below the peak effect there is an elastic depinning transition F_p from a pinned state to elastic flow (open circles). As the peak effect is approached, the depinning becomes plastic, as indicated by the F_{pl} line (filled circles), and there is a higher drive transition from plastic flow to a dynamically reordered elastic flow state, indicated by the F_{cr} line (open squares). Both F_p and F_{pl} correspond to the depinning threshold F_c . Reprinted with permission from S. Bhattacharya and M.J. Higgins, Phys. Rev. Lett. **70**, 2617 (1993). Copyright 1993 by the American Physical Society.

peak of the peak effect where plastic flow is believed to occur. It was proposed that when the vortex lattice depins elastically, dV/dF_D saturates to a constant value and exhibits no spike feature, whereas when the vortex lattice depins plastically, the vortex structure is initially strongly disordered but dynamically orders at higher drives into a defect free structure, producing a spike in the dV/dF_D curve [21]. According to this interpretation, the change in the velocity-force curves reflects a transition from elastic to plastic depinning and also provides evidence for a dynamical transition from plastic flow to a moving ordered structure at higher drives. Figure 10 shows the proposed dynamic phase diagram for this scenario. At magnetic fields below the peak effect, the vortex lattice is ordered and depins elastically directly to a moving ordered state, marked in the figure as elastic flow. The peak effect coincides with a transition from a pinned ordered lattice to a disordered pinned structure that depins plastically and dynamically reorders at higher drives. As H_{c2} is approached, the drive at which the dynamical reordering occurs diverges.

A change from elastic to plastic depinning at the peak effect is consistent with the experimental observations, but the reason for this change must be explained. One argument invokes the increase in the size of the London penetration depth λ as H_{c2} is approached. Since the vortex-vortex interaction strength is controlled by gradients in the local magnetic

field, as λ increases these gradients become smaller and the vortex-vortex interactions become weaker. When the vortex-vortex interactions are weak enough, dislocations can proliferate in the vortex lattice, destroy the triangular ordering, and cause a transition to plastic depinning. In the elastic regime, when the stiff triangular lattice formed by the vortices interacts with randomly placed pinning sites, it is too energetically costly for the vortices to deform their triangular lattice in order to take advantage of the pinning energy, so many of the pinning sites remain unoccupied and therefore ineffective. Once dislocations appear in the vortex lattice, however, the softened or amorphous lattice can deform easily in order to allow vortices to sit in the disordered pinning sites, so that a much higher fraction of the pinning sites are occupied and the effectiveness of the pinning increases dramatically. In other words, the stiffer triangular vortex lattice couples to the substrate more weakly than the softer amorphous vortex structure. One analogy that has been used to describe why elastic depinning occurs at a lower driving force than plastic depinning is that the elastic depinning process is akin to the easy motion of a stiff solid such as an ice cube over a carpet, while the plastic depinning process is like attempting to move a soft solid such as a gelatin cube over a carpet. The soft solid easily adjusts to fit in the asperities of the carpet and can be moved only with difficulty [76].

The idea that softer systems are more strongly coupled to the pinning substrate applies only when the number of pinning sites is greater than or equal to the number of particles in the system. For example, consider a substrate composed of a flat surface decorated by a small number of well-defined pinning sites that can each capture no more than a single vortex. When there are more vortices than pinning sites, some of the vortices have no pinning site available in which to sit and are confined only by the vortex-vortex interaction force from their neighbors. These interstitial vortices can still be effectively pinned if enough of their neighbors are directly pinned; however, the strength of this interstitial pinning depends on the shear modulus of the vortex lattice and not merely on the strength of the pinning sites. In a stiff elastic vortex lattice, the strong shear modulus makes it difficult or impossible to depin the interstitial vortices separately from the vortices in the pinning sites, leading to an elastic depinning transition. If the vortex-vortex interactions are weakened substantially, then the interstitial vortices can be depinned at lower drives than the vortices in the pinning sites, resulting in a plastic depinning transition. In simulations of 2D systems containing a small number of pinning sites, when the vortex interactions are modified in order to

tune the shear modulus from a high value to a low value, a very high shear modulus results in a low depinning threshold as the stiff vortex lattice depins elastically, while for a reduced shear modulus the depinning threshold increases and reaches a maximum at the onset of plastic depinning [77]. For even smaller shear modulus values, the depinning threshold decreases again when the vortices at the pinning sites are no longer able to exert a confining force on the interstitial vortices [77]. It is not clear whether this model can be applied to the experimentally observed peak effect in superconducting systems since the number of intrinsic pinning sites is generally at least as large as if not greater than the number of vortices, which would imply that the pinning force should be maximal for low or zero shear modulus [78].

3.2. Dynamical ordering transitions

It was first noted in neutron scattering experiments by Thorel *et al.* that vortices can exhibit increased ordering in the moving state [79], while 2D vortex simulations by Shi and Berlinsky showed that the number of topological defects in the vortex lattice decreases with increasing drive [80]. Koshelev and Vinokur (KV) performed 2D simulations of vortices driven over random pinning and mapped out a dynamic phase diagram containing a pinned phase, a plastic flow phase characterized by a highly defected vortex lattice, and a dynamically ordered phase at high drives where the vortices form a sixfold ordered structure [47]. These simulations also included a thermal fluctuation force, and showed that in the absence of pinning, there is a bulk melting temperature T_m above which the vortices lose their sixfold ordering. In the presence of pinning, as the temperature T increases toward T_m , the depinning threshold F_c decreases while the driving force at which dynamical reordering occurs shifts to higher drives, with a divergence near T_m . The divergence of the reordering force at the point at which the flow becomes liquidlike or plastic is similar to the divergence observed in the experimentally determined dynamic phase diagram of Bhattacharya and Higgins shown in figure 10 [21]; however, the transition observed by KV [47] occurs as a function of temperature rather than as a function of magnetic field. Additionally, there is no peak in the depinning threshold in the simulation studies since the thermal fluctuations monotonically reduce F_c . This work does, however, provide further evidence that there are at least three generic dynamic phases in driven vortex systems with disorder: pinned, plastic flow, and elastic flow, with transitions between these states. KV argued that vortices moving over a random landscape experience dynamical fluctuations induced by the pinning that can be treated as an effective shaking

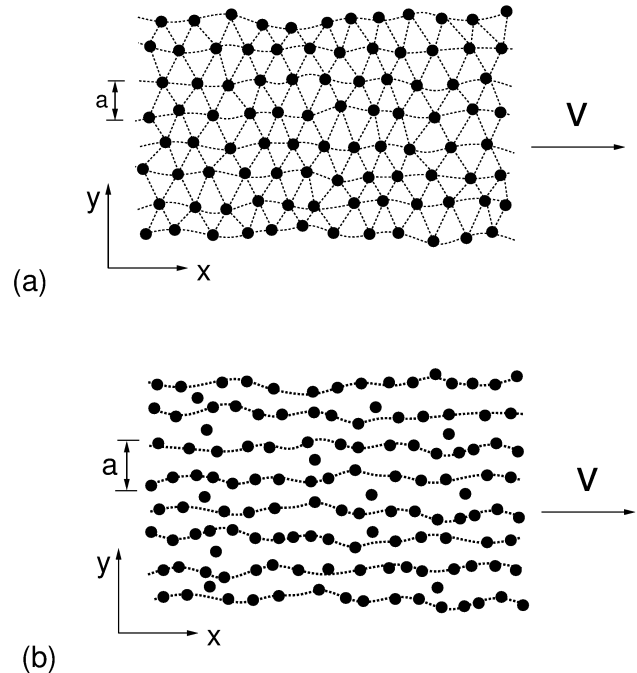


Figure 11. Schematic illustrations of two possible moving states for a lattice of particles driven along the x direction. (a) The moving Bragg glass, which contains no dislocations. (b) A moving smectic state, which is periodic transverse to the driving direction but has liquid order along the driving direction. Reprinted with permission from L. Balents, M.C. Marchetti, and L. Radzihovsky, *Phys. Rev. B* **57**, 7705 (1998). Copyright 1998 by the American Physical Society.

temperature T_{sh} , so that when the combination of the bulk temperature T and T_{sh} are greater than or equal to T_m , the system is in a disordered plastic flow phase. As F_D increases, T_{sh} decreases since the vortices are moving too rapidly to respond to the perturbations induced by the pinning sites, and using analytical arguments KV find $T_{sh} \propto 1/F_D$. The vortices dynamically order when $T + T_{sh} < T_m$, which explains the divergence in the driving force at which dynamic reordering occurs as T approaches T_m . Several further experiments and simulations also find similar evidence for three dynamical phases [52, 56, 81, 82, 83, 84, 87, 88].

It is interesting to ask whether there are different kinds of plastic flow or different dynamically ordered moving phases. In some ways the dynamically ordered phase is easier to address, since if it has some crystalline properties, then the presence or absence of certain symmetries can be used to distinguish different ordered moving phases. Giamarchi and Le Doussal argued that in the moving phase, the pinning-induced shaking temperature is anisotropic rather than isotropic, so that the dynamically ordered state is not a moving crystal but a moving anisotropic Bragg glass [51]. A Bragg glass is an equilibrium glass state that

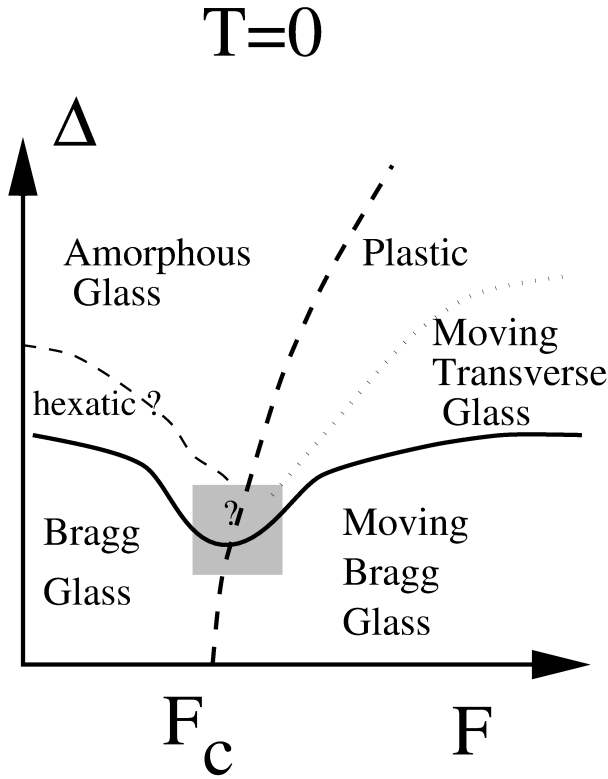


Figure 12. Schematic dynamic phase diagram as a function of disorder strength Δ versus driving force F for $d = 3$ dimensions. Δ corresponds to the pinning force F_p , while F corresponds to the driving force F_D . The heavy dashed line is a depinning transition. The behavior in the shaded square region is unclear. An interesting possibility would be a direct depinning of a hexatic into the moving transverse glass, but other scenarios are possible. Reprinted with permission from P. Le Doussal and T. Giamarchi, *Phys. Rev. B* **57**, 11356 (1998). Copyright 1998 by the American Physical Society.

arises for systems with quenched disorder in which there are no dislocations present [89]. Within the moving Bragg glass phase, the flow consists of vortices traveling in coupled channels, and if an additional driving force is applied perpendicular to the original driving force, there is a finite transverse depinning threshold [51]. In the moving frame, the transverse depinning threshold can be viewed as an effective pinning force in the direction perpendicular to the channel direction that is experienced by the moving vortex channels, each of which acts like an elastic object. In further theoretical studies, it was argued that the anisotropy of the shaking temperature is strong enough that it produces dislocations in the vortex lattice, destroying the Bragg glass state, but that these dislocations are aligned by the driving force, producing a moving smectic phase illustrated schematically in figure 11 that has long range or quasi-long range order transverse to the driving direction but short range order parallel to the driving direction

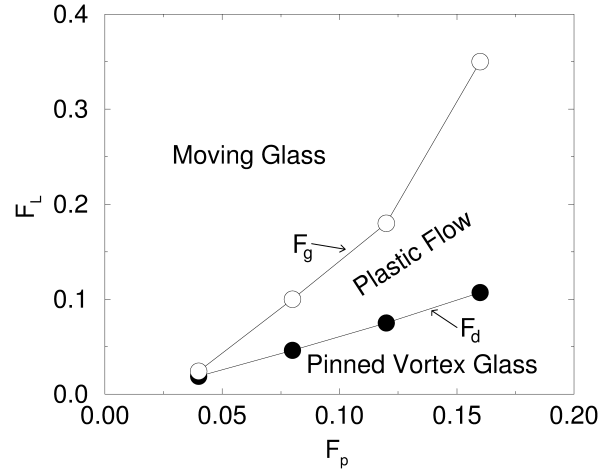


Figure 13. The dynamic phase diagram from simulations of a 2D vortex system for driving force F_L vs pinning force F_p highlighting a pinned phase, plastic flow phase, and a dynamical partially ordered moving glass phase. Filled circles are the depinning line F_d , corresponding to F_c , while the open circles indicate the dynamical reordering transition. Here F_L corresponds to the driving force F_D . Reprinted with permission from K. Moon, R.T. Scalettar, and G.T. Zimányi, *Phys. Rev. Lett.* **77**, 2778 (1996). Copyright 1996 by the American Physical Society.

[53, 54]. Such a smectic phase would be generic to 2D systems. Giamarchi and Le Doussal then proposed that the moving anisotropic Bragg glass and moving smectic phase are different regimes of the same system [55], as shown in the schematic phase diagram of figure 12 as a function of disorder strength versus driving force. At low disorder strengths the system forms a dislocation-free Bragg glass that depins elastically into a moving Bragg glass. At higher disorder strength there is a transition from a Bragg glass to an amorphous glass phase that depins plastically and then dynamically reorders into a moving smectic, also termed a moving transverse glass. It is possible that a pinned hexatic phase could exist between the pinned Bragg glass and the pinned amorphous glass [89].

Using Bitter decoration experiments, Pardo *et al.* found direct evidence for a moving smectic phase as well as a weaker pinning regime in which only an anisotropic crystal appears [90], while other imaging experiments show ordered vortices moving along coupled 1D channels [91]. Additional theoretical works and simulations also provide evidence of moving crystal phases and smectic phases [52, 83, 38, 92, 93, 94, 95, 96]. In other studies, a transverse depinning threshold is observed in the moving crystal or smectic phase, but is absent in the plastic flow phase when the system acts like a liquid [52, 83, 38, 97, 98, 99]. In figure 13, the dynamical phase diagram of driving force

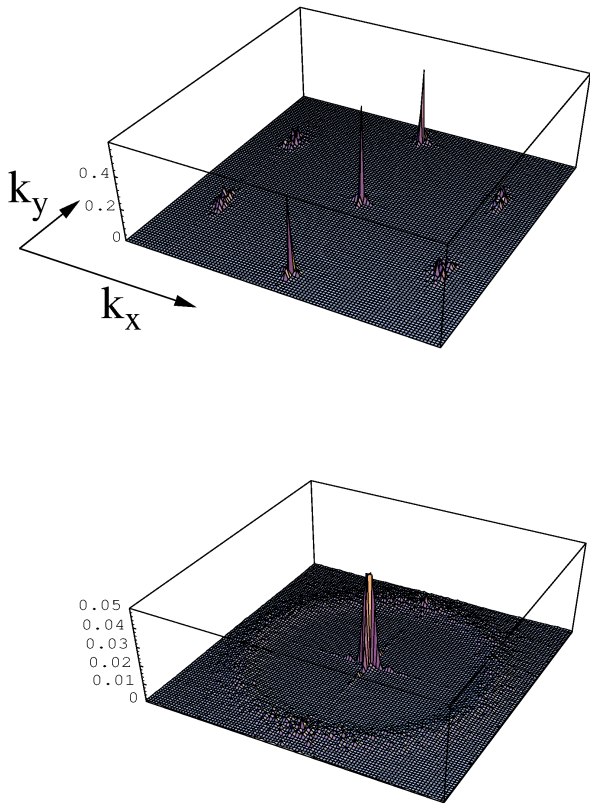


Figure 14. The structure factor $S(\mathbf{k})$ from the system in figure 13 at a pinning strength of $F_p = 0.16$. Upper panel: At a driving force of $F_L = 0.6$ in the dynamically ordered phase, there are two peaks indicative of a smectic structure. Lower panel: At $F_L = 0.2$ in the plastic flow phase, there is a ring shape indicative of a liquid or amorphous structure. Here F_L corresponds to the driving force F_D . Reprinted with permission from K. Moon, R.T. Scalettar, and G.T. Zimányi, Phys. Rev. Lett. **77**, 2778 (1996). Copyright 1996 by the American Physical Society.

versus pinning strength from 2D simulations of Moon *et al.* [52] contains a pinned vortex phase, a plastic flow phase, and a moving ordered phase or moving glass. The lines on the phase diagram are determined from velocity-force curve measurements as well as changes in the structure factor

$$S(\mathbf{k}) = \frac{1}{N} \left| \sum_i^N \exp(-i\mathbf{k} \cdot \mathbf{R}_i) \right|^2. \quad (5)$$

In the plastic phase, $S(\mathbf{k})$ has a ringlike structure indicative of glass or liquid ordering, as shown in the lower panel of figure 14, while in the dynamically ordered phase, the upper panel of figure 14 shows that the ring structure is replaced by two peaks indicative of a moving smectic phase. If a true moving crystal had formed, $S(\mathbf{k})$ would contain six

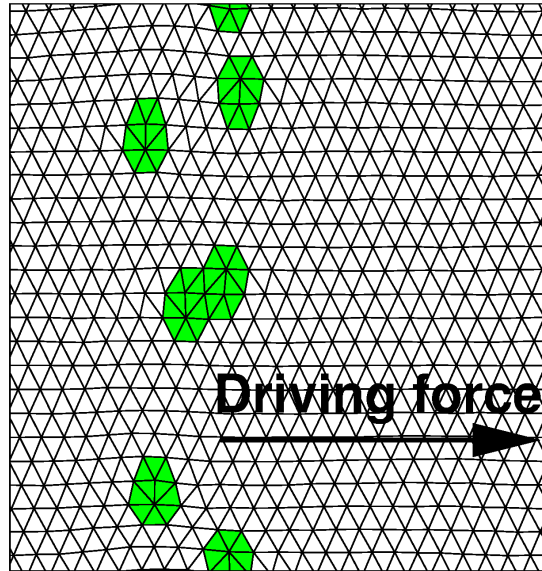


Figure 15. Alignment of dislocations in a coherently moving smectic phase from a 2D vortex simulation. White regions contain sixfold coordinated vortices while green regions contain fivefold or sevenfold coordinated vortices. Reprinted with permission from H. Fangohr, S.J. Cox, and P.A.J. de Groot, Phys. Rev. B **64**, 064505 (2001). Copyright 2001 by the American Physical Society.

peaks of equal weight. An example of aligned dislocation structures in the moving smectic phase from 2D vortex simulations appears in figure 15. Fivefold and sevenfold coordinated dislocations in the sixfold coordinated lattice pair up with each other and preferentially align so that they can glide along the driving force direction [84]. Moon *et al.* also identified several aligned dislocations in the smectic state [52].

The exact nature of the moving phase, and whether it forms a true smectic structure or a moving dislocation-free Bragg glass, depends on the dimensionality of the system and the strength of the disorder. Olson *et al.* performed 2D simulations of vortices interacting with random pinning arrangements in which there were more pinning sites than vortices, and tuned the strength A_v of the vortex-vortex interactions or the effective shear modulus from zero to high values [93], obtaining the velocity-force curves shown in the inset of figure 16(a). As A_v increases, the depinning threshold F_c decreases. The main panel of figure 16(a) shows that the corresponding dV/dF_D curves have a peak at the depinning threshold which increases in size with decreasing A_v , and that for high drives all of the dV/dF_D curves saturate to the same constant value. Figure 16(c) shows the fraction P_6 of sixfold coordinated vortices versus F_D . To measure P_6 , the coordination number z_i of each vortex is obtained by performing a Voronoi construction [85], and taking

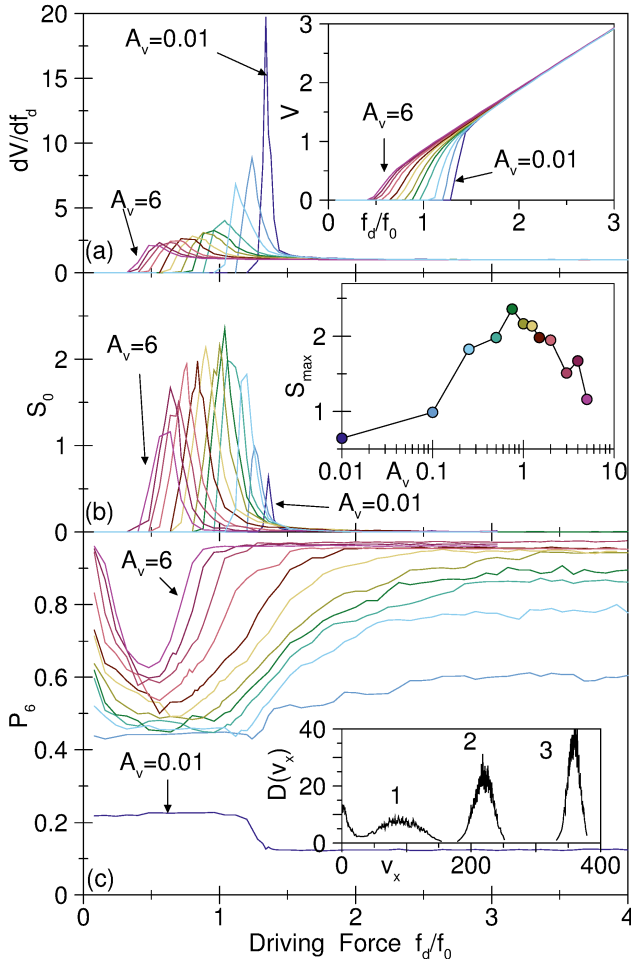


Figure 16. (a) Inset: Velocity V vs driving force f_d/f_0 curves from 2D simulations of vortices moving over a disordered substrate as the vortex-vortex interaction strength A_v , or effective shear modulus, is varied from $A_v = 6$ to $A_v = 0.01$. Main panel: dV/df_d vs driving force f_d/f_0 . (b) The corresponding velocity noise power S_0 vs f_d/f_0 . The inset shows the maximum value S_{\max} of S_0 for each value of A_v . (c) The fraction of six-fold coordinated vortices P_6 vs f_d/f_0 for varied A_v , showing that above depinning, P_6 increases with increasing f_d/f_0 . Here f_d/f_0 corresponds to the driving force F_D and dV/df_d corresponds to dV/dF_D . Reprinted with permission from C.J. Olson, C. Reichhardt, and F. Nori, Phys. Rev. Lett. **81**, 3757 (1998). Copyright 1998 by the American Physical Society.

$P_6 = N^{-1} \sum_i \delta(z_i - 6)$. For a perfect triangular lattice, $P_6 = 1.0$. In these simulations, the vortices are initialized in a triangular lattice, so that as the driving force is increased in the pinned state, short-lived vortex rearrangements or avalanches occur that cause P_6 to drop with increasing F_D until it reaches a minimum value at the depinning threshold. Above depinning, P_6 gradually increases with increasing drive, reaching a value of nearly 1.0 for the larger values of A_v where the vortex lattice is fairly stiff, but saturating to a value significantly lower than 1.0 for lower values of A_v , indicating that numerous dislocations persist in

the dynamically reordered state. The power spectrum of the time series of the vortex velocity fluctuations $V(t)$ is obtained from

$$S(\omega) = \left| \int V(t) e^{-i2\pi\omega t} dt \right|^2. \quad (6)$$

Figure 16(b) shows the noise power S_0 [86], obtained by integrating $S(\omega)$ over a fixed frequency range, $S_0 = \int_{\omega_2}^{\omega_1} df S(\omega)$. In the plastic flow phase, $S(\omega)$ has the form $S(\omega) \propto 1/f^\alpha$ with $\alpha = 1.5$ to 2.0, indicating the existence of large noise power at low frequencies due to the slowly changing plastic flow channel structure similar to that illustrated in figure 1(a). At higher drives the spectrum becomes white with $\alpha = 0$ or develops a peak at a single frequency, corresponding to narrow band noise, and this coincides with a drop in S_0 and the saturation of P_6 to its highest dynamically ordered value. The inset of figure 16(b) shows the maximum value S_{\max} reached by S_0 across all driving forces as a function of A_v . At higher A_v , the noise power is small since there are few defects in the system, while for small A_v when the depinning threshold is highest, the noise power is also small due to the loss of collective vortex-vortex interaction effects which are needed in order to produce large-scale velocity fluctuations.

A dynamic phase diagram as a function of A_v versus F_D constructed from the simulation measurements appears in figure 17. The width of the pinned phase decreases as A_v increases since a stiffer system is not as well pinned by random disorder. The open circles and crosses indicate the locations of the peaks in the noise power and dV/dF_D curves, respectively. For $A_v < 1.0$, the system depins into a plastic flow phase and then reorders into a moving phase in which the dislocations have their Burgers vectors aligned perpendicular to the driving direction, forming a smectic structure in which $S(\mathbf{k})$ contains only two prominent peaks. For $A_v > 1.0$, after the vortices depin plastically and dynamically reorder into a smectic state, at higher drives a second dynamical reordering occurs into a defect-free anisotropic crystal with six peaks in $S(\mathbf{k})$. The drive at which the vortices dynamically reorder into the crystalline state diverges as A_v decreases. Inset (A) of figure 17 shows a representative velocity noise power spectrum $S(\omega)$ obtained in the plastic flow phase, where $1/f^{1.5}$ noise appears, while in inset (B) of figure 17, $S(\omega)$ in the moving crystal phase has a washboard character with a narrow band noise peak. These results indicate that noise fluctuations can serve as another powerful tool for examining transitions between plastic and dynamically ordered phases. In Section 4 we provide a further discussion of noise measurements for nonequilibrium states.

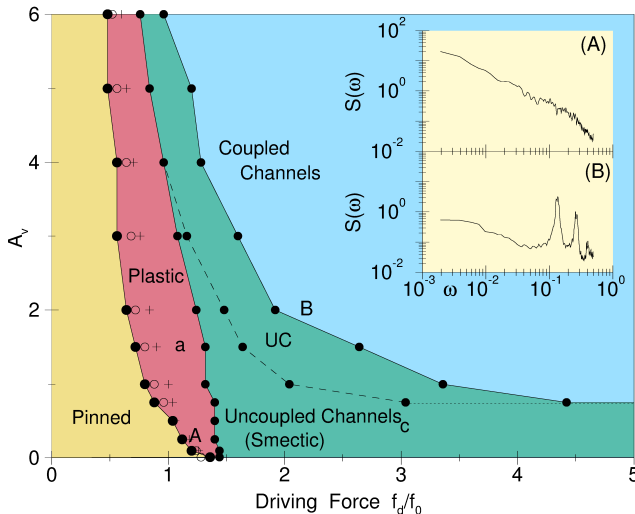


Figure 17. The dynamic phase diagram for the system in figure 16 as a function of vortex-vortex interaction strength A_v vs driving force f_d/f_0 , showing a pinned phase, plastic phase, uncoupled channel (UC) phase, and coupled channel or moving lattice phase. Here f_d/f_0 corresponds to the driving force F_D and A_v is an effective shear modulus. The open circles and crosses indicate the locations of the peaks in the noise power and dV/dF_D curves, respectively. Inset (A) shows the velocity noise power spectrum $S(\omega)$ obtained in the plastic flow phase at the point marked A at $A_v = 1.0$, where there is $1/f^\alpha$ noise. Inset (B) shows $S(\omega)$ obtained in the coupled channel phase at the point marked B at $A_v = 2.0$ where there is a narrow band noise signal. Adapted with permission from C.J. Olson, C. Reichhardt, and F. Nori, Phys. Rev. Lett. **81**, 3757 (1998). Copyright 1998 by the American Physical Society.

In 2D systems such as these, finite size effects can arise. If a sufficiently large system were simulated, it is possible that some aligned dislocations would appear in what is labeled a moving crystal state in figure 17, indicating that the moving crystal or coupled channel phase is actually smectic at large scales. If this is the case, the moving smectic would exhibit another length scale in the form of the average spacing between dislocations. This length scale is controlled by the ratio of the vortex-vortex interaction strength to the vortex-pinning interaction strength. Thus, it is possible to form a strong smectic in which each flowing channel of vortices contains numerous dislocations separated by distances of the order of a few lattice constants, as well as a weak smectic in which large groups of channels are coupled and the dislocations are separated by hundreds or thousands of lattice constants. Such finite size effects could impact the results of Pardo *et al.* [90], where the observation of a moving crystal phase rather than a moving smectic phase could indicate that the length scale at which dislocations appear was larger than the region over which the experimental images were obtained.

Despite the large number of studies on dynamical reordering in 2D vortex systems, there are still many

open questions. The distances between the aligned dislocations in the smectic phase may depend on the drive and on the disorder strength, and might exhibit additional divergences. The nature of the dynamical reordering transition is unknown. It might be similar to an equilibrium freezing transition; alternatively, it might be better understood as a type of absorbing phase transition similar to directed percolation, as described in Section 12. There could be a true transition between the moving smectic and moving crystal phases, and if so, the nature of this transition is also unknown. Additional transitions between different phases could occur, such as anisotropic plastic to moving nematic to moving smectic to moving crystal, and methods would need to be identified to distinguish between these phases if they are truly distinct phases. If the disorder is very weak, it is possible that only a moving floating crystal could occur, with the effects of the pinning vanishing completely; alternatively, it is possible that the pinning effects never completely disappear. There are also some studies that find that the orientation of the mostly triangular dynamically ordered moving state can rotate as a function of driving force, but the exact reason for this rotation has not yet been identified; it could be due to extra dissipation created by additional modes of motion of the vortex core [100].

4. Depinning and First Order Dynamical Phase Transitions in 3D Systems

Most of the results in Section 3 were obtained in 2D or effectively 2D systems, where the depinning and dynamic reordering transitions are generally continuous or second order in nature. In this Section we discuss systems in which some of these transitions are sharper or first order in character. Transitions of this type can occur in overdamped 3D vortex systems and in 2D layered systems with geometries similar to those illustrated in figure 3. First order behavior can also arise in systems containing inertia or stress overshoot effects.

The system in which 3D depinning and dynamic effects have been most extensively studied is vortices in type-II superconductors. The vortices are line-like objects, and in the limit where the lines are stiff, the 2D approximation of their behavior described in Section 3 works well; however, there are many superconducting systems that are strongly anisotropic or contain a series of superconducting layers, and in these systems the vortex lines can break up or decouple along the direction of the applied magnetic field [1]. Even for isotropic 3D superconductors or only weakly anisotropic superconductors, near T_c or H_{c2} the vortex lines may become soft enough to break up along their

length in the presence of strong pinning. Thus, an important question is how the dynamics of interacting vortices changes when plasticity is allowed to occur in the third direction.

There are numerous features observed in real superconductors, particularly near the peak effect, that have not been successfully captured in 2D simulations. In general, 2D simulations show that as the vortex-vortex interactions weaken relative to the vortex-pinning interactions, the critical depinning threshold increases gradually [52, 87, 96, 101, 102], while in many experiments, the increase in F_c is usually much sharper. Paltiel *et al.* [103] showed that the onset of the peak effect in 2H-NbSe₂ is very sharp when edge contamination effects are removed, and argued that the vortex order-to-disorder transition associated with the peak effect is a first order transition [104]. Near the peak effect, strong hysteresis in the velocity-force curves is commonly observed [105, 106, 107] along with a variety of memory effects [108, 109, 110, 111, 112], indicating the presence of metastability which is consistent with an underlying first order phase transition. Imaging experiments reveal the coexistence of ordered and disordered pinned phases separated by sharp, well defined boundaries, lending support to the first-order nature of the order-disorder transition [113]. In 3D strongly layered superconducting systems, it is generally agreed that the 3D to 2D decoupling or melting transition is first order [114]. The fact that 2D simulations do not produce many of these features is consistent with the idea that isotropic 2D systems of the type illustrated in figure 1(a,b) generally do not exhibit sharp transitions. The melting transitions in most 2D systems are continuous, taking the form of either a Kosterlitz-Thouless transition, a second order transition, or at most a weak first order transition, while when random disorder is added to 2D systems, it becomes even less likely that first order transitions can occur [115].

The question is whether driven 3D systems in the presence of random disorder exhibit transitions that are first or second order in nature, and whether these features are consistent with what is observed in vortex experiments. Most theoretical and simulation work has focused on 3D elastic line models or 3D layered models of the type illustrated in figure 3(b,c). In 3D elastic line models, the vortices can exhibit plasticity in the $x-y$ plane perpendicular to their length, but not along the z direction parallel to their length. One issue with such elastic models is how to treat the behavior when the line wandering along the z -direction becomes large enough that crossing or entanglement of the lines can occur. The vortex lines can be modeled as unbreakable objects like directed polymers that cannot pass through each other, or they can be allowed to cross

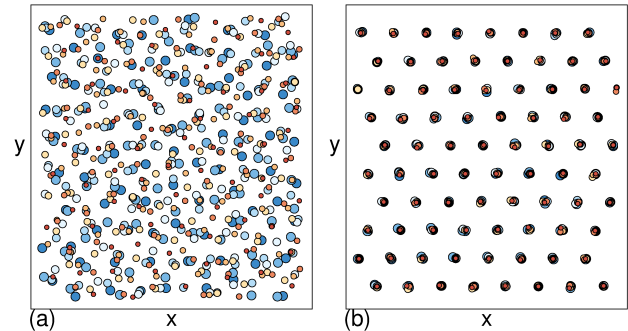


Figure 18. Top view of a simulation of a 3D layered system of magnetically interacting vortices in the presence of pinning in the form of random point defects. Circles are the vortices in each layer, with different colors and sizes indicating the different layers; the pinning sites are not shown. (a) A disordered phase in which the vortices are decoupled and move independently in each layer. (b) An ordered state in which the vortices are aligned in the z direction and form a triangular lattice in the $x-y$ plane. Adapted with permission from C.J. Olson, C. Reichhardt, and V.M. Vinokur, *Phys. Rev. B* **64**, 140502(R) (2001). Copyright 2001 by the American Physical Society.

each other with line breaking and reconnection taken into account. An alternative 3D model consists of coupled planes that each contain a fixed number of 2D vortices called pancake vortices [116]. Each pancake vortex has a repulsive interaction with vortices in the same layer but experiences an attraction to vortices in adjacent layers. In this model, the 2D vortices can stack up into 3D line-like objects but can also undergo decoupling transitions in which the line-like object breaks apart and the vortices move independently in each layer.

4.1. Depinning and dynamical phase transitions

Simulations of 3D elastic lattice line models show that dynamical ordering can occur between a plastic flow state and a moving crystal; however, a first order or peak effect transition is not observed [117, 118], suggesting that some form of 3D plasticity or line breaking that is neglected by the models must be important in the experimental systems. Olson *et al.* considered a 3D layered model of magnetically interacting vortices as illustrated in figure 18(b), which shows a top view of the system in which the vortices in $N_L = 8$ layers are aligned with each other along the z axis and form a triangular lattice in the $x-y$ plane [119]. In the absence of pinning and as a function of temperature, this model shows a single first order melting transition where the lines break up into decoupled layers similar to those shown in figure 18(a). At $T = 0$ it also shows a first order transition as a function of increasing pinning strength from a 3D ordered state to a 2D disordered decoupled state. For weak pinning under an applied drive F_D , the

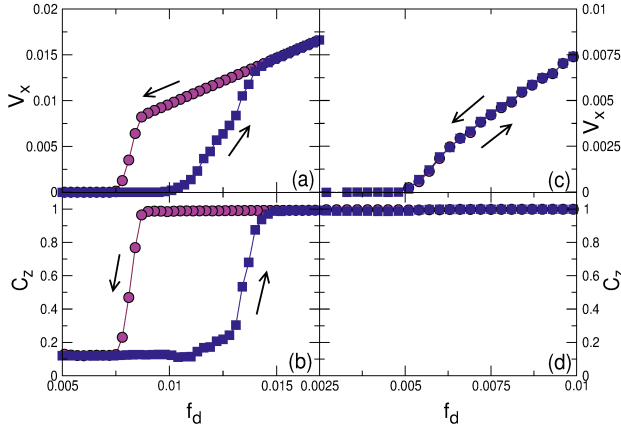


Figure 19. (a) Average vortex velocity V_x in the driving direction vs driving force f_d in the disordered decoupled phase for simulations of the 3D layered system in figure 18(a). The vortices depin plastically and dynamically reorder at higher drives. Strong hysteresis is present for sweeping the drive up (blue squares) and down (red circles), indicative of behavior that is first order in nature. (b) C_z vs f_d . The quantity C_z measures the correlations of the vortex lines along the z direction, $C_z = 1 - \langle (2R_z/a_0)\Theta(a_0/2 - R_z) \rangle$ where $R_z = |\mathbf{R}_{i,l} - \mathbf{R}_{i,l+1}|$, $\mathbf{R}_{i,l}$ is the location of vortex i in layer l , a_0 is the vortex lattice constant, Θ is the Heaviside step function, and the average is performed over all vortices in neighboring layers. Below depinning and for low drives, C_z is small, and at higher drives there is a dynamical transition into an ordered 3D solid. (c) V_x vs f_d curves for the ordered 3D solid illustrated in figure 18(b). The depinning is elastic and there is no hysteresis in the velocity response. (d) C_z vs f_d for the ordered 3D solid also shows no hysteresis. Here V_x corresponds to the velocity V and f_d corresponds to the driving force F_D . Adapted with permission from C.J. Olson, C. Reichhardt, and V.M. Vinokur, Phys. Rev. B **64**, 140502(R) (2001). Copyright 2001 by the American Physical Society.

3D ordered system depins elastically into a moving 3D line solid, and there is no hysteresis in the velocity-force curves, as shown in figure 19(c). In both the pinned and moving phase, a measure C_z of the correlations of the vortex lines along the z direction gives $C_z = 1.0$, as shown in figure 19(d). The lack of hysteresis or any discontinuous behavior upon sweeping the driving current up and down suggests that elastic depinning in this 3D system is a continuous transition; however, a scaling analysis of the velocity-force curves has not been performed. When the strength of the pinning is increased or the effective vortex-vortex coupling between layers is reduced by thermal effects or other means, then the pinned state is no longer a 3D ordered state but is instead a disordered decoupled 2D state of the type illustrated in figure 18(a). This decoupled 2D state depins plastically, as shown in figure 19(a), and at higher drives the system exhibits a sharp transition into a moving 3D ordered solid, as indicated by the abrupt increase of C_z from a low value to $C_z = 1.0$ within the moving phase in figure 19(b). Both the velocity-force curves and C_z are strongly hysteretic

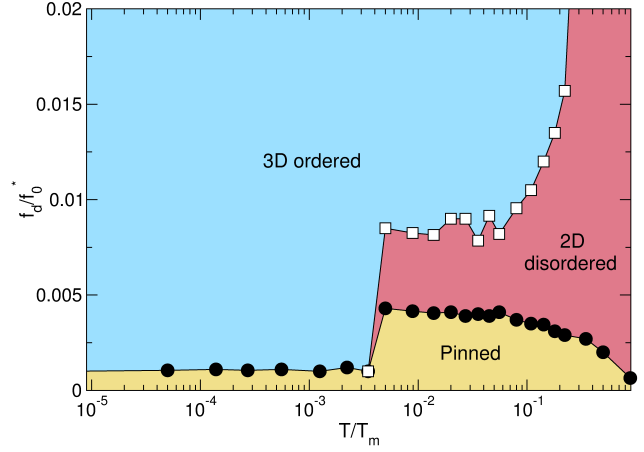


Figure 20. The simulated dynamic phase diagram as a function of f_d/f_0 vs temperature T/T_m for the 3D magnetically coupled layered vortex system shown in figures 18 and 19 with weak pinning. T_m is the melting temperature and f_d/f_0 corresponds to the driving force F_D . Black circles indicate the depinning threshold F_c , while white squares show the dynamical reordering line. At low T , the 3D solid depins elastically as shown in figure 19(c,d), while at higher T there is a transition to a pinned 2D disordered state that depins plastically and undergoes a first order dynamical transition into a moving 3D solid at higher drives, as shown in figure 19(a,b). There is a sharp increase in the depinning threshold at the transition from the 3D ordered pinned state to the 2D decoupled pinned state. Adapted with permission from C.J. Olson, C. Reichhardt, and V.M. Vinokur, Phys. Rev. B **64**, 140502(R) (2001). Copyright 2001 by the American Physical Society.

upon sweeping the drive up and down, with the coupled 3D ordered state persisting down to much lower drives during the decreasing drive sweep. The net vortex velocity in the 3D ordered phase is higher than in the 2D decoupled phase, indicating that the pinning is less effective for the 3D ordered state.

Figure 20 shows the dynamic phase diagram for the 3D layered vortex system from Figures 18 and 19 with weak pinning as a function of F_D versus temperature T/T_m , where T_m is the melting temperature of the clean system. At low T the vortices depin elastically from a 3D pinned state to a moving 3D solid, while at higher T there is a first order transition within the pinned state to a disordered 2D state which is associated with a sharp increase in the depinning threshold F_c . From the 2D disordered state, the vortices depin plastically and at higher drive undergo a first order dynamical transition into an ordered 3D moving solid. The driving force at which the dynamical ordering occurs shows a divergence as T approaches T_m from below, similar to the behavior observed in the 2D simulations of Koshelev and Vinokur [47]. As T is further increased, the depinning threshold decreases since 2D vortices can be easily thermally depinned. These results show that many of the features observed experimentally in the peak effect regime, including a

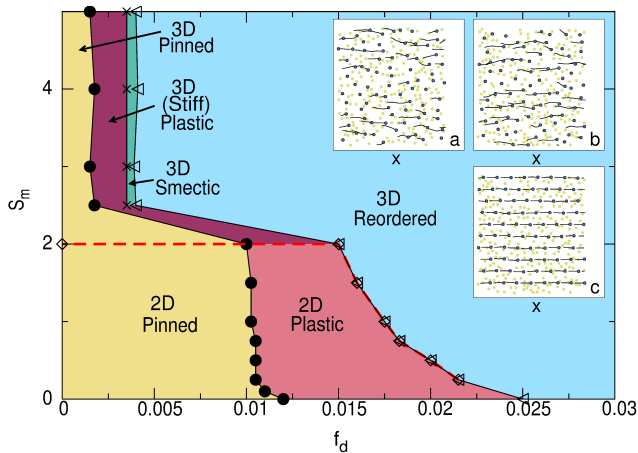


Figure 21. Simulated dynamic phase diagram as a function of interlayer coupling strength S_m vs driving force f_d for $T = 0$ for the 3D magnetically coupled layered vortex system shown in figures 18 to 20 with weak pinning. There is a first order phase transition, indicated by the dashed red line, from a 3D ordered solid into a 2D disordered decoupled phase. The other phases are plastic flow of stiff 3D lines, a 3D smectic phase, a 3D dynamically reordered phase, and a 2D disordered plastic flow phase. Insets (a) and (b) show the top and bottom layer, respectively, of the pinning sites (green dots), vortex positions (blue dots) and trajectories (lines) in the 2D plastic flow phase, while inset (c) illustrates one layer of the 3D ordered moving phase. Here f_d corresponds to the driving force F_D . Adapted with permission from C.J. Olson, G.T. Zimányi, A.B. Kolton, and N. Grønbech-Jensen, Phys. Rev. Lett. **85**, 5416 (2000). Copyright 2000 by the American Physical Society.

first-order transition from a pinned elastic solid to a pinned disordered solid and a discontinuous dynamical ordering transition, can be captured by a 3D model that allows plasticity in the z -direction.

Other numerical studies of the same 3D layered vortex model at $T = 0$ focused on the effect of modifying the strength of the interlayer coupling S_m [120]. Figure 21 shows a dynamical phase diagram for this model as a function of S_m versus F_D at a fixed pinning strength. For strong interlayer coupling $S_m > 2.0$, the system forms a 3D ordered pinned state that depins into a 3D plastic flow state in which the vortices form stiff lines that can flow plastically around each other in the $x - y$ plane. At higher drives there is a transition into a 3D smectic phase followed by a transition to a 3D moving crystal phase. In this 3D regime the dV/dF_D curve exhibits a single peak similar to that found in 2D simulations of completely stiff vortex lines. As S_m decreases, there is a first order transition into a disordered decoupled 2D state that depins plastically and at higher drives undergoes a first order transition into a 3D ordered moving line state. The dV/dF_D curves have distinct double-peak features associated with this two step depinning and dynamical reordering process. The top insets in figure 21 show that the vortex positions and trajectories obtained

simultaneously in the top and bottom layers of the sample in the 2D decoupled plastic flow phase are distinct, while the bottom inset illustrates vortex flow in the top layer of the sample in the 3D dynamically ordered phase where the flow in all layers is identical. Additional studies of the same model show dynamical ordering from a 2D decoupled state to a 3D ordered structure [121, 122], and many of the memory and metastability effects that are observed in experiments can be captured in the 3D layered vortex model by superheating and supercooling the sample across the first order transition [123].

In 2D systems the most general moving ordered state at high drives is a moving smectic phase; however, simulations of the 3D layered vortex model show evidence of only small regions of 3D moving smectic phases, and it is not clear if such 3D smectic states are robust or whether they are a result of finite size effects. Other models for 3D vortex systems include 3D anisotropic frustrated X-Y systems of the type used by Chen and Hu [124] to examine the weak pinning regime in which the system forms an ordered assembly of 3D lines without topological defects or a 3D Bragg glass state. In this work, a first order transition separates the moving 3D ordered state from a moving smectic state, which transitions continuously into a liquid state as a function of temperature. Hernández and Domínguez studied a similar model and observed that a first order transition from a 3D ordered pinned state to a 2D disordered state is associated with a large increase in the depinning threshold [125].

4.2. Phase locking effects

In the moving ordered Bragg glass state, Chen and Hu observed a pronounced washboard signal in the velocity noise spectrum, with a narrow band noise peak called a washboard peak at a characteristic frequency of $f_0 = V/a_0$ [124], where V is the velocity along the driving direction and a_0 is the vortex lattice constant. Similar washboard noise spectra have been observed in the ordered state in 2D systems [96, 117]; however, the washboard peak is particularly sharp in the 3D system [124], indicating that the moving 3D ordered state undergoes fewer random fluctuations than the moving 2D ordered state. Washboard noise and broad band noise features have also been observed experimentally in layered superconductors [127, 128]. When narrow band noise is present, interference effects can arise if an ac drive is applied to the sample in addition to the dc drive. When the ac drive frequency matches the washboard frequency or its harmonics, the two frequencies lock and a series of Shapiro steps appear in the velocity-force curves. Such effects were first observed by Fiory [129] for the moving vortex lattice, while the washboard effect for vortices moving over

random pinning was explained by Schmid and Hauger [130]. Phase locking, including enhanced ordering effects, of vortices moving over random pinning has been studied in experiments [128, 131, 132, 133] and simulations [126], while related studies have been performed for colloids driven over a periodic substrate [134]. Narrow band noise and phase locking steps have also been studied in experiments on sliding CDW systems [4]. In this case, the scaling of the shape of the velocity-force curve as it enters and exits individual phase locked steps is similar to the scaling observed at an elastic depinning transition, with $V \propto (F_D - F_s)^\beta$, where F_s is the drive at which the phase locking occurs and $\beta < 1.0$ [135]. It is not known whether vortices obey scaling of this type as they enter and exit phase locking steps, nor is it known whether the character of the Shapiro steps is different in 2D and 3D vortex systems, or whether different phase locking signatures would appear depending on whether the system is in a moving smectic state or a moving crystal state.

If a longitudinal drive is applied to the vortices in order to place them in a dynamically ordered state, and then a transverse ac drive is added, the vortices can become even more ordered and can exhibit transverse phase locking. Even though the dc drive causes the vortices to move in the longitudinal direction, the narrow band noise signal of the reordered state produces a periodic modulation of the vortex motion in the transverse direction as well, making it possible for the transverse ac drive to lock to the narrow band frequency. Kolton *et al.* [136] examined transverse phase locking in the moving ordered phase for vortices driven over random disorder. Figure 22(a) shows that there is a clear phase locking step in the longitudinal vortex velocity as a function of the longitudinal dc drive F_D when a transverse ac drive is present. The vortex trajectories in figure 22(b) show that below the locking step, the vortices are moving in channels in the longitudinal direction (y direction in the figure) but there is some spread in the trajectories along the transverse direction. Above the locking step, the trajectories are similar, as illustrated in figure 22(d), but on the step a highly ordered sinusoidal pattern appears, as shown in figure 22(c). In the power spectra of the velocity time series, shown in figure 22(e-g), there is a sharp resonance on the locking step due to the highly ordered motion. Although longitudinal phase locking effects have been observed experimentally [133], there has not yet been an experimental observation of transverse phase locking.

Voltage noise measurements that can be used to detect the existence of a washboard frequency provide a useful experimental method of determining where the different dynamical phases occur as well as the amount of order in the moving structure. An illustration

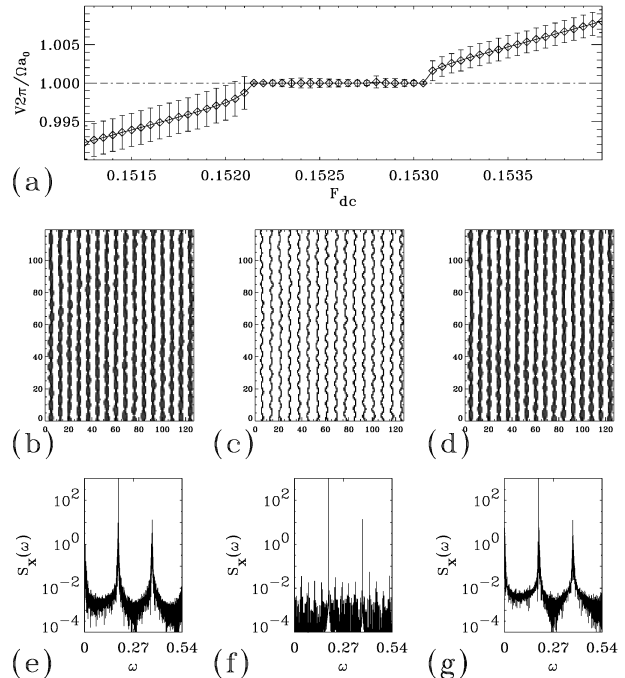


Figure 22. (a) Simulations of velocity V vs dc driving force F_{dc} in the window around the main transverse phase locking step in a system with a fixed ac drive applied transverse to the dc drive for vortices moving over random disorder in the dynamically ordered phase. (b,c,d) Typical time-averaged coarse-grained vortex densities. Here the dc driving force is applied along the y axis and the transverse ac drive is applied along the x axis. (e,f,g) Typical voltage power spectra $S_x(\omega)$ of the transverse vortex velocity. (b,e) A phase-unlocked state below the locking step. (c,f) A phase-locked state on the locking step. (d,g) A phase-unlocked state above the locking step. Reprinted with permission from A.B. Kolton, D. Domínguez, and N. Grønbech-Jensen, Phys. Rev. B **65**, 184508 (2002). Copyright 2002 by the American Physical Society.

of how the power spectra and noise fluctuations are correlated with the amount of order in the vortex system appears in figure 23, which shows the evolution of the velocity noise spectrum $S(\omega)$ in the moving state for increasing vortex density for the 3D elastic line model studied by Bullard *et al* [117]. The inset of each panel shows the corresponding structure factor $S(\mathbf{k})$ of the moving state. For the plastic flow phase in figure 23(a), the noise is broad band and the structure factor has a ring feature indicative of an amorphous state. Figure 23(b) shows that at a higher density the system forms a moving smectic as indicated by the appearance of two peaks in $S(\mathbf{k})$ at finite \mathbf{k} , while $S(\omega)$ begins to develop a series of smeared peaks as a washboard frequency emerges. In figure 23(c) the system is even more ordered and there are now six peaks in $S(\mathbf{k})$; however, the ordering is still anisotropic as two of the peaks are much more pronounced than the others. The washboard frequency peak in $S(\omega)$ is more prominent, reflecting the stronger ordering

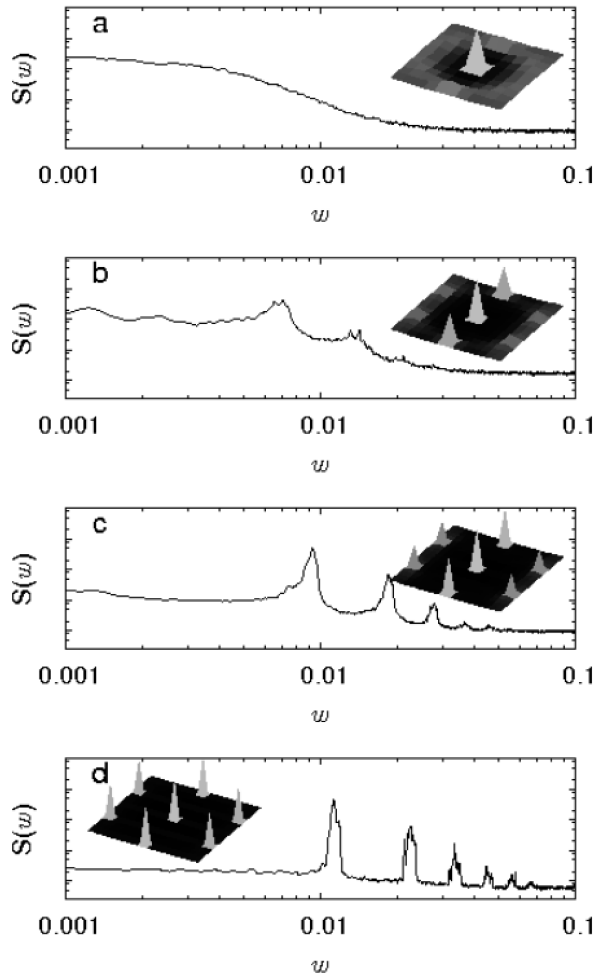


Figure 23. The vortex velocity power spectra $S(\omega)$ from simulations of a 3D elastic line vortex model in the moving phase for increasing vortex density, from top to bottom. The insets show the corresponding structure factor $S(\mathbf{k})$. (a) Plastic flow phase. (b) Smectic flow phase. (c) Anisotropic crystal phase. (d) Moving crystal phase. Reprinted with permission of Springer from T.J. Bullard, J. Das, G.L. Daquila and U.C. Täuber, *Eur. Phys. J. B* **65**, 469 (2008). Copyright 2008 by the The European Physical Journal.

in the moving system. In figure 23(d) a defect-free moving lattice state forms in which $S(\mathbf{k})$ contains six peaks that are nearly equal in weight, while $S(\omega)$ shows sharp spikes at the washboard frequency and its higher harmonics. The washboard frequency increases with increasing vortex density as the vortex lattice constant decreases.

There are still many questions to ask about the dynamics of 3D depinning, and very little is known beyond the behavior of directed line models. A 3D isotropic lattice of particles could arise in systems such as a 3D Wigner crystal [137, 138], 3D colloidal Yukawa systems [139, 140] and 3D cubic lattices of skyrmions [141, 142]. Systems of this type could exhibit a rich

variety of plastic flow and dynamically ordered phases in which the particles could dynamically order into 1D columns or 2D slabs aligned with the drive or into other anisotropic ordered structures. It would be interesting to determine whether such reordering transitions are continuous or first order. Other systems in which 3D reordering transitions could be studied include 3D liquid crystals moving in random disorder as well as pattern forming systems or Lennard-Jones particles, where additional effects could arise such as the formation of moving labyrinth phases. Finally, there have been many studies of packing and glass transitions in dimensions higher than 3 to determine where mean-field behavior emerges. It may be interesting to examine depinning and dynamical ordering transitions in systems with 4 or more dimensions to explore whether a similar mean-field limit can be reached.

5. Depinning and First Order Dynamical Phase Transitions in Other Layered Systems

5.1. Systems with many layers

Continuous and first order depinning phenomena can occur in other 3D and 2D layered systems beyond superconducting vortices, such as in sliding CDWs [4], layered Wigner crystals [143], and particles moving along the easy direction through periodic asymmetric 1D constrictions [144]. For example, layering effects can produce first order dynamical depinning transitions in 2D or 3D sliding CDWs. Although many CDW systems are thought to exhibit purely elastic behavior, experiments have revealed a variety of hysteretic, switching, and discontinuous behaviors, which have been argued to indicate that a purely overdamped elastic description of CDWs often breaks down [4, 35, 145, 146]. Vinokur and Nattermann [147] theoretically examined the depinning transition for a layered CDW system and found that the velocity-force curves exhibit a two-step depinning processes, with an initial continuous depinning into a plastic flow phase of decoupled layers followed by a second sharp hysteretic transition at higher drives into a coherent moving structure. For weaker disorder, the system undergoes a single depinning transition into a coherently sliding 3D solid. The velocity-force curves in figure 24 show a depinning transition at F_c followed by a sharp hysteretic jump in V at the dynamical reordering transition into a coherently moving 3D solid. The inset of figure 24 shows a dynamical phase diagram as a function of driving force versus temperature in the strong pinning limit where pinned, plastic flow, and moving solid phases appear. The overall behavior of this system is very similar to that observed in simulations of a 3D layered vortex system, described in Section 4.

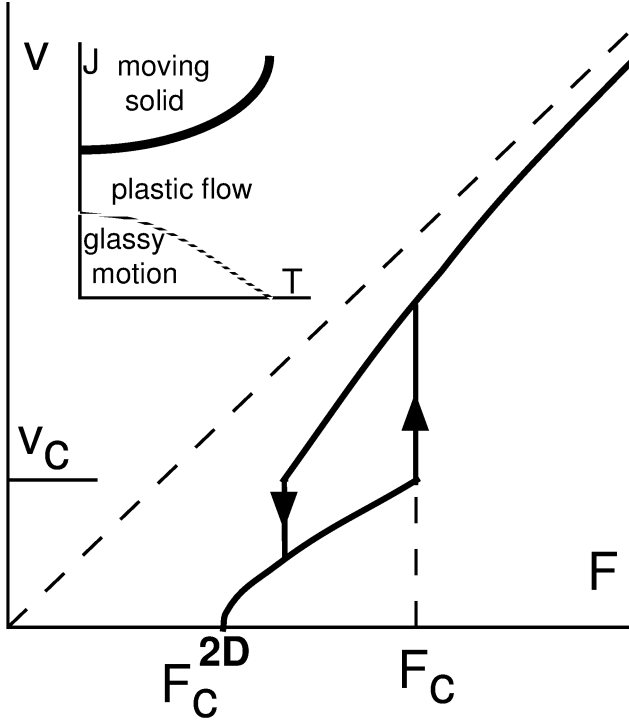


Figure 24. The theoretical velocity V versus driving force F response for a 3D layered sliding CDW system. A continuous transition to plastic flow at F_c^{2D} is followed by a sharp hysteretic transition into a coherent moving 3D state at F_c . The inset shows the dynamic phase diagram for driving force J vs temperature T , highlighting the evolution of the two depinning transitions a function of temperature. Here, F and J correspond to the driving force F_D , F_c^{2D} corresponds to the critical depinning threshold F_c , while F_c in the figure corresponds to the dynamical ordering transition. Reprinted with permission from V.M. Vinokur and T. Nattermann, Phys. Rev. Lett. **79**, 3471 (1997). Copyright 1997 by the American Physical Society.

Marchetti *et al.* considered an overdamped anisotropic mean field model of a system of particles that are elastically coupled along the driving direction and viscoelastically coupled transverse to the driving direction, allowing the possibility for slip of neighboring rows of particles [148]. The equation of motion is

$$\dot{\phi}_i^i(t) = K \sum_{\langle j \rangle} (\phi_i^j - \phi_i^i) + F + F_p + \sigma_{i,i}^\alpha \quad (7)$$

where the first term gives the elastic coupling to the neighboring particles along the direction of drive with elastic constant K , F is the external driving force corresponding to F_D , F_p is the pinning force, and σ is the viscoelastic interaction term characterized by a coupling parameter η . Various forms can be used for the viscoelastic time response, and in [148] a linear response was applied, permitting the system to be tuned from purely elastic to purely viscous by varying the coupling constants. Figure 25(a) illustrates the velocity-force response of the system in the purely

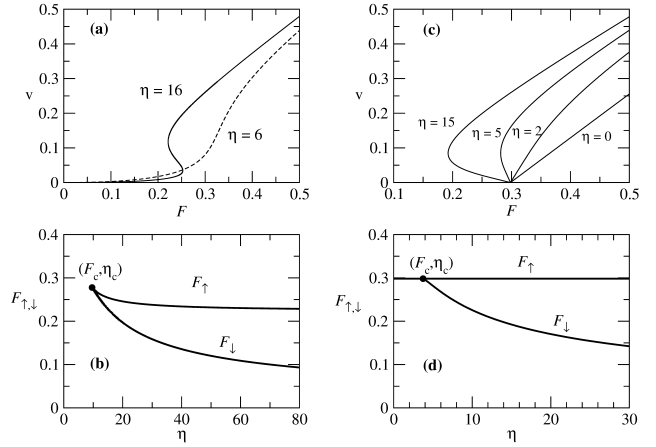


Figure 25. (a) The velocity-force response for an anisotropic model with a random substrate, elastic coupling in the direction of drive, and viscous coupling in the transverse direction, where η is the strength of the viscous coupling term. Here F corresponds to the driving force F_D . In the purely viscous case shown here, there is a critical viscous coupling η_c above which the velocity-force curves become hysteretic. (b) The corresponding phase diagram showing as a function of η the driving forces F_\uparrow and F_\downarrow at which the hysteretic transitions to the coupled sliding state occur for sweeping the drive up and down, respectively. (c) The velocity-force curves for a system with finite elasticity, where in the absence of transverse viscous coupling ($\eta = 0$) the depinning is continuous and non-hysteretic. (d) The corresponding driving force vs η phase diagram shows that there is again a critical viscous coupling above which hysteretic behavior occurs. Reprinted with permission from M.C. Marchetti, A.A. Middleton, K. Saunders, and J.M. Schwarz, Phys. Rev. Lett. **91**, 107002 (2003). Copyright 2003 by the American Physical Society.

viscous limit of $K = 0$ for different values of the viscous coupling η , while the corresponding phase diagram of driving force versus η in figure 25(b) shows that there is a critical viscous coupling η_c above which the system develops a hysteretic response. When a finite elasticity is introduced by setting $K = 1$, the velocity-force curves for different values of η take the shapes illustrated in figure 25(c). For $\eta = 0$ the depinning transition is continuous, while for higher values of the viscoelastic coupling the depinning becomes sharp and is hysteretic, as shown in the dynamic phase diagram in figure 25(d). Followup studies and variations of this model that allow plasticity to arise from nonconcave interaction potentials also show that coherent and incoherent flows can coexist in parameter space [149].

5.2. Systems with few layers

It is also possible to observe dynamical phase transitions in systems with only a small number of layers. Le Doussal *et al.* showed that in a d -dimensional two-layer model, both continuous and sharp dynamical transitions can occur if plasticity between the two layers is allowed [150]. Experimental

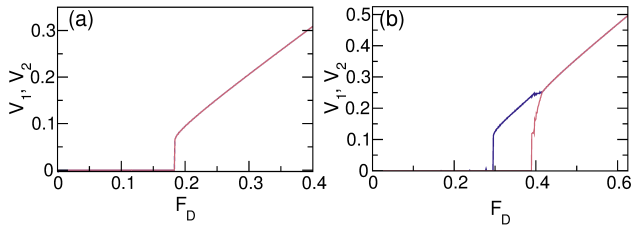


Figure 26. The simulated velocity-force curves for two coupled 1D channels of Yukawa particles moving over random pinning of strength $F_p = 6.0$. The channels are separated by a distance d and the velocities in the two channels are denoted by V_1 (blue) and V_2 (red). There are four times as many particles as pinning sites, and both particles and pinning sites are evenly divided between the two channels. (a) At $d = 1.13$, the depinning is elastic and there is no slip between the channels. (b) At $d = 1.47$, the channels depin at different drives but show a dynamical locking transition at higher drives near $F_D = 0.4$. Adapted with permission from C. Reichhardt and C. J. Olson Reichhardt, *Phys. Rev. B* **84**, 174208 (2011). Copyright 2011 by the American Physical Society.

realizations of systems of interacting particles confined in one to three layers can be achieved for vortices in mesoscopic channels [151], coupled 1D Wigner crystal wires [152], colloidal systems [153], dusty plasmas [154], and ions in line traps [155]. Reichhardt and Reichhardt [156] considered Yukawa repulsively interacting particles in two coupled 1D channels separated by an interchannel distance d in the presence of random pinning. The particles form zig-zag structures to minimize their interaction energy. An interesting feature of this layered system is that the pinning strength can be adjusted separately in each layer, producing a different effective damping in the moving phase for each layer. Despite its simplicity, this model exhibits a remarkably rich variety of dynamic phases and hysteretic responses. For example, when the interchannel distance is small and there are an equal number of randomly placed pinning sites of equal strength in each layer, the velocity-force curves for each channel in figure 26(a) show that the particles depin elastically and are locked together in the two layers. Here V_1 is the velocity of channel 1 and V_2 is the velocity of channel 2. When the interchannel distance is increased in order to reduce the interchannel coupling, figure 26(b) shows that each channel depins at a different value of F_D . At low drives, only one channel is moving; at intermediate drives, the second channel depins and the channels slip past each other; and at higher drives, there is a transition to a locked phase where the particles in the two channels move together. This simple system thus produces four different phases, illustrated in the dynamic phase diagram as a function of driving force versus interchannel distance d in figure 27: phase P, where both channels are pinned; phase C, where one

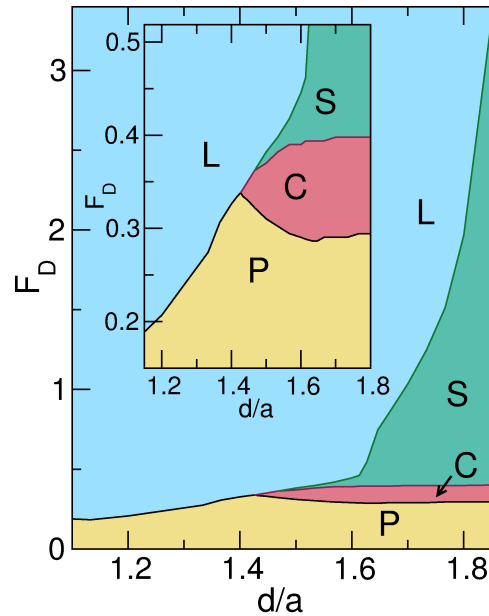


Figure 27. The simulated dynamic phase diagram for the two coupled 1D channels of Yukawa particles from Fig. 18 for driving force F_D vs interchannel distance d/a . P: pinned phase. C: coexistence between pinned and moving channels. S: sliding phase in which both channels are moving at different velocities and slip past one another. L: locked channel phase. Inset: A detail of the main panel shows that near the elastic to plastic depinning transition at $d/a = 1.4$ there is peak in the critical depinning threshold. Adapted with permission from C. Reichhardt and C. J. Olson Reichhardt, *Phys. Rev. B* **84**, 174208 (2011). Copyright 2011 by the American Physical Society.

channel is pinned and the other is flowing; phase S, a sliding phase where both channels are flowing but are not locked; and phase L, a moving locked phase. The depinning transition is elastic for $d \leq 1.4$ and plastic for $d > 1.4$, while the drive at which the system dynamically orders from a sliding state to a locked state diverges with increasing d . The inset of figure 27 shows a detail of the crossover from elastic to plastic depinning near $d = 1.4$, where a peak in the critical depinning threshold appears at the transition. This phase diagram shows behavior remarkably similar to that observed in the complex peak effect phenomenon for 3D vortex systems described in Section 3, where a peak in the critical depinning threshold is associated with a transition from elastic to plastic depinning, and the drive needed to dynamically order the system diverges as the coupling between neighboring vortices decreases.

If the pinning strength is increased, additional dynamical features appear in the model of two coupled 1D channels. Figure 28 shows the velocity-force curves for each channel in a sample with pinning that is strong enough to permit the formation of moving solitons that can coexist with pinned particles in a single channel.

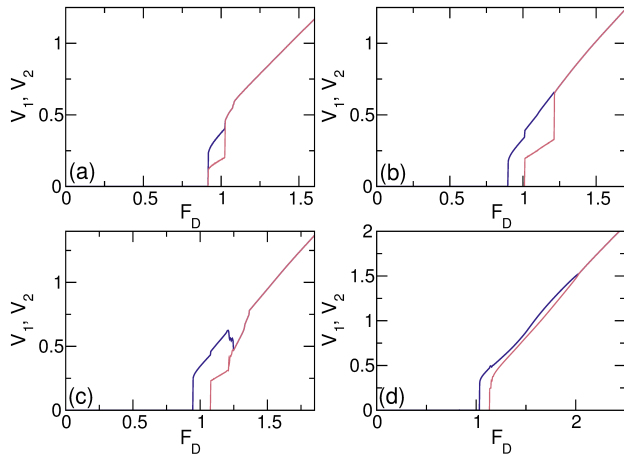


Figure 28. The simulated velocity-force curves V_1 (blue) and V_2 (red) vs F_D for two coupled 1D channels of Yukawa interacting particles moving over random pinning of strength $F_p = 15.0$, where the channels are separated by a distance d . The pinning strength has been increased compared to figures 26 and 27. (a) At $d = 1.147$, both channels depin at the same time to a sliding state with $V_1 > V_2$, and the channels lock at higher drives. (b) At $d = 1.2$, the channels depin at different drives, and there is a jump up in V_1 when V_2 becomes finite. (c) At $d = 1.27$, at the onset of the dynamical locking phase V_1 drops while V_2 increases. (d) At $d = 1.47$, the channels do not lock until a much higher drive is applied. Adapted with permission from C. Reichhardt and C. J. Olson Reichhardt, Phys. Rev. B **84**, 174208 (2011). Copyright 2011 by the American Physical Society.

Figure 28(a) shows that for $d = 1.2$, both channels depin at the same time, but there is a regime in which $V_1 > V_2$, and when the moving channels become locked, there is a sharp jump in both V_1 and V_2 . In figure 28(b) for $d = 1.27$, each channel depins at a different value of F_D . The depinning transition in channel 2 is sharp and coincides with a jump up in V_1 , while a dynamical coupling transition occurs near $F_D = 1.25$. Figure 28(c) shows that at $d = 1.27$, the channels depin separately, while at the dynamic locking transition, a jump up in V_2 is associated with a jump down in V_1 , producing a negative differential conductivity in channel 1. For $d = 1.47$ in figure 28(d), the channels do not couple until a much higher drive is applied. The general shape of the dynamical phase diagram in figure 27 is preserved for models containing up to 8 interacting channels. In an 8 channel system, within the sliding phase a series of locking and unlocking transitions of different groups of layers occurs, and only at higher drives do all of the channels finally lock together.

Other mechanisms can transform a non-hysteretic depinning transition into a hysteretic one. Schwarz and Fisher examined an elastic manifold driven over random disorder, which exhibits a non-hysteretic depinning transition in the overdamped limit [157]. Stress overshoots, in which a moving segment of the

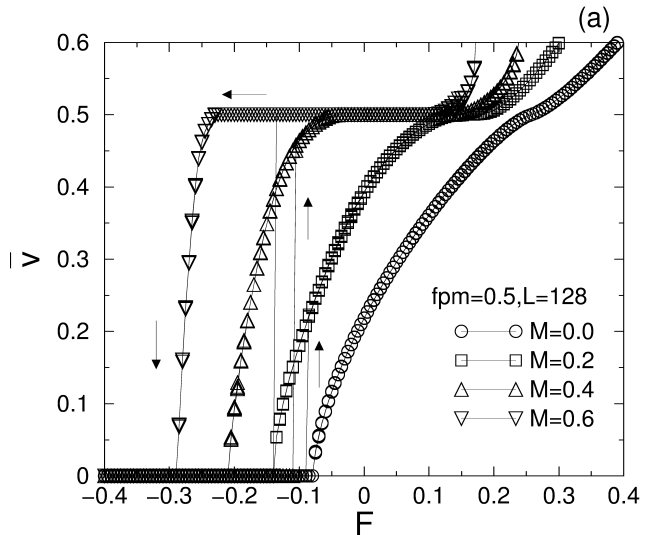


Figure 29. Simulated velocity-force curves for a mean field elastic model in the presence of random disorder, where the strength of inertial overshoot effects is determined by the parameter M . At $M = 0$ the system depins elastically, while at finite M the system exhibits a hysteretic response. Here \bar{v} corresponds to the velocity V and F corresponds to the driving force F_D . Reprinted with permission from J.M. Schwarz and D.S. Fisher, Phys. Rev. E **67**, 021603 (2003). Copyright 2003 by the American Physical Society.

manifold generates stress in the non-moving segments, can be introduced by adding inertial and elastic wave effects, and when stress overshoots are present, the critical depinning threshold is reduced and the depinning transition becomes increasingly hysteretic. This is illustrated in figure 29, which shows the velocity-force curves from simulations of a mean field model where M is the inertial or stress overshoot parameter. There is no hysteresis in the depinning transition at $M = 0$, and the hysteresis grows with increasing M . Hysteretic depinning transitions can also arise in underdamped Frenkel-Kontorova models [49, 158], where there can be a coexistence of large regions of moving particles with areas of pinned particles. Less is known about how inclusion of inertia could affect systems that exhibit plastic depinning.

5.3. Kinetic precursors and spinodals

Numerous aspects of first order phase transitions remain current topics of active research, particularly the kinetics of such transitions and the presence of precursor dynamics as the transition is approached [159, 160, 161, 162]. For example, below the transition there can be fluctuating droplets containing the new phase. Since the size of these fluctuating droplets increases as the first order phase transition is approached, it is possible for a droplet to reach the

critical droplet size that nucleates the new phase at a point below the actual phase transition, making it possible for the system to exhibit critical features in spite of the fact that the transition is first order [160]. Features of this type could be strongly enhanced by the inhomogeneities introduced by a pinning landscape. Additionally, the ideas of spinodal points in mean field models and pseudo-spinodal points in systems with finite range interactions that describe the extent of metastability could be applied to nonequilibrium first order dynamical transitions [161, 162]. For example, if a system undergoing phase separation or coarsening as a function of time were simultaneously driven over random disorder, the fluctuating forces induced by the pinning could stabilize the coarsening process at some limit, or they could enhance the speed of the coarsening or destroy the coarsening process altogether.

6. Depinning and Dynamic Phases on Periodic Pinning Arrays

Another class of systems that can exhibit depinning transitions and various types of nonequilibrium phase transitions is particles driven over periodic substrates. As mentioned in the introduction, there has already been substantial work on a variety of frictional systems, which in some cases can be modeled as atoms or molecules moving over a periodic substrate. Such work is beyond the scope of this review, and we refer the reader to an excellent recent review of this field [10]. There are, however, examples of systems that can be effectively modeled as overdamped particles moving over periodic arrangements of pinning sites where plasticity can occur that exhibit behavior similar to the dynamical phases that arise for random pinning arrangements. Such systems include superconducting vortices driven over periodic pinning arrays and colloids moving over periodic optical or magnetic substrates.

6.1. Dynamic phases of superconducting vortices on periodic substrates

Many superconducting applications require high critical currents or strong vortex pinning, so considerable effort has been devoted to understanding how to arrange pinning sites in special geometries that maximize the pinning effectiveness [1, 2, 58, 163]. Since the ground state of the vortex lattice is triangular, a natural approach is to arrange the pinning sites in periodic structures with 2D [2, 58, 163, 164], 1D [165], or quasiperiodic [166] ordering. Experiments in superconductors with periodic pinning arrays show that the critical depinning threshold exhibits a series of peaks at magnetic fields at which the number of vortices N is an integer multiple n of the number of pinning sites

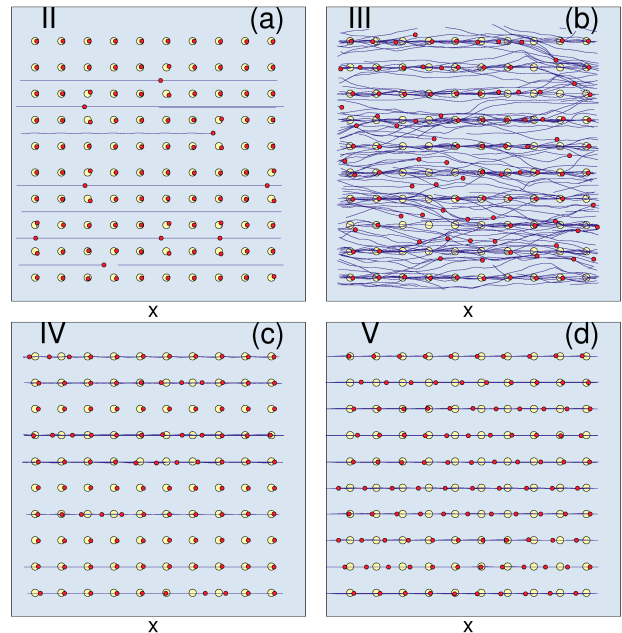


Figure 30. Vortex locations (red dots), pinning site locations (yellow circles) and trajectories (blue lines) for simulations of superconducting vortices interacting with a square pinning array at a filling fraction of $n = 1.06$ for increasing drive. (a) Phase II, the 1D flow of interstitial vortices between pinned vortices. (b) Phase III, chaotic or turbulent flow. (c) Phase IV, a 1D soliton type flow along the pinning sites. (d) Phase V, a 1D flow of all the vortices along the pinning sites. Adapted with permission from C. Reichhardt, C.J. Olson, and F. Nori, *Phys. Rev. Lett.* **78**, 2648 (1997). Copyright 1997 by the American Physical Society.

N_p , $n = N/N_p$, while direct imaging [2, 164] and simulations [59, 164, 167] indicate that the vortices form ordered arrangements at the integer commensurate fillings. Since the vortex density is controlled by an applied magnetic field, the filling $n = 1$ is called the first matching field. At nonmatching fillings, there can be either a disordered structure or an ordered lattice containing well defined interstitials, vacancies, or grain boundaries.

One of the key differences between vortex motion over periodic pinning arrays and most models of atomic friction is that the pinning sites for the vortices are localized, so that the potential energy landscape experienced by the vortex resembles a muffin tin rather than an egg carton. Additionally, the vortex interactions are much longer range than atomic interaction potentials, so that on strong pinning landscapes two separate vortex species can be present: the vortices directly trapped by the pinning sites, and the vortices located in the interstitial regions between pinning sites. The interstitial vortices still feel a confining potential due to repulsion from their neighboring vortices, some or all of which may be trapped at the pinning sites. For $n \lesssim 1$, just below

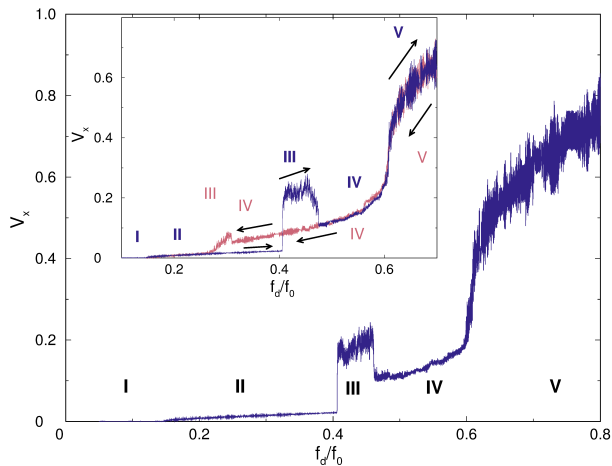


Figure 31. The simulated velocity-force curves for the periodic pinning vortex system in figure 30. Here V_x corresponds to the velocity V and f_d/f_0 corresponds to the driving force F_D . The inset shows the hysteresis in the velocity-force curves when the driving force is swept up (blue) and down (red). Phase I is the pinned phase. The nature of the transitions between phases are as follows: I to II, second order; II to III, first order; III to IV, first order; IV to V, second order. Adapted with permission from C. Reichhardt, C.J. Olson, and F. Nori, Phys. Rev. Lett. **78**, 2648 (1997). Copyright 1997 by the American Physical Society.

the first matching field, all the vortices are located at pinning sites and there are a fixed number of vacancies, while for $n \gtrsim 1$, just above the first matching field, a portion of the vortices are trapped at interstitial sites. When a sample containing interstitial vortices is subjected to a driving current, two depinning transitions should occur, with the first transition corresponding to the depinning of the interstitial vortices, while the second is the depinning of the vortices trapped at pinning sites.

Reichhardt *et al.* [62, 168] numerically examined the depinning dynamics of vortices in a 2D square pinning array. At $n = 1.0$ there is a single continuous non-hysteretic depinning transition at a critical value F_c corresponding to the maximum pinning force F_p exerted by an individual pinning site, indicating that the interactions between the vortices cancel and the system responds in the same manner as in the single particle limit. At $n = 1.06$, the interstitial vortices depin at a lower driving force and follow 1D trajectories between the pinned vortices, as illustrated in figure 30(a). Figure 31 shows the velocity-force curve for this system, with the pinned phase labeled phase I and the 1D interstitial vortex flow phase labeled phase II. As F_D increases there is a transition from the phase II flow to a turbulent or chaotic flow in which the moving interstitial vortices cause vortices at the pinning sites to depin, producing the strongly fluctuating trajectories illustrated in figure 30(b). This disordered pinning and depinning flow phase is labeled

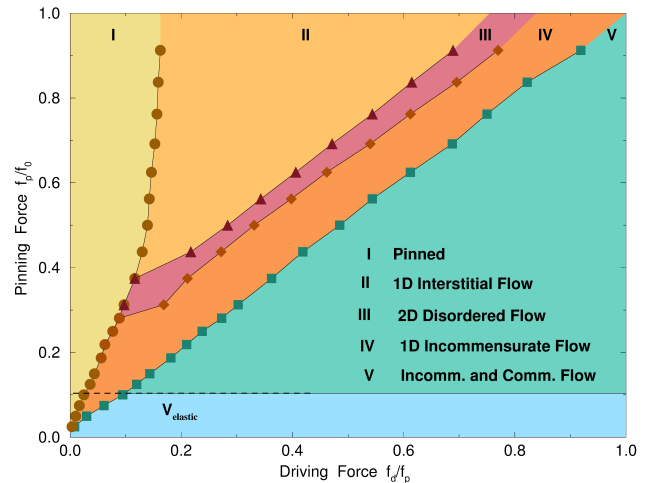


Figure 32. Simulated dynamic phase diagram for vortices in periodic pinning for the same system in figures 30 and 31 showing the evolution of the phases as a function of pinning strength f_p/f_0 vs driving force f_d/f_p at $n = 1.06$. Here f_p/f_0 corresponds to F_p and f_d/f_p corresponds to F_D . Adapted with permission from C. Reichhardt, C.J. Olson, and F. Nori, Phys. Rev. B **58**, 6534 (1998). Copyright 1998 by the American Physical Society.

phase III, and its onset coincides with a sharp jump up in the velocity-force curve in figure 31 since a larger number of vortices are now moving. At higher F_D there is another transition from phase III to a 1D soliton-like flow of vortices along the pinning sites, labeled phase IV and illustrated in figure 30(c). The transition between phases III and IV is associated with a sharp drop in the vortex velocity, as shown in figure 31, which is termed negative differential mobility. Flow in phase IV consists of excitations or pulses of motion that translate over the substrate much more rapidly than the individual vortices. At even higher drive, there is a transition to a state called phase V in which all of the vortices are flowing along the pinning sites, as illustrated in figure 30(d). Since there are more vortices than pinning sites in this example, the flow in phase V is smectic, and neighboring rows gradually slide past each other over time. The inset in figure 30 shows that there no hysteresis associated with the IV-V transition, strong hysteresis across the III-IV and II-III transitions, and no hysteresis in the I-II transition. The I-II transition falls into the same class as the depinning of an individual particle from a periodic substrate, with the velocity-force curve obeying $V = (F_D - F_c)^\beta$ with $\beta = 0.5$. The II-III transition is a first order transition from a non-chaotic state to a chaotic state, while the III-IV transition is a first order transition from a chaotic state to a non-chaotic state. The IV-V transition is a continuous non-hysteretic transition.

The dynamic phase diagram constructed from a series of simulations for the system in figure 31 is shown in figure 32 as a function of pinning force F_p

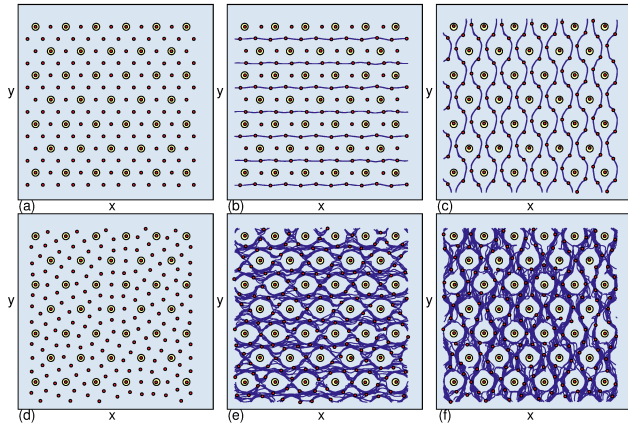


Figure 33. Ordered and disordered plastic flow phases for simulations of superconducting vortices in a periodic triangular array of pinning sites showing vortex locations (red dots), pinning site locations (yellow circles), and trajectories (blue lines). (a,b,c) A filling of $n = 4.0$. (a) In the pinned phase, the vortices form an ordered state. (b) For driving in the x -direction just above depinning, a portion of the vortices flow in 1D channels. (c) For driving in the y -direction, all the interstitial vortices flow in a sinusoidal pattern. (d,e,f) A filling of $n = 5.0$. (d) The frustrated pinned phase. (e) For driving in the x direction, a disordered or chaotic flow state occurs. (f) For driving in the y direction, a similar disordered flow state occurs. Adapted with permission from C. Reichhardt and C.J. Olson Reichhardt, Phys. Rev. B **79**, 134501 (2009). Copyright 2009 by the American Physical Society.

versus driving force F_D at a filling of $n = 1.06$. At low F_p , the interstitial vortices cannot be localized between the pinning sites, and the system forms a grain boundary state which depins elastically. As F_p is further increased, the interstitial vortices become localized and phase II and phase III flows begin to appear. The critical depinning threshold for the I-II transition saturates at large F_p since it is determined by the confinement of the interstitial vortices rather than by the pinning sites themselves, and this energy scale is set by the vortex lattice constant instead of by the pinning strength. The III-IV and IV-V transitions both increase linearly in F_D with increasing F_p . For $n < 1.0$ (not shown), there is also a two-step depinning process in which the vacancies in the vortex lattice depin first followed by the vortices at the pinning sites; however, phase III flow does not occur [168]. Other simulations of the motion of vortices through periodic arrays of obstacles also show negative differential conductivity as well as a dynamically pinned or jammed state in which the vortices form pileups and then force their way through the obstacle when the drive is high enough, allowing the motion to start again [169].

For higher fillings and other pinning geometries, additional dynamic flow phases occur which generically fall into two categories: a smooth non-chaotic flow

of interstitial vortices between pinned vortices and/or immobile interstitial vortices, and chaotic flow states [168, 170, 171, 172, 173, 174, 175]. The depinning into a smooth non-chaotic phase when the pinned equilibrium vortex lattice structure is ordered is illustrated in figure 33(a) for a triangular pinning array at $n = 4.0$ where the vortices form an ordered triangular lattice below depinning [176]. Figure 33(b) shows the flow of the vortices at this filling just above depinning for driving in the x -direction. A portion of the interstitial vortices flow in 1D channels between the pinning sites, while the vortices at the pinning sites remain pinned and a third of the interstitial vortices also remain pinned. If the drive is instead applied along the y direction, the flow is again ordered and forms the pattern illustrated in figure 33(c), with all the interstitial vortices flowing. For higher drives, additional dynamical transitions occur as the remaining vortices depin. In figure 33(d), the pinned vortex phase at $n = 5.0$ is disordered due to a frustration effect, and the depinning for driving in either the x or y directions results in disordered flows such as those shown in figure 33(e,f).

In experiments on superconductors with square periodic pinning arrays near $n = 1.01$ [63], the velocity-force curves exhibit the same signatures found in simulations of the dynamical phases I through V, as shown in figure 34(a), where there is a jump up in velocity at the II-III transition and a jump down in velocity at the III-IV transition. Figure 34(b,c,d) shows schematics of the flow patterns in phases II, III and IV. In the same set of experiments, strong hysteresis appears across the II-III and III-IV transitions [63]. S. Avci *et al.* also experimentally investigated the dynamics of vortices in periodic pinning arrays where strong matching effects occur, and found features in the velocity-force curves that are consistent with those observed for the dynamic phases I through V, as illustrated in figure 35 [177]. Other transport experiments in periodic pinning arrays have also found similar transport signatures corresponding to dynamic phases I through V, as well as hysteresis in the velocity-force curves [178].

Of the various dynamical phases observed for motion through periodic pinning arrays, phases II and IV are locked in periodic non-chaotic orbits. It would be interesting to measure the Lyapunov exponents in the different phases. It may also be possible to achieve layering effects by constructing pinning arrays in which every other pinning row has a different strength or size. Another method for extracting information about the nature of the dynamical flow is the velocity noise signature, since the periodicity of the pinning sites should always induce a periodicity in the velocity as a function of time, but the magnitude of this periodic

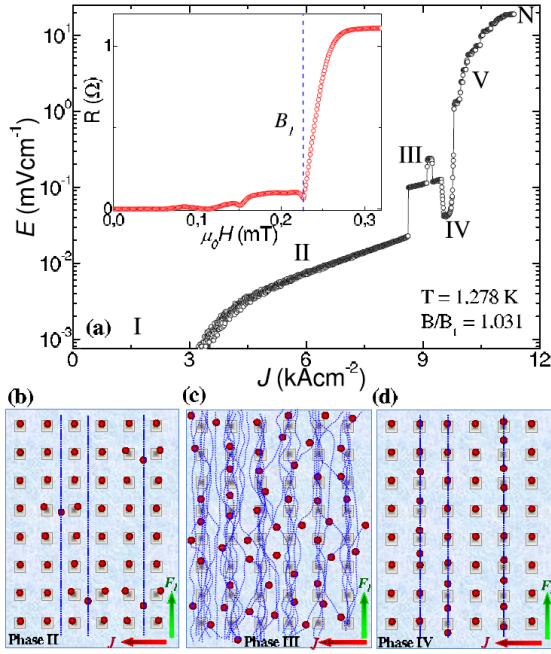


Figure 34. (a) Experimentally measured velocity-force curve for vortices in a square pinning array at a filling of $n = 1.0$ as a function of voltage E vs current J . Here E corresponds to the velocity V and J corresponds to the driving force F_D . Labels indicate the dynamical phases. I: pinned; II: 1D interstitial motion of the type illustrated in panel (b); III: turbulent flow; IV: 1D soliton flow; V: motion of all the vortices; N: transition of the sample to the normal state. (b-d) Schematic images of vortex flow. (b) 1D interstitial motion in phase II. (c) Turbulent flow in phase III. (d) 1D soliton flow in phase IV. Reprinted with permission from J. Gutierrez, A.V. Silhanek, J. Van de Vondel, W. Gillijns, and V.V. Moshchalkov, *Phys. Rev. B* **80**, 140514(R) (2009). Copyright 2009 by the American Physical Society.

signal will vary depending on whether the flow is in an ordered state or a disordered state. Simulations show that very different velocity noise spectral signatures arise depending on the nature of the flow pattern, ranging from narrow band noise to broad band noise [170]; however, experimental noise measurements have not yet been performed. It would be interesting to determine whether the addition of an ac drive to the dc drive could produce an ordering of the chaotic flow states. There have already been experimental studies [179] and simulations [180, 181] of vortex motion in periodic pinning arrays that reveal Shapiro step locking effects near $n = 1.0$; it would be interesting to examine whether similar effects appear at higher fillings. There have also been studies of dynamical transitions in the vortex flow for systems with asymmetric pinning sites, where different types of flow patterns emerge for driving along different directions with respect to the substrate asymmetry [182]. Another open question is how the vortex dynamics would change for periodic pinning placed in 3D systems or 3D layered systems, and whether phases I through V would still occur, or

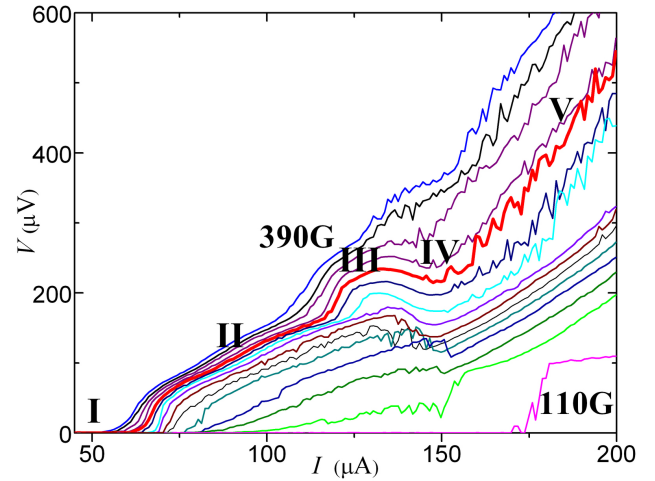


Figure 35. Experimentally measured velocity-force curves for superconducting vortices in a square pinning array as a function of voltage V vs current I for changing magnetic field or changing vortex density, from 110 G (lower right) to 390 G (upper right). V corresponds to the vortex velocity and I corresponds to the driving force F_D . Evidence of dynamical phases I through V (labeled) appears in the form of jumps and dips in the average vortex velocity. Reprinted with permission from S. Avci, Z.L. Xiao, J. Hua, A. Imre, R. Divan, J. Pearson, U. Welp, W.K. Kwok, and G.W. Crabtree, *Appl. Phys. Lett.* **97**, 042511 (2010). Copyright 2010, AIP Publishing LLC.

whether additional phases would arise. It would also be possible to study a system in which the density of pinning sites at the top of the sample (containing the tops of the vortex lines) is different from the bottom of the sample (containing the bottoms of the vortex lines), and to vary the ratio of these densities in order to determine whether a new type of commensuration effect can occur between the number of vortices and the two different periodicities of the pinning array.

6.2. Dynamic phases of colloids on periodic substrates

Colloids are an outstanding experimental system in which to explore issues in equilibrium and nonequilibrium statistical mechanics due to their size scale, which allows direct access to the microscopic degrees of freedom [183, 184]. Recent advances in optics allow the creation of a variety of substrates over which the colloids can be driven [185]. There have been numerous studies of the pinned ground states and ordering of colloids interacting with 1D [186, 187, 188, 189] and 2D periodic substrates [190, 191, 192, 193]. For 2D periodic arrays, the substrate can have either an egg carton form [190, 192, 193] that does not allow interstitial particles, or it can have a muffin tin form that allows interstitial colloids to coexist with pinned colloids [189, 194]. When individual colloids are driven through periodic arrays at different angles with respect to the array symmetry

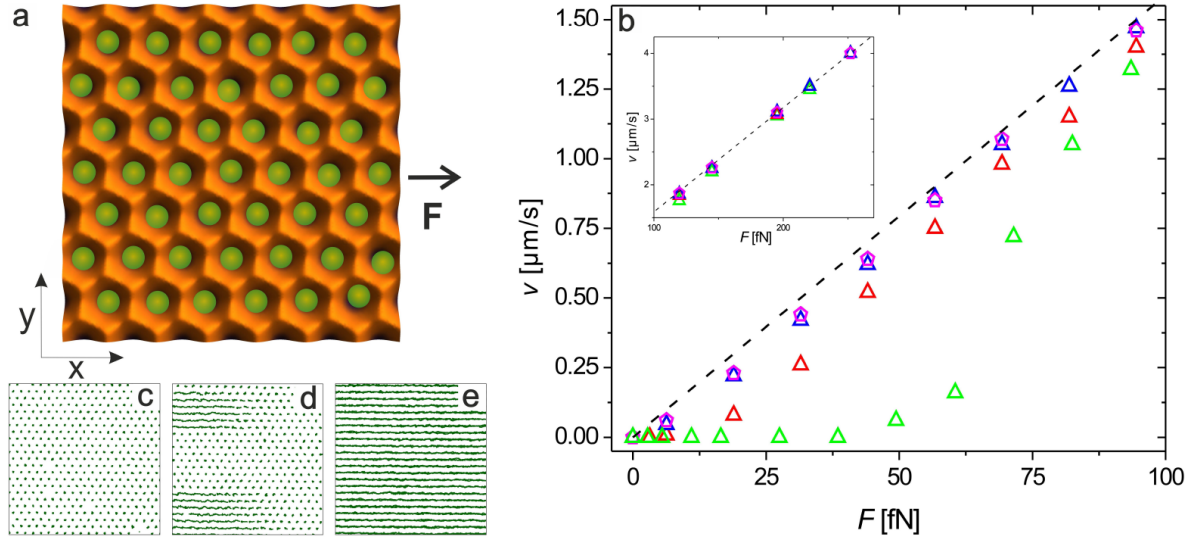


Figure 36. (a) Schematic of an experiment in which a colloidal monolayer is driven with force F across an energy landscape created by the interference of laser beams. The potential strength and length scale of the substrate potential can be adjusted by varying the laser intensity and the angle at which the laser beams intersect. Here F corresponds to F_D . (b) The experimentally measured mean colloidal velocity V of a crystalline monolayer with lattice constant $a = 5.7\mu\text{m}$ vs driving force F for a commensurate substrate with $n = 1$ (green), incommensurate substrates with $n = 0.83$ (red) and $n = 0.71$ (blue), and quasiperiodic (magenta) substrates. The dashed line corresponds to free sliding on a flat substrate. Inset: V vs F for larger F where $V \propto F$. (c,d,e) Colloid trajectories for $n = 1$ commensurate conditions at (c) $F = 0$, (d) $F = 49$, and (e) $F = 82$. Reprinted by permission from Macmillan Publishers Ltd: Nature Materials, T. Bohlein, J. Mikhael, and C. Bechinger, Nature Mater. **11**, 126 (2012), copyright 2012.

direction, a variety of directional locking effects appear in which the motion of the colloids locks to high symmetry directions of the substrate [195, 196]. Other studies focused on the properties of the dynamic steady state flows of colloids moving over ordered substrates [197]. Colloids moving over periodic substrates can also be studied for practical applications such as novel particle separation techniques, since in some cases one species of colloid locks to a symmetry direction of the substrate lattice while another species does not, so that a mixture of different colloid species can be segregated in the direction transverse to the drive over time [195, 196, 198, 199, 200, 201].

6.2.1. Colloids on egg carton substrates – Bohlein *et al.* experimentally examined the motion of a monolayer of charge-stabilized colloids with a repulsive Yukawa colloid-colloid interaction potential driven over a periodic substrate [7, 8]. Figure 36(a) shows a schematic of the optically created triangular substrate lattice, where each potential minimum traps a single colloid and the external driving force is applied along the x -direction. Figure 36(b) illustrates the colloid velocity versus applied force, where the dashed line indicates the velocity signature in the absence of a substrate. At the $n = 1$ commensurate condition, the velocity is roughly zero for $F_D < 45$ and the colloids are in the pinned state shown in figure 36(c). When $F_D = 49$ the system depins and motion occurs in the form

of sliding kinks, as illustrated in figure 36(d), while at higher drives all the colloids flow simultaneously, as shown in figure 36(e). At incommensurate fillings, the depinning threshold F_c is substantially reduced, but flow above depinning still involves running kinks (solitons) or antikinks (antisolitons).

Vanossi *et al.* conducted numerical simulations of the same system and examined the velocity-force curves at commensurate and incommensurate fillings [202]. Figure 37(a) shows a schematic of their system, in which the colloids interact with an egg carton corrugated substrate potential. As illustrated in figure 37(b), at $n = 0.95$ where there are fewer colloids than potential minima, different families of antisolitons appear in the initial configuration. The substrate is relatively weak so the antisolitons are large objects containing many colloids that float above the substrate potential. Figure 37(c) shows velocity-force curves obtained for different values of n and different substrate strengths, with the substrate-free limit indicated by a dashed line. At the commensurate (CO) filling of $n = 1.0$ the depinning threshold $F_c \approx 1.0$ and the velocity-force curve has sublinear scaling behavior; however, the exponent β in the expression $V \propto (F_D - F_c)^\beta$ was not analyzed. At the antisoliton-incommensurate (AI) filling of $n = 0.95$, depinning occurs in two steps, and at low drives the motion consists of antisolitons traveling in the direction opposite to the drive, achieved when each colloid moves one lattice constant

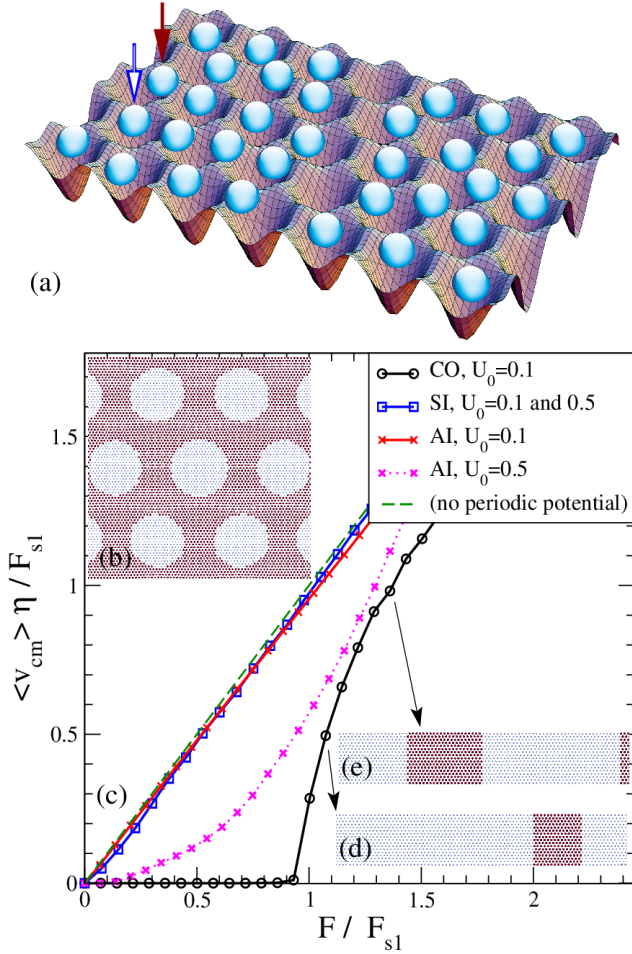


Figure 37. (a) Schematic of a simulation of colloids interacting with a 2D triangular periodic substrate. An individual colloid can sit in a minimum (white arrow) or on a maximum (red arrow) of the substrate potential. (b) The initial conditions at a filling of $n = 0.95$. Light dots represent colloids in substrate minima; dark dots indicate colloids on substrate maxima. Here the substrate potential is relatively weak, so the dark areas are antisoliton regions that are floating above the substrate potential, while the white areas are commensurate regions in which the colloids sit in the substrate minima. (c) The velocity-force curves for fillings of $n = 1.0$ (CO or commensurate, black), $n = 0.95$ (AI or antisoliton-incommensurate, red and pink), and $n = 1.05$ (SI or soliton-incommensurate, blue) showing that the commensurate case has the highest depinning threshold. U_0 is the substrate corrugation strength, corresponding to the pinning strength F_p , while $\langle v_{cm} \rangle$ corresponds to the velocity V and F/F_{s1} corresponds to the driving force F_D . (d,e) Illustration of sliding-generated solitons in the $n = 1$ commensurate lattice at the points on the velocity-force curve marked with arrows. The width of the soliton increases with increasing driving force. Reprinted with permission from A. Vanossi, N. Manini, and E. Tosatti, Proc. Natl. Acad. Sci. (USA) **109**, 16429 (2012). Copyright 2012 National Academy of Sciences, USA.

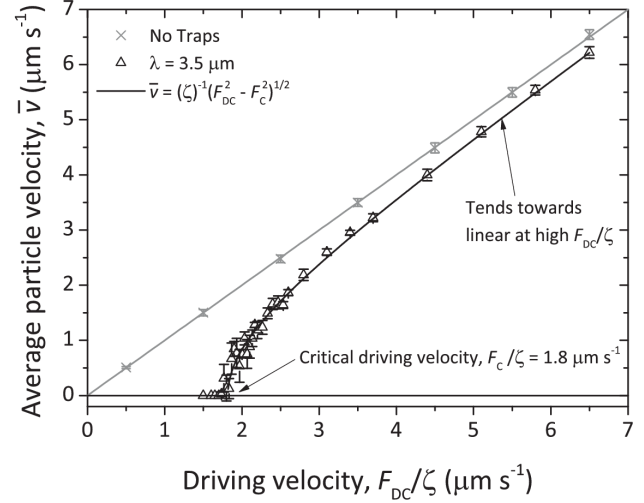


Figure 38. The experimentally measured velocity-force curves for colloids moving over a 1D periodic substrate, showing the presence of a critical depinning threshold F_c . At higher drive the velocity approaches the substrate-free limit (light line). Here \bar{v} corresponds to the velocity V and F_{DC}/ζ corresponds to the driving force F_D . The solid line is a fit to $V \propto (F_D^2 - F_c^2)^{1/2}$. Reprinted with permission from M.P.N. Juniper, A.V. Straube, D.G.A.L. Aarts, and R.P.A. Dullens, Phys. Rev. E **93**, 012608 (2016). Copyright 2016 by the American Physical Society.

in the driving direction every time an antisoliton passes over it. In the soliton-incommensurate (SI) case of $n = 1.05$, the depinning threshold is even smaller and the solitons move in the driving direction. Figure 37(d,e) shows that in the CO case, the width of the moving soliton regions increases as the external driving force is increased. For both weak and strong substrates, the solitons consist of regions in which excess particles that lack a substrate minimum in which to sit partially float above the substrate lattice as an incommensuration, and the barrier for motion of these regions is small. For weak substrates such as that shown in figure 37, the antisolitons have the same floating incommensuration structure as the solitons, and are similarly weakly pinned. In contrast, for strong substrates, the antisolitons that appear at the AI filling of $n = 0.95$ are composed of missing particles, and can move only if the adjacent particles hop over the substrate potential maximum. As a result, the barrier for motion on strong substrates is much higher in the AI state than in the SI state. Other simulation studies of the sliding states of colloids moving over periodic substrates show that the pinning threshold is maximum exactly at the commensurate state, while away from commensuration, soliton flow states arise [203]. As a function of substrate strength, sharp transitions from a pinned state to a flowing state are observed in simulations, leading to super-lubricity type behaviors [204].

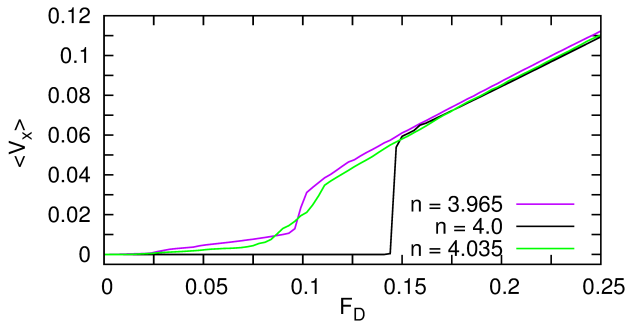


Figure 39. Simulated velocity-force curves for colloids interacting with a square muffin tin substrate at fillings of $n = 3.965$, 4.0 , and 4.035 , showing that the depinning threshold is highest at the commensurate case $n = 4.0$. Here $\langle V_x \rangle$ corresponds to the velocity V . Adapted with permission from D. McDermott, J. Amelang, C.J. Olson Reichhardt, and C. Reichhardt, *Phys. Rev. E* **88**, 062301 (2013). Copyright 2013 by the American Physical Society.

Experimental studies of colloids moving under combined ac and dc driving forces over 1D periodic substrates [205] show phase locking steps in the velocity-force curves similar to those observed for vortices and sliding CDW's under combined ac and dc drives. Locking can occur when collective effects are present that make it possible for a density wave or soliton excitation along the 1D colloidal chain to act like a quasi-particle with dynamics similar to that of a single particle moving over a periodic substrate [205]. Simulations of this system indicate that the motion of such solitons can produce additional steps in the velocity-force curves beyond the typical integer Shapiro steps [206].

Juniper *et al.* experimentally measured the dc velocity-force curves for colloids on a 1D periodic substrate and find that the optical substrate can be effectively modeled as a sinusoidal potential for small trap spacing, and that Brownian noise effects are relevant near depinning but are absent in the high driving limit [207]. Figure 38 shows that the average particle velocity for this system in the absence of a substrate obeys $V \propto F_D$, while when the substrate is present, a finite critical depinning threshold appears and the velocity approaches the clean limit at higher drives. The solid line is a fit to $V \propto (F_D^2 - F_c^2)^{1/2}$; however, near F_c it is possible to fit the data to the single particle elastic depinning behavior of $V \propto (F_D - F_c)^\beta$ with $\beta < 1.0$.

6.2.2. Colloids on muffin tin substrates Simulation studies of colloids interacting with muffin tin type potentials reveal the existence of a variety of dynamic phases [64]. Figure 39 illustrates the velocity-force curves for a system with a square muffin tin pinning array at fillings of $n = 3.965$, 4.0 , and 4.035 . At

$n = 4.0$, the colloids form a commensurate ordered triangular lattice in which the pinning sites trap 1/4 of the colloids, and the remaining colloids form an ordered arrangement in the interstitial region. A two-step depinning process occurs for the $n = 4.0$ filling, with the initial depinning of the interstitial colloids occurring near $F_D = 0.14$, while the second depinning transition of the colloids in the pinning sites occurs at a drive much higher than the range illustrated in figure 39. At $n = 3.965$, grain boundaries form in the pinned state that separate two different degenerate orientations of the $n = 4$ pinned state, and the depinning transition is substantially reduced. At depinning, the grain boundaries or antikink excitations become mobile, while at $n = 4.035$ the initial depinning is of the kinklike grain boundaries that form. For either incommensurate filling, a transition occurs at higher drives from grain boundary-dominated dynamics to the coherent flow of interstitial particles, while for higher drives there is a transition to a state in which all of the colloids are flowing.

Figure 40(a) illustrates the colloid positions, trajectories, and pinning site locations for the $n = 4.035$ filling from figure 39, and figure 40(b) shows the corresponding Voronoi construction of the colloid positions, where light blue polygons indicate sixfold coordinated particles while the darker polygons are fivefold or sevenfold coordinated particles. At this filling, the system forms two domain walls, and just above depinning at $F_D = 0.05$, figure 40(a) shows that these domain walls begin moving in the direction of the drive in the form of kinks or solitons. The nature of the soliton motion is more clearly visible in figure 40(g), which shows a blowup of the motion of a domain wall. At $F_D = 0.08$, illustrated in figure 40(c,d), the domain walls grow in size and fluctuate, but there are still commensurate regions in which the colloids are immobile. At $F_D = 0.2$, the flow transitions to the ordered interstitial motion shown in figure 40(e,f), and the domain wall structure present at lower drives is lost. The blowup of the ordered interstitial channel motion in figure 40(h) shows that the colloids at the pinning sites and a portion of the interstitial colloids remain pinned. It would be interesting to examine the depinning of the domain walls in more detail since this could provide an example of elastic depinning of a line-like object. In many models, domain wall depinning is represented as the motion of a strictly elastic system; however, as shown in figure 40(c,d), the domain wall can break up when it moves, so it is possible that in many real examples of domain wall depinning, some plasticity or breaking of the domain wall may occur.

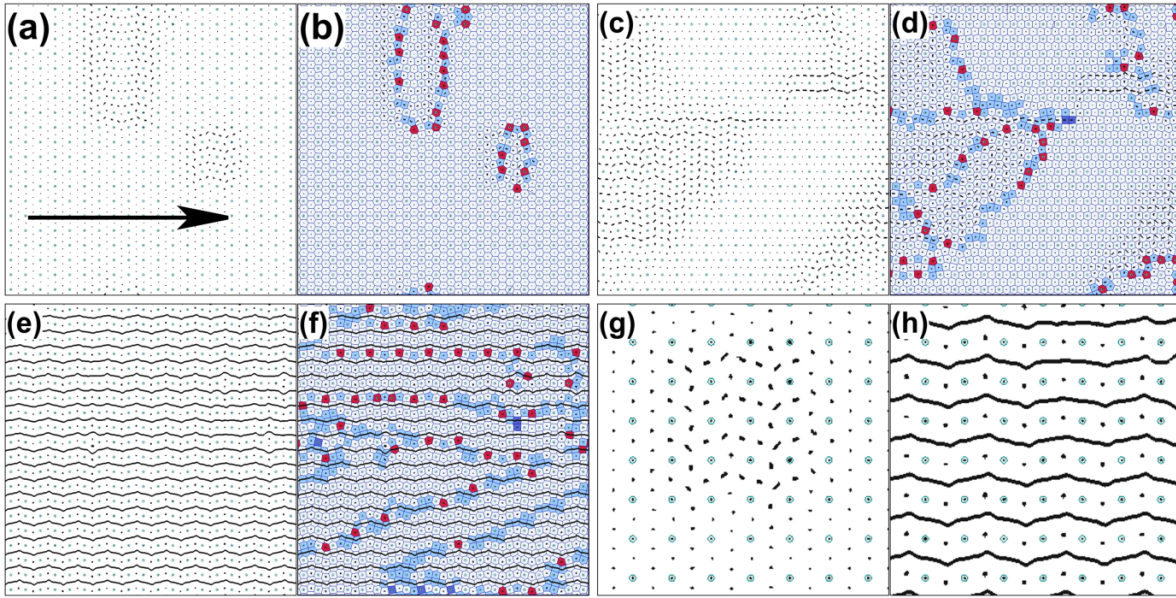


Figure 40. (a,c,e) The pinning site locations (open circles), particles (dots), and trajectories (lines) from simulations of the system in figure 39 for colloids driven in the x direction over a square muffin tin pinning array at $n = 4.035$. The arrow indicates the driving direction. (b,d,e) The corresponding Voronoi constructions. Light blue polygons indicate sixfold coordinated particles, while red and dark blue polygons are sevenfold and fivefold coordinated, respectively. (a,b) At $F_D = 0.05$, the grain boundaries depin. (c,d) At $F_D = 0.08$ there is a fluctuating grain boundary state. (e,f) At $F_D = 0.2$, interstitial colloid flow occurs. (g) A blowup of the trajectories from the flowing grain boundary state in panel (a). (h) A blowup of the flow of the interstitial particles in panel (e). Reprinted with permission from D. McDermott, J. Amelang, C.J. Olson Reichhardt, and C. Reichhardt, *Phys. Rev. E* **88**, 062301 (2013). Copyright 2013 by the American Physical Society.

6.3. Future directions

Beyond spherical colloids, it is also possible to consider colloidal dimers or trimers, patchy colloids, and Janus colloids, all of which can form a variety of self-assembled equilibrium structures [208]. Simulation studies of effective colloidal dimers and trimers moving over a periodic substrate show that a variety of dynamical states can occur, such as flows in which the dimers align with the driving direction, while the velocity-force curves can exhibit transitions between ordered and sinusoidal flows [209, 210]. In other numerical studies of dimer motion on ordered substrates, absolute negative mobility arises when a combination of ac and dc driving forces are applied to colloidal dimers [211]. For colloids driven over quasi-1D periodic substrates, different types of ordered and disordered flowing states can occur depending on the filling factor and the magnitude of the external dc drive [212, 213]. One of the next systems to examine would be the driven motion of colloids with more complex interactions over periodic substrates, since it may be possible to produce dynamically generated self-assembly. It would also be interesting to consider multiple species of colloids moving over periodic pinning arrays to understand possible segregation or mixing effects.

Most of the studies of particles driven over

periodic substrates have been performed in 2D. One possible avenue of future research would be to study the dynamical phases of particles moving through 3D pinning arrays. Colloids represent an ideal system for such studies since it is possible to create 3D arrays of optical traps. In 3D, issues such as glass transitions start to become important, and it is possible that the depinning transitions or dynamic phases could change under conditions at which a glass-forming length scale becomes larger than the length scale of the periodicity of the pinning sites. It would also be interesting to characterize the moving phases of colloids and other particle systems moving over periodic pinning arrays using something akin to an effective temperature. For particles moving over random disorder, the dynamically generated fluctuations from the pinning sites often have Boltzmann-like statistics, making it possible to apply an effective temperature description [214]; however, for particles moving over periodic arrays, the fluctuations are much more directional and generally do not have Boltzmann-like features. In certain cases where the pinned state is strongly frustrated, it may be possible for the frustration effects to survive into the moving state, permitting the moving state for certain incommensurate fillings to be characterized as having effective thermal fluctuations even though the commensurate moving states do not.

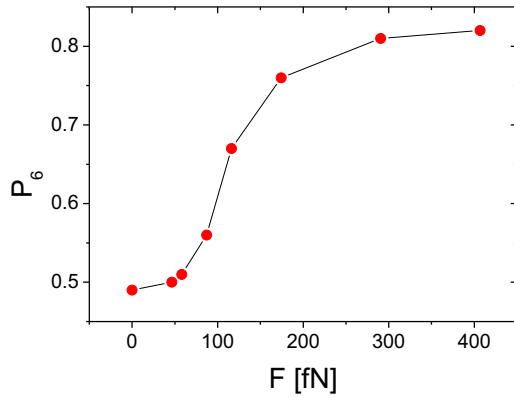


Figure 41. The fraction of sixfold coordinated colloids P_6 vs driving force F for an experimental system of colloids driven over a quasiperiodic substrate. Here F corresponds to the driving force F_D . Reprinted with permission from T. Bohlein and C. Bechinger, *Phys. Rev. Lett.* **109**, 058301 (2012). Copyright 2012 by the American Physical Society.

7. Dynamic Phases on Quasiperiodic Substrates

Substrates with quasicrystalline ordering can be created for both superconducting vortices and colloids. Since quasicrystals are nonperiodic yet have long range order [215], the dynamic phases of particles driven over quasiperiodic substrates could exhibit features that are a combination of those observed in periodic and random pinning arrays. In the high drive limit, particles driven over random pinning dynamically reorder into a triangular moving solid or a moving smectic state, while for periodic pinning arrays the particles generally form a moving smectic state, so on a quasicrystalline pinning array, a moving solid or a moving smectic could emerge depending on whether the long range order or the nonperiodicity dominates.

In numerical studies of the dynamics of both superconducting vortices and colloids moving over a fivefold or Penrose quasiperiodic array of pinning sites [216, 217], at low drives the particles form a pinned quasicrystal similar to that found in the pinned state for colloids interacting with quasiperiodic substrates in the strong trapping limit [218, 219]. The system depins into a plastic flow phase, and then at higher drives dynamically orders into a moving Archimedean structure state in which the particles form combinations of square and triangular rows that are aligned in the direction of drive [216]. Archimedean ordering was also experimentally observed in the pinned state for colloids on quasicrystalline substrates in the weaker substrate limit, and was argued to arise

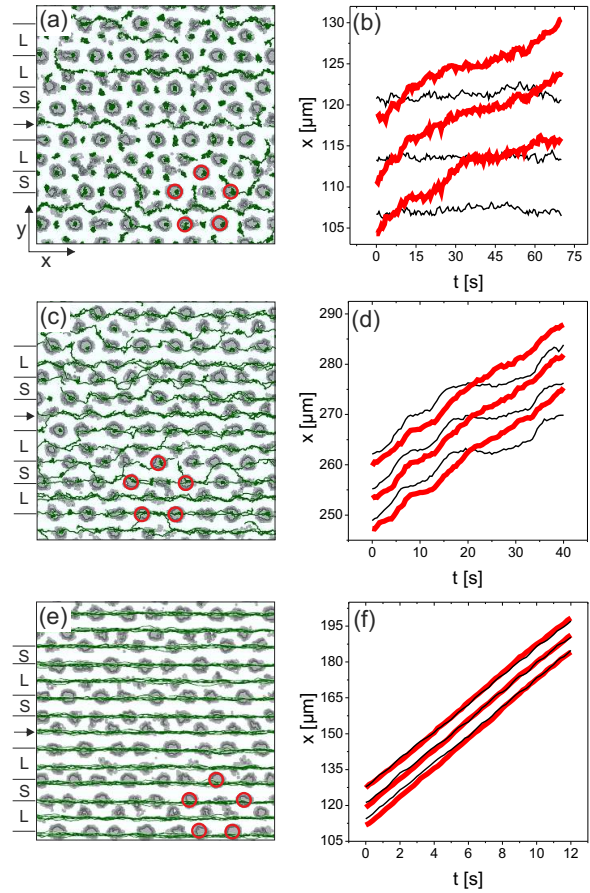


Figure 42. Experimental results for colloids driven in the x direction over a quasiperiodic substrate. (a,c,e) The particle trajectories (green) and the quasiperiodic substrate (grey) at driving forces from figure 41 of (a) $F = 47$ fN (c) $F = 87$ fN, and (e) $F = 291$ fN. The fivefold symmetry of the substrate is highlighted in red. Here F corresponds to the driving force F_D . (b,d,f) The x coordinate vs time t for three sets of adjacent interstitial (thick red lines) and noninterstitial (thin black lines) particles. (b) The noninterstitial particles are pinned and the interstitial particles are moving at $F = 47$ fN. (d) The noninterstitial particles transiently pin and depin while the interstitial particles move continuously at $F = 87$ fN. (f) Interstitial and noninterstitial particles move with the same velocity in the dynamically ordered phase at $F = 291$ fN. Reprinted with permission from T. Bohlein and C. Bechinger, *Phys. Rev. Lett.* **109**, 058301 (2012). Copyright 2012 by the American Physical Society.

as a compromise between the periodic ordering favored by the colloid-colloid interactions and the quasiperiodic ordering of the substrate [218]. If the driving direction is altered, simulations show that the Archimedean ordering emerges only for particular orientations of the drive with respect to the fivefold symmetry directions of the substrate, while square moving lattices and disordered states occur when the drive is oriented along non-symmetry directions of the substrate [216].

Bohleyn and Bechinger experimentally studied colloids driven along the x axis, a symmetry direction, of a fivefold quasiperiodic substrate, and observed a transition from a plastic flow state at low drives to a dynamically ordered moving Archimedean crystal at higher drives [8]. Figure 41 shows a plot of P_6 , the fraction of sixfold coordinated colloids, versus driving force. At low drives, $P_6 \approx 0.5$ and the flow consists of interstitial particles moving past pinned particles. At higher drives, P_6 increases to a maximum value of $P_6 = 0.8$ in the dynamically ordered regime, but does not reach $P_6 = 1.0$ despite the reordering since the Archimedean moving lattice structure contains a number of four-sided polygons. Figure 42(a) shows the particle trajectories and the quasiperiodic substrate potential in the plastic flow phase at $F_D = 47$ for the system in figure 41, while a plot of the x position of adjacent interstitial and noninterstitial colloids as a function of time in figure 42(b) shows that at this drive there is a coexistence of pinned noninterstitial and moving interstitial colloids. Intermittent trapping of the noninterstitial colloids occurs at $F_D = 87$ fN, as shown in figure 42(c,d), and at $F = 291$ fN in figure 42(e,f), the system has entered the dynamically ordered flowing state and the trajectories form straight lines centered on rows of pinning sites. These experiments also demonstrated that for driving at different angles with respect to the substrate, changes in P_6 similar to those found in simulations occur when the colloidal motion becomes locked to certain angles. Moving square ordering was not observed in the experiments, which could be due to the different scale of the pinning sites or the magnitude of the driving force compared to the simulations. In numerical studies of particles driven over quasiperiodic substrates by a combination of ac and dc drives, phase locking similar to that observed for particles moving over ordered arrays occurs; however, for the quasiperiodic substrate strong irrational phase locking steps are present [220].

Many open questions remain in the dynamics of driven particles on quasicrystalline arrays, such as what phases appear on arrays with sevenfold, tenfold, or higher-fold ordering [221] or what effects occur when phason dynamics are also relevant [222]. In the moving state it would also be interesting to study the dynamically generated fluctuations to determine whether it is possible to describe the behavior of the system in terms of an effective dynamically induced temperature.

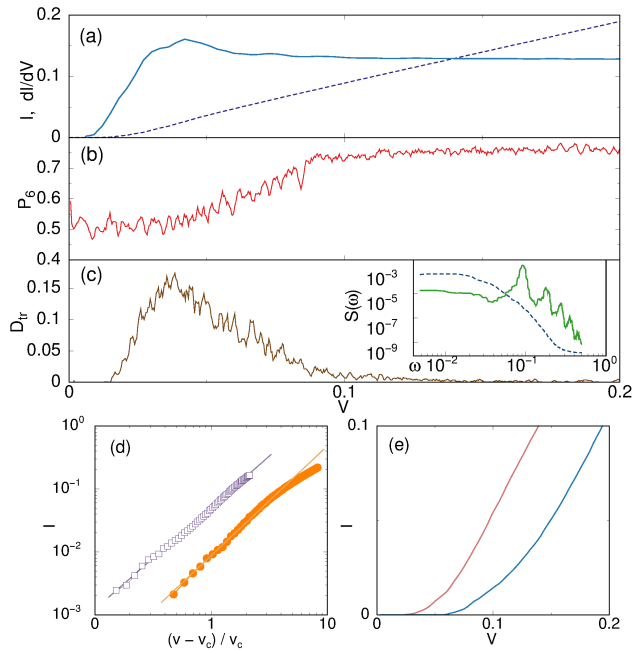


Figure 43. Results from simulations of a 2D Wigner crystal interacting with charged defects. (a) Dashed line: Current I vs voltage V . I corresponds to the electron velocity V while the voltage V corresponds to a driving force F_D . Solid line: dI/dV , corresponding to a dV/dF_D curve. (b) The corresponding fraction of sixfold coordinated electrons P_6 vs voltage V . (c) The transverse diffusion D_{tr} of the electrons vs voltage V . Inset: power spectrum $S(\omega)$ of the velocity time series for the plastic flow phase (dashed line), showing broad band noise, and for the moving smectic phase (solid line), showing narrow band noise. (d,e) The scaling of the velocity-force curves, which obey velocity $V = (F_D - F_c)^\beta$ with $\beta = 1.61$ and $\beta = 1.71$. Adapted with permission from C. Reichhardt, C.J. Olson, N. Grønbech-Jensen, and F. Nori, Phys. Rev. Lett. **86**, 4354 (2001). Copyright 2001 by the American Physical Society.

8. Depinning and Dynamics in Charge Transport

8.1. Wigner crystal depinning

Wigner crystals [3] are another system that exhibits depinning and sliding behavior. This electronic crystalline state is normally associated with insulating behavior, but it has a finite threshold for conduction under an applied drive. 2D Wigner crystal states that arise in semiconductor systems can be pinned by charged doping sites in the material. Experiments on 2D Wigner crystal systems show threshold and nonlinear conduction features [223, 224]. Sliding states can also occur for electrons on liquid He films, where the pinning is produced by dimpling effects [225].

In simulations of classical electrons with long range Coulomb interactions, Cha and Fertig observed a transition from a clean or ordered triangular Wigner crystal state to a disordered state as function of the strength of the quenched disorder substrate, and

found that in the disordered regime the depinning is plastic [40]. In other simulations [41] performed using overdamped dynamics for the same model of the electron crystal state, the substrate potential produced by the charged doping sites is represented as a smooth pinning landscape with large-scale fluctuations. The interaction energy in this system is given by

$$U = \sum_{i \neq j} \frac{e^2}{|\mathbf{r}_i - \mathbf{r}_j|} - \sum_{ij} \frac{e^2}{\sqrt{(|\mathbf{r}_i - \mathbf{r}_j^{(p)}|^2 + d^2)}} \quad (8)$$

where \mathbf{r}_i is the location of electron i . The first term is the electron-electron repulsion which favors formation of a triangular lattice. The second term represents the interaction of the electrons with impurities at positions $\mathbf{r}_j^{(p)}$ that are assumed to be positively charged defects offset by a distance d from the 2D plane containing the classical electrons. For strong disorder or small d , the numerical studies of Reichhardt *et al.* [41] indicate that the electrons depin into a plastic phase, followed at higher drives by a dynamical reordering into a moving Wigner crystal phase. Figure 43(a) shows the electron velocity, representing a measured current, versus driving force, representing an applied voltage, along with the corresponding dV/dF_D curve. The corresponding fraction P_6 of sixfold coordinated electrons versus F_D appears in figure 43(b), while figure 43(c) shows a measure D_{tr} of the fraction of electrons that wandered a distance larger than $a_0/2$ in the direction perpendicular to the drive during a fixed time interval, where a_0 is the electron lattice constant. There is a clear finite depinning threshold, and a peak in dV/dF_D coincides with the drive at which P_6 begins to increase and D_{tr} begins to decrease. Near $F_D = 0.1$, the system enters a moving smectic phase as indicated by the saturation of dV/dF_D and P_6 . In the moving smectic phase, D_{tr} goes to zero since the electrons flow along well-defined channels and cease to wander in the direction transverse to the drive. In the plastic flow phase, the velocity noise spectrum $S(\omega)$ has a broad band signal, as shown in the inset of figure 43(c), while in the moving smectic phase a narrow band noise feature emerges. There is no hysteresis in the velocity-force curves obtained in these simulations, but near the depinning threshold the electron velocity scales as $V \propto (F_D - F_c)^\beta$ with $\beta = 1.61$ to $\beta = 1.71$, as shown in figure 43(d,e). These exponents are similar to those observed in other studies of plastic depinning.

Figure 44 shows the dynamic phase diagram for the Wigner crystal system as a function of driving force versus pinning offset distance d , where small d corresponds to high F_p . For $d > 1.5$ or weak pinning, the pinned ground state is ordered and the system depins elastically into a moving Wigner crystal state, while for smaller d or stronger pinning, plastic depinning occurs and there is a dynamical

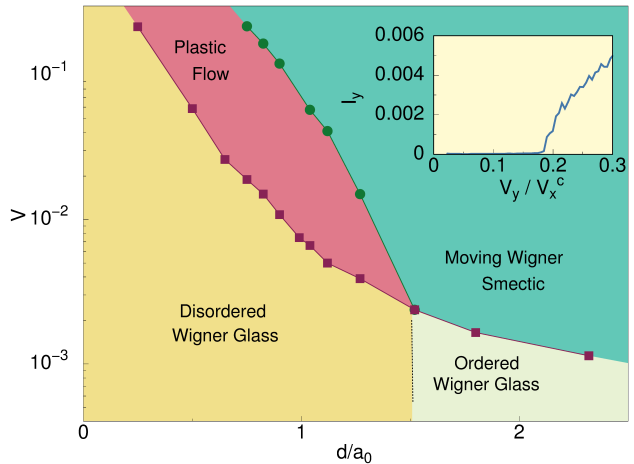


Figure 44. Dynamic phase diagram from simulations of the driven disordered Wigner solid as a function of the driving voltage V vs inverse pinning strength d/a_0 for the system in figure 43 highlighting a disordered pinned phase (Wigner glass), an ordered pinned phase, a plastic flow phase, and a moving Wigner smectic phase. The voltage V corresponds to a driving force F_D and the pinning offset distance d/a_0 is inversely proportional to the pinning strength F_p . Inset: Velocity-force curve showing the transverse depinning of the moving smectic phase. The current I_y corresponds to the velocity V_y in the transverse direction, while the voltage V_y/V_x^c corresponds to a transverse driving force F_D^y/F_c^x , where F_c^x is the depinning threshold for longitudinal driving. Adapted with permission from C. Reichhardt, C.J. Olson, N. Grønbech-Jensen, and F. Nori, *Phys. Rev. Lett.* **86**, 4354 (2001). Copyright 2001 by the American Physical Society.

reordering transition at higher drives into a moving smectic phase. The moving smectic has a strong transverse depinning threshold that can be observed by applying an additional transverse dc drive to the moving smectic state, as illustrated in the inset of figure 44. The flowing smectic channels do not break apart at the transverse depinning transition, which has elastic properties as indicated by the $\beta < 1$ curvature of the transverse velocity-force curve. Due to the long-range nature of the substrate disorder potential, the relative size of the transverse depinning threshold F_c^y compared to the longitudinal depinning threshold F_c^x is much larger than is observed in systems with short range pinning potentials, such as superconducting vortex systems [97, 98, 99]. Other numerical studies on the depinning of Wigner crystals in a constricted channel show that the velocity-force curve scales as $V = (F_D - F_c)^\beta$ with $\beta = 0.66$ in the elastic depinning regime and $\beta = 0.95$ in the quasielastic regime [226], while simulations using correlated pinning give $\beta = 1$ to $\beta = 1.7$ in the plastic depinning regime [227].

Transport experiments on 2D electron gases (2DEGs) show evidence of finite depinning thresholds and hysteretic velocity-force response curves [228] as well as negative differential resistance [229], which

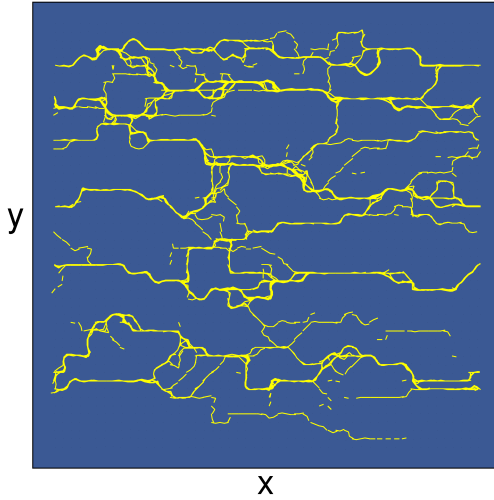


Figure 45. The current paths of charge flow (yellow) from a simulation of a 2D metallic dot array system just above the plastic depinning threshold. Adapted with permission from C. Reichardt and C.J.O. Reichardt, *Phys. Rev. Lett.* **90**, 046802 (2003). Copyright 2003 by the American Physical Society.

could imply that in some cases, a purely overdamped equation of motion as a model for a Wigner crystal is inadequate and does not capture the true dynamics. Alternatively, such results could indicate that in these systems the electrons form more exotic crystalline states such as stripes or bubbles, which can produce different dynamics as we discuss in Section 11. The appearance of narrow band velocity noise in simulations suggests that Shapiro step phenomena could be produced by imposing an additional ac drive on the dc drive, as previously predicted for sliding Wigner crystal states [230]; however, experiments of this type have not been conducted. In the case of liquid helium, the pinning is produced by the interactions of the electrons with the surface of the fluid, so it would be interesting to model this system by using deformable pinning sites.

8.2. Charge transport in metallic dot arrays

Another system that exhibits features such as a finite conduction threshold and nonlinear transport is charge transport in coupled metallic dot arrays. Middleton and Wingreen (MW) performed analytical and simulation studies of both 1D and 2D models of coupled metallic islands in which charges hop from one island to the next across a Coulomb barrier under a driving force consisting of an externally applied voltage [5]. The velocity of the charges is proportional to an experimentally measurable current. MW observed a finite threshold for conduction associated with critical scaling of the velocity according to $V = (F_D - F_c)^\beta$, with $\beta = 5/3$ in analytical calculations, $\beta = 2.0$ in 2D simulations, and $\beta = 1.0$ in 1D simulations.

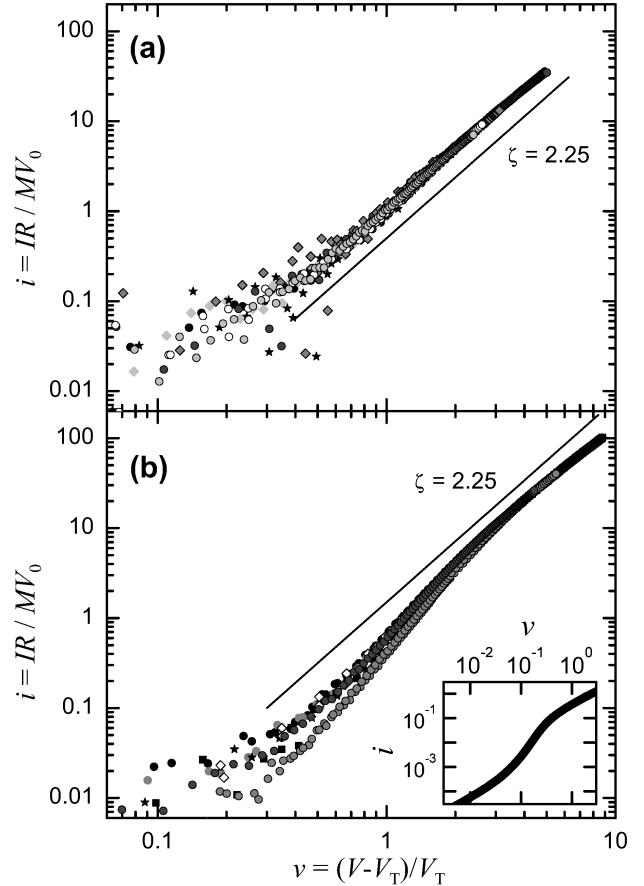


Figure 46. (a) The scaled current i vs voltage ν curves for experimental measurements of charge transport in a uniform gold nanodot array, where V_T is the threshold applied voltage at which conduction becomes finite. Here the current i corresponds to the charge velocity V , while the voltage ν corresponds to the driving force F_D . The line indicates a fit to velocity $V \propto (F_D - F_c)^\beta$ with $\beta = 2.25$. In the figure ζ corresponds to the scaling exponent β . (b) Velocity-force curves for a gold dot array containing large scale voids. There are two scaling regimes, with $\beta = 2.25$ in the higher voltage or large drive regime. Inset: The two-step transport response is also captured in simulations. Reprinted with permission from R. Parthasarathy, X.-M. Lin, and H.M. Jaeger, *Phys. Rev. Lett.* **87**, 186807 (2001). Copyright 2001 by the American Physical Society.

They also found that the charge flows in transverse meandering channels similar to those observed for superconducting vortices above the plastic depinning transition. Figure 45 shows an example of such charge conduction channels just above the plastic depinning threshold from simulations of a 2D metallic dot array [231]. Near depinning thresholds observed in experiments on coupled metallic islands, the velocity scales as $V \propto (F_D - F_c)^\beta$ with $\beta = 1.5$ to $\beta = 2.0$ [232]. Other experiments on GaAs quantum dot arrays reveal a scaling exponent for a single dot of $\beta = 0.5$, consistent with single particle depinning, while in coupled dot arrays, $\beta = 1.47$ [233].

Parthasarathy *et al.* performed experimental

transport studies on monolayers of gold nanocrystals formed into arrays that have either long range order or large scale voids [234]. Figure 46(a) shows the scaling observed in successive velocity-force curves obtained with ordered arrays, which exhibit a finite depinning threshold and a scaling exponent of $\beta = 2.25$, while figure 46(b) shows that an array containing large scale voids has two scaling regimes, with $\beta = 2.25$ at large drives and a lower exponent at low drives. Subsequent simulations [231] of uniform arrays give exponents of $\beta = 1.94$ for 2D arrays and $\beta = 1.0$ for 1D arrays, while systems with large voids exhibit two scaling regimes. At small drives in the void system, $\beta = 1.0$ and the charges flow through a sparse array of static 1D channels that avoid the voids, placing the system in an effectively 1D regime for which Middleton and Wingreen predicted an exponent $\beta = 1.0$ [5]. At higher drives, the flow in the void system becomes fully 2D, producing a larger value of β . The simulation work in [231] also showed a transition as a function of increasing drive from meandering plastic flow channels at low drives to a coherent flow of effectively 1D chains of charges along the arrays at high drives. This transition is associated with a change from broad band velocity or conductance fluctuation noise at low drives to narrow band noise at higher drives; however, there have been no experiments to confirm whether such a dynamical transition to a coherent flow occurs in actual metallic dot arrays. Additionally, it is not clear if there is universality in the scaling exponents for the plastic depinning. Several experiments on dot arrays show discontinuous and hysteretic behavior in the velocity-force curves [233, 235] which have not been captured in simulations. It is possible that such effects arise from the spatial ordering of the dot array itself, and that they correspond to features associated with periodic pinning arrays rather than with disordered pinning. If so, additional elements such as time-dependent dissipation or local heating effects would need to be added to the simulation models in order to capture these behaviors.

As advances in nanotechnology continue, greater control over the topology and disorder of the dots should be achievable, making it possible to carefully tune the pinning effect as well as to control longer-range correlations and monitor local dissipation effects. An understanding of how to control charge flows through tailored dot array geometries would be important for certain applications of these devices. Future work in this field could include studying the driven dynamics of fully 3D coupled dot arrays with and without layering effects [236].

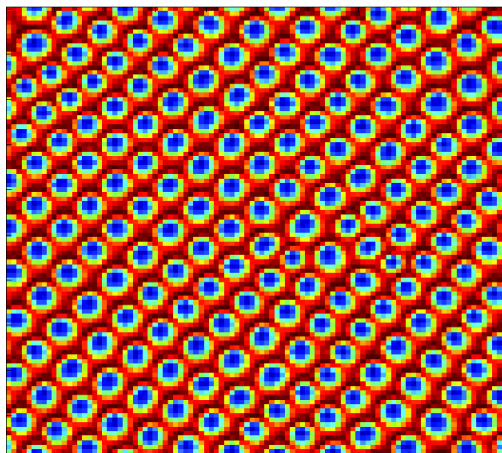


Figure 47. A continuum simulation of a skyrmion lattice in the absence of a substrate. The skyrmions form a triangular lattice similar to the Abrikosov lattice observed for superconducting vortices. Reprinted with permission from S.-Z. Lin, C. Reichhardt, C.D. Batista, and A. Saxena, *Phys. Rev. Lett.* **110**, 207202 (2013). Copyright 2013 by the American Physical Society.

9. Depinning and Dynamics of Skyrmions

In the systems described in the preceding Sections, the equation of motion is dominated by overdamped dynamics; however, other terms such as inertia or Magnus terms can become relevant in certain instances. Recently it was discovered that chiral magnets can support skyrmion states, composed of magnetic excitations called skyrmions that have particle-like properties and that can form a triangular lattice similar to that observed for superconducting vortices [237, 238, 239]. Since this initial discovery, a growing number of compounds have been identified that support skyrmions, including some at room temperature [239, 240, 241, 242]. Skyrmions also hold promise for a variety of applications including magnetic storage, memory, and magnetic logic devices [243]. Skyrmions have many similarities to vortices in superconductors in that they are both particle-like objects with repulsive interactions that favor formation of a triangular lattice, as illustrated in figure 47 [244]. Additionally, both skyrmions and vortices can be driven with an applied current and exhibit depinning transitions [239, 245, 246, 247, 248]. The velocity of superconducting vortices can be determined based on the magnitude of the voltage response induced by their motion; however, the skyrmion velocity produces no voltage drop and cannot be measured so easily. The motion of skyrmions does, however, produce changes in the measured Hall response, and from these changes it is possible to determine the depinning threshold and construct a skyrmion velocity-force curve [239, 246, 249]. Skyrmion motion under

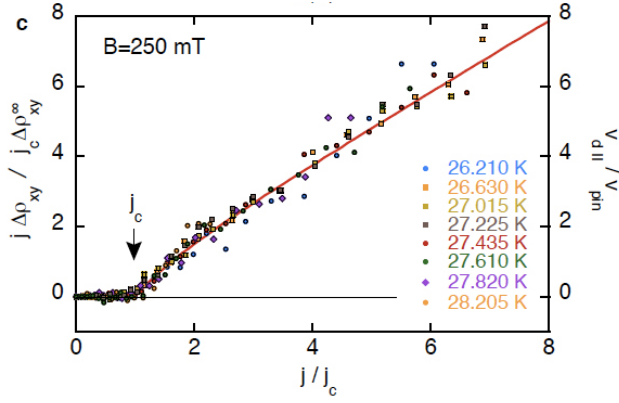


Figure 48. Experimental measurements obtained at different temperatures of effective skyrmion velocity deduced from changes $\Delta\rho_{xy}$ in the Hall resistance versus driving current j/j_c scaled by the critical depinning current j_c , showing a finite depinning threshold and a sliding phase. Here the change in the Hall resistance $\Delta\rho_{xy}$ corresponds to the velocity V , the driving current j corresponds to the driving force F_D , and the critical current j_c corresponds to the depinning threshold F_c . Reprinted with permission from Macmillan Publishers Ltd: Nature Physics, T. Schulz, R. Rita, A. Bauer, M. Halder, M. Wagner, C. Franz, C. Pfleiderer, K. Everschor, M. Garst, and A. Rosch, Nature Phys. **8**, 301 (2012), copyright 2012.

an applied drive can also be directly visualized using Lorentz microscopy [247, 250]. Figure 48 shows an experimentally measured effective skyrmion velocity-force curve for several different temperatures, where the x -axis has been scaled by the depinning threshold. There is a clear finite depinning threshold along with a nonlinear feature near depinning, while at higher drives the velocity increases linearly with drive [246].

Due to the topological nature of skyrmions, their dynamics is dominated by a Magnus term which induces a velocity component that is perpendicular to the net force acting on the skyrmion [239, 246, 248, 251, 252]. In simulation studies using a continuum model of skyrmions based on a Landau-Lifshitz-Gilbert equation, it was argued that the Magnus term causes skyrmions to deflect around attractive pinning sites rather than falling into them, producing a reduction of the depinning threshold compared to that observed in overdamped systems [248]. Lin *et al.* [251] introduced a 2D particle model for skyrmions based on Theile's equation [253] that includes skyrmion-skyrmion interactions and pinning effects. In this model, the dynamics of a skyrmion i is governed by the following equation of motion:

$$\alpha_d \mathbf{v}_i + \alpha_m \hat{z} \times \mathbf{v}_i = \mathbf{F}_i^{ss} + \mathbf{F}_i^{sp} + \mathbf{F}^D, \quad (9)$$

where \mathbf{v}_i is the skyrmion velocity, α_d is the dissipative term that aligns the skyrmion velocity with the net force, α_m is the Magnus term which rotates the skyrmion velocity into the direction perpendicular to the net force, \mathbf{F}_i^{ss} is the skyrmion-skyrmion repulsive

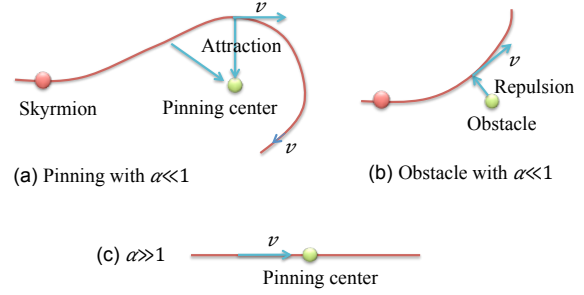


Figure 49. (a,b) A schematic of a skyrmion system in which the Magnus term α_m dominates the dissipative term α_d . Here the ratio of the two terms is written as $\alpha = \alpha_d/\alpha_m$. The skyrmion is shown interacting with an attractive (a) and repulsive (b) pinning site. For the attractive pinning site, the Magnus term generates a velocity component that is perpendicular to the attractive force of the pinning site, causing the skyrmion to spiral around the pinning site rather than becoming trapped. (c) In the overdamped limit with $\alpha \gg 1$, a particle interacting with an attractive pinning site travels directly to the center of the pinning site and becomes trapped. Reprinted with permission from S.-Z. Lin, C. Reichhardt, C.D. Batista, and A. Saxena, Phys. Rev. B **87**, 214419 (2013). Copyright 2013 by the American Physical Society.

interaction of Bessel function form which favors triangular ordering, \mathbf{F}_i^{sp} is the pinning force, and \mathbf{F}^D is the external dc driving force. In most superconducting systems, $\alpha_m/\alpha_d \ll 1.0$; however, in skyrmion systems $\alpha_m/\alpha_d = 10$ to 40. In most of the experimental studies performed so far, the skyrmions are in the clean limit and form ordered triangular lattices. More recent studies in thin films show evidence of stronger pinning that permits a coexistence between pinned and moving skyrmions, allowing plastic depinning to occur [240, 242]. The Magnus term can alter the depinning transition in many ways. For example, the Magnus term introduces a strong time dependence to the dynamics, so that a skyrmion entering a pinning site undergoes a spiraling motion, illustrated schematically in figure 49(a). This is in contrast to the behavior of overdamped particles such as vortices, which simply travel directly to the bottom of the pinning potential, as shown schematically in figure 49(c) [251]. The Magnus term can also cause a skyrmion that passes through a pinning site to undergo what is called a side jump, in which skyrmion trajectories entering one half of the pinning site are more strongly deflected than those entering the other half [50, 252].

The spiraling motion of skyrmions and the capture probabilities for different types of pinning sites have been studied in various continuum and particle based models [252, 254] and observed in experiments [31]. Reichhardt *et al.* [50] conducted particle-based simulations of skyrmions interacting with random pinning under the Magnus-dominated condition $\alpha_m/\alpha_d = 10$. Figure 50(a) shows the

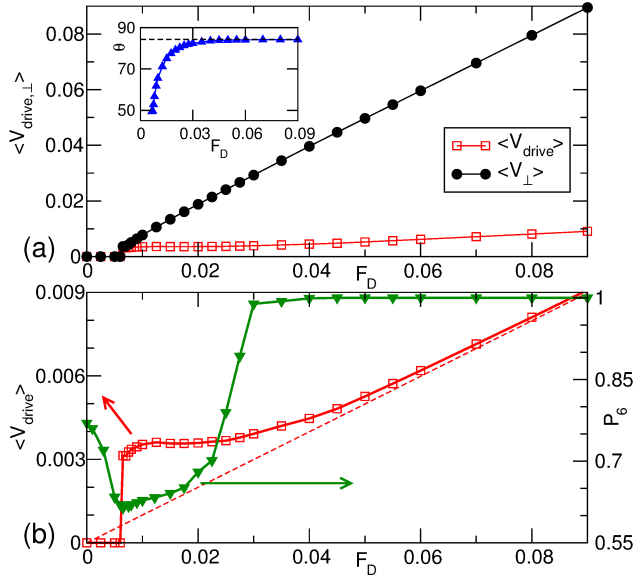


Figure 50. Average skyrmion velocity in the direction of the drive $\langle V_{\text{drive}} \rangle$ (open squares) and perpendicular to the drive $\langle V_{\perp} \rangle$ (filled circles) vs driving force F_D from 2D particle-based simulations of skyrmions in the strong Magnus regime $\alpha_m/\alpha_d = 10$ interacting with randomly placed pinning sites. The inset shows the Hall angle θ vs F_D ; the dotted line indicates the value of the Hall angle in a clean, substrate-free system. (b) The corresponding $\langle V_{\text{drive}} \rangle$ (open squares) and the fraction of sixfold coordinated particles P_6 (filled triangles) vs F_D , where the dashed line indicates the results from a clean system. A dynamical reordering transition occurs at $F_D = 0.03$. Here $\langle V_{\text{drive}} \rangle$ corresponds to the velocity V or V_x in the driving direction, and $\langle V_{\perp} \rangle$ corresponds to the velocity V_y perpendicular to the driving direction. Adapted with permission from C. Reichhardt, D. Ray, and C.J. Olson Reichhardt, Phys. Rev. Lett. **114**, 217202 (2015). Copyright 2015 by the American Physical Society.

skyrmion velocity in the direction of drive, V or V_x , and perpendicular to the drive, V_y , versus driving force F_D in the strong pinning limit where the depinning is plastic. There is a finite depinning threshold and $V_x \ll V_y$ due to the Magnus term, which produces a Hall angle in the substrate-free limit of $\theta = \tan^{-1}(\alpha_m/\alpha_d) = 84.25$, meaning that the skyrmions move nearly perpendicular to the direction of the net force acting on them. The inset of figure 50(a) shows the measured Hall angle $\theta = \tan^{-1}(V_y/V_x)$ versus F_D , where the dashed line indicates the value of θ in the clean limit. The Hall angle has a strong drive dependence due to the side jump effect induced by the pinning, with the size of the side jumps decreasing with increasing F_D . The changing Hall angle indicates that the net direction of the skyrmion flow is changing as a function of drive. In figure 50(b), the corresponding fraction of sixfold coordinated skyrmions P_6 versus F_D indicates that the system is the most disordered just above the depinning transition, and that a dynamical reordering transition to a nearly defect-free state occurs

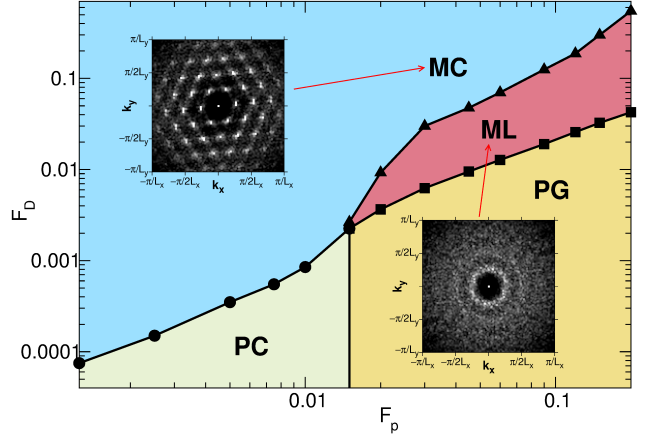


Figure 51. Simulated dynamic phase diagram for the skyrmion system from figure 50 as a function of driving force F_D vs pinning force F_p . PC: pinned crystal phase; PG: pinned glass phase; ML: moving liquid phase; MC: moving crystal phase. Insets show the structure factor $S(\mathbf{k})$ calculated in the moving crystal (upper left) and moving liquid (lower right) phases. Adapted with permission from C. Reichhardt, D. Ray, and C.J. Olson Reichhardt, Phys. Rev. Lett. **114**, 217202 (2015). Copyright 2015 by the American Physical Society.

at high drive, as shown by the increase in P_6 to $P_6 = 1.0$ near $F_D = 0.3$. Figure 50(b) also contains a plot of V_x versus F_D where the dashed line indicates the behavior expected in the clean limit. The depinning transition is discontinuous, and the skyrmion velocities are *larger* than the clean limit values due to an overshoot or pinning-induced speed-up effect. Such behavior never occurs in overdamped inertia-free systems. Speed-up effects have also been observed for the depinning of single skyrmions from pinning sites, and are generated when the Magnus term rotates the velocity component induced by the pinning into the velocity component induced by the drive [252, 255].

Figure 51 illustrates the dynamical phase diagram as a function of driving force F_D versus pinning strength F_p for the system in figure 50. At low F_p and low F_D , there is a pinned skyrmion crystal that depins elastically with increasing drive into a moving skyrmion crystal. As the pinning strength increases, there is a critical value F_p^c at which topological defects proliferate in the pinned phase and the system depins plastically into a liquid like state, as indicated by the plot of $S(\mathbf{k})$ in the lower inset of figure 50. At higher drives, dynamical reordering occurs into a moving crystal phase free of dislocations, as shown by the six-fold ordering of $S(\mathbf{k})$ plotted in the upper inset of figure 50. A difference between the dynamically ordered skyrmion phases and the dynamically ordered vortex phases is that the skyrmions order into an isotropic moving crystal rather than into a moving smectic state, since

the shaking temperature induced in the presence of a strong Magnus term is distinct from the shaking temperature produced in the overdamped limit. In the moving phase in superconducting vortex systems, the pinning generates vortex velocity fluctuations that are stronger in the direction of drive than perpendicular to the drive, while for skyrmion systems, the Magnus term causes the velocity fluctuations induced by the pinning to be more isotropic.

The study of the collective dynamics of skyrmions is still in its infancy, and potentially represents an entirely new field of Magnus-dominated collective dynamical phases. Open questions include whether the Magnus term changes the scaling behaviors at elastic or plastic depinning transitions compared to the overdamped limit. The plastic flow itself could have different properties when the Magnus term dominates than in overdamped systems, and the velocity noise fluctuations in the plastic flow and/or the moving ordered phases could be different from those observed in overdamped systems. In 3D systems, skyrmions form line-like objects similar to vortex lines, so it would also be interesting to study the 3D dynamical plastic flow of skyrmions when the Magnus term is important. Another direction of study is to consider skyrmions moving through periodic pinning arrays, which could be created with various nanostructuring techniques. Simulations of individual skyrmions moving over 2D periodic [256] and 1D periodic [257] substrates show threshold behavior, directional locking, and Shapiro steps that have features distinct from the overdamped case, so it would be interesting to explore the behavior of collectively interacting skyrmions moving on periodic pinning arrays. The Magnus term could affect thermal creep, the velocity-force curves [258], and avalanche behaviors. Some studies have provided evidence that inertial effects may be important for skyrmion dynamics [255], and there is evidence that 3D point-like skyrmion objects could be stabilized in certain systems, which would open up a new class of the dynamics of 3D point-like objects [141].

10. Jamming and Pinning

The jamming of loose assemblies of particles with only contact interactions, such as grains, bubbles, or emulsions, has received considerable attention over the last 15 years since Liu and Nagel proposed a jamming phase diagram in which, at high enough particle density, the particles come into contact and the system transitions from a fluid-like state to a rigid jammed state [259, 260, 261, 262]. The density at which the system begins to support a finite shear is called point J. An appealing feature of this picture is that the physics that describes point J may also

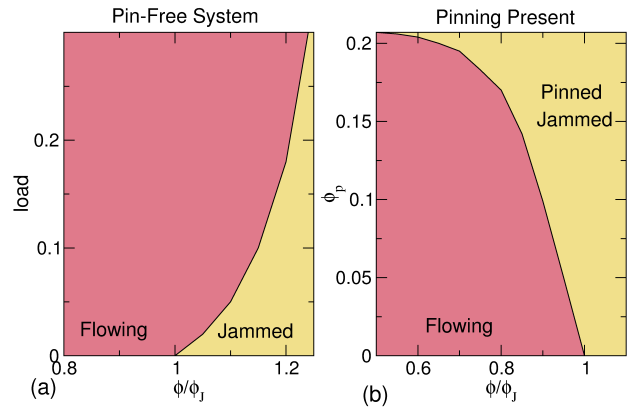


Figure 52. Schematic jamming phase diagrams. (a) In a pin-free system, as a function of load or shear vs particle density ϕ/ϕ_J , jamming occurs for sufficiently large load and sufficiently high ϕ/ϕ_J , where ϕ_J is the density called point J at which the system jams in the absence of load. Jamming occurs only for $\phi/\phi_J \geq 1$. (b) When pinning is present, the particle density at which jamming occurs under zero load drops below $\phi/\phi_J = 1.0$ as the pinning density ϕ_p increases.

describe other phenomena such as the onset of yielding under load or the onset of rigidity as the temperature is lowered. One difference between jamming and depinning is that the jamming transition is controlled solely by the particle-particle interactions and does not involve quenched disorder. Jamming is typically discussed in the context of assemblies of particle-like objects that interact with each other through a short range steric repulsion, making it possible to define a unique particle density at which all the particles have just barely come into contact with each other. In contrast, in most of the systems in which depinning transitions have been studied, even the short-range particle-particle interactions that have been considered are longer range than steric, so that in the absence of pinning the system can act like a crystal or solid down to very low particle densities. Although it is possible for systems containing particles which do not interact with each other to exhibit a depinning transition, such systems cannot exhibit a jamming transition, which is a truly collective effect. These points suggest that depinning and jamming transitions represent quite distinct phenomena; however, there are many cases in which depinning transitions exhibit properties similar to those associated with a jamming transition. For example, in regimes in which there are fewer pinning sites than particles, the entire system can remain pinned even when a driving force is applied due to particle-particle interactions that confine and trap the interstitial particles which are not directly trapped by pinning sites. This resembles a localized jamming effect in which the interstitial particles between the pinning sites act like a solid. In systems where the particle-particle interactions are short-ranged and have

a well-defined cutoff distance, if a random substrate potential is introduced, both jamming and pinning can occur. Examples of such systems include sterically stabilized colloids, bubbles, or grains moving over a rough landscape, and in these systems the interplay between jamming behavior and depinning transitions can be explored.

In figure 52 we illustrate an example of how jamming and pinning can be connected. One of the pairs of axes on the Liu-Nagel phase diagram is particle density ϕ/ϕ_J versus external load [259, 261], as shown schematically in figure 52(a) for a pin-free system. Below the critical jamming density ϕ_J , the system is in a liquidlike state and can flow under any applied load, while for $\phi/\phi_J > 1.0$, a finite load must be applied before the system begins to flow, and the magnitude of this load increases with increasing ϕ/ϕ_J . Adding pinning to the jamming system produces the phase diagram shown schematically in figure 52(b) as a function of pinning site density ϕ_p versus particle density ϕ/ϕ_J at zero load. When $\phi_p = 0$, there are no pins and the system jams only when $\phi/\phi_J \geq 1.0$; however, for finite pinning density, the onset of jamming drops to particle densities $\phi/\phi_J < 1.0$, and a state emerges that is both jammed and pinned. This suggests that a new axis could be added to the jamming phase diagram proposed by Liu and Nagel showing the interplay between jamming and pinning.

Reichhardt *et al.* considered a model of a bidisperse assembly of 2D hard disks interacting with a random pinning array and subjected to a uniform driving force [263]. This system has a well-defined pin-free jamming density corresponding to an areal disk coverage of $\phi = \phi_J = 0.844$. If only a single pinning site is present in the system, the depinning threshold is finite only when $\phi/\phi_J \geq 1$ and the system jams into a solid state that can be held in place by a single obstacle. Depending on the strength of the single pinning site, the depinning transition may be either plastic or elastic. At disk densities $\phi/\phi_J < 1$, the system may or may not exhibit a finite depinning threshold depending on the ratio of the number of pinning sites to the number of disks. Figure 53(a) shows the disk velocity versus applied drive for a sample in which the pinning strength is $F_p = 2.0$ and the pinning density is $\phi_p/\phi_J = 0.415$. At a disk density of $\phi/\phi_J = 0.014$, each disk can be pinned independently since there are many more pinning sites than disks, and the depinning threshold is $F_c = F_p$. At a higher disk density of $\phi/\phi_J = 0.761$, the depinning threshold remains finite even though there are more disks than pinning sites, indicating that the disks trapped directly at the pinning sites are able to block or jam the flow of the interstitial disks and prevent them from moving. Figure 53(c) illustrates the pinned

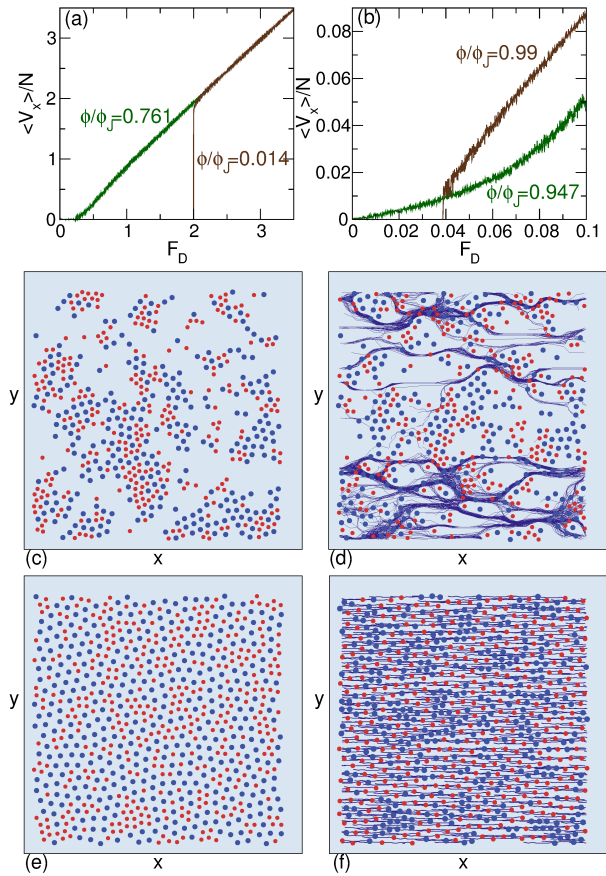


Figure 53. (a,b) Velocity-force curves from simulations of a system of binary hard disks at an area coverage or disk density of ϕ/ϕ_J , where ϕ_J is the pin-free jamming density. Here $\langle V_x \rangle$ corresponds to the velocity V and F_D is the driving force. (a) Samples with a pinning density of $\phi_p/\phi_J = 0.415$. At a disk density of $\phi/\phi_J = 0.014$ (brown), there are more pins than disks and the system is in the single particle pinning limit, while at $\phi/\phi_J = 0.761$ (green) a pinned jammed configuration appears. (b) Samples with sparse pinning at a density of $\phi_p/\phi_J = 0.09$. There is no depinning threshold at $\phi/\phi_J = 0.947$ (green), while at $\phi/\phi_J = 0.99$ (brown) a finite depinning threshold appears. (c,d) The pinned (c) and flowing (d) configurations for the system in panel (a) at $\phi/\phi_J = 0.761$, showing plastic depinning. The two sizes of disks are indicated by two sizes and colors of dots, while lines show the disk trajectories in the flowing state. (e,f) The pinned (e) and flowing (f) configurations for the system in panel (b) at $\phi/\phi_J = 0.99$, showing elastic depinning. Adapted with permission from C.J. Olson Reichhardt, E. Groopman, Z. Nussinov, and C. Reichhardt, *Phys. Rev. E* **86**, 061301 (2012). Copyright 2012 by the American Physical Society.

state for the $\phi/\phi_J = 0.761$ sample from figure 53(a), showing that the pinned state is strongly clustered. The local disk density is equal to ϕ_J within each cluster and there are large disk-free regions between clusters. Under an applied drive, the system depins plastically as illustrated in figure 53(d). If the density of pinning sites is reduced, the depinning threshold vanishes but the velocity-force curve can still show nonlinearity, as shown in figure 53(b) for samples in which there are

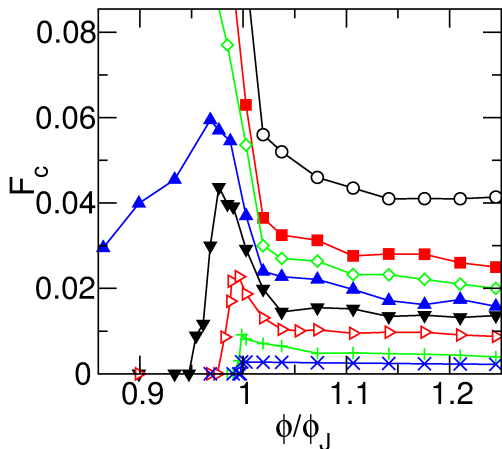


Figure 54. The depinning threshold F_c vs disk density ϕ/ϕ_J for simulations of the system in Figure 53 at pinning densities of $\phi_p/\phi_J = 0.828, 0.415, 0.277, 0.138, 0.09267, 0.0346, 0.00692,$ and 0.00138 , from top to bottom. For ϕ/ϕ_J below the peak in F_c , the disks depin plastically, while for ϕ/ϕ_J above the peak in F_c , the disks depin elastically. Adapted with permission from C.J. Olson Reichhardt, E. Groopman, Z. Nussinov, and C. Reichhardt, Phys. Rev. E **86**, 061301 (2012). Copyright 2012 by the American Physical Society.

only a small number of pinning sites present, $\phi_p/\phi_J = 0.09$. Here, the depinning threshold is zero when the disk density $\phi/\phi_J = 0.947$ but the velocity-force curve is nonlinear, indicating that plastic flow is occurring. In contrast, at $\phi/\phi_J = 0.99$, the depinning threshold is finite and the system forms a uniform pinned solid, shown in figure 53(e), which depins elastically into the uniform moving state illustrated in figure 53(f). These results show that elastic jammed solids can in some cases show a finite depinning threshold, while liquidlike states do not.

Figure 54 shows the evolution of the depinning threshold F_c as a function of ϕ/ϕ_J for varied pinning densities ranging from $\phi_p/\phi_J = 0.828$ to $\phi_p/\phi_J = 0.00138$. For the low pinning densities, the depinning threshold $F_c = 0$. There is a peak in F_c at ϕ^* just below $\phi/\phi_J = 1.0$. For disk densities $\phi/\phi_J < \phi^*$, the disks depin plastically, while for $\phi/\phi_J > \phi^*$, the disks depin elastically. For $\phi_p/\phi_J > 0.3$, the depinning threshold is always finite, and F_c is much higher at particle densities $\phi/\phi_J < 1$ below the jamming density than for $\phi/\phi_J > 1$, above the jamming density. Other numerical studies also show that the introduction of a small number of pinning sites can reduce the disk density at which jamming occurs [264].

Relatively little work has been done on connecting jamming and depinning, leaving the field wide open with a range of topics for further study. Since critical properties are associated with point J, it would be interesting to understand whether the pinning-induced jamming that occurs at densities below point

J preserves these critical properties or destroys them. Another open question is whether dynamical ordering transitions are possible in pinned jamming systems when the jamming density has been depressed below point J, since in principle the system could organize to a state in which the particles do not interact with each other.

11. Dynamics of Driven Systems with Competing Interactions

In the systems discussed in the preceding Sections, the particle-particle interactions are purely repulsive, so that in monodisperse 2D samples in the clean limit, the ground states have triangular ordering. A natural question to ask is whether collections of particles with different types of clean limit ground states can exhibit similar nonequilibrium dynamical phases, or if entirely new types of phases can arise. In one such class of system, the interactions between the particles includes a competition between a long-range repulsion and a short-range attraction. In the absence of quenched disorder, systems of this type are known to form a rich variety of crystalline, bubble, stripe, void crystal, and densely packed triangular states [265]. In soft matter systems, patterns of this type can arise in colloidal assemblies, phase separating mixtures, and binary fluids [265]. In hard condensed matter systems, pattern formation is relevant for stripes in quantum Hall systems [266], charge ordering in cuprates [267, 268], pattern formation in systems with Jahn-Teller interactions [269], flux states in type-I superconductors [270], and vortices in in multiband superconductors [271, 272, 273, 274, 275]. In quantum Hall systems, the existence of stripe crystals instead of Wigner crystals has been proposed to explain the strongly anisotropic transport found at certain magnetic fields [276], as well as narrow band noise fluctuations [277] and the hysteresis in certain transport measurements [278].

11.1. Pairwise competing interactions

As an example of a pattern forming system, Reichhardt *et al.* [9, 279] considered a model in which the particle-particle interaction contains a long-range Coulomb repulsion combined with a short-range attractive term. The interaction energy for particles located a distance R_{ij} apart has the following form:

$$U(R_{ij}) = \frac{1}{R_{ij}} - e^{-BR_{ij}}. \quad (10)$$

A clump crystal forms at low particle densities, with the particles forming a triangular lattice within each clump and the clumps themselves forming a larger scale triangular lattice due to the long-range repulsive interaction term. At intermediate particle densities, a

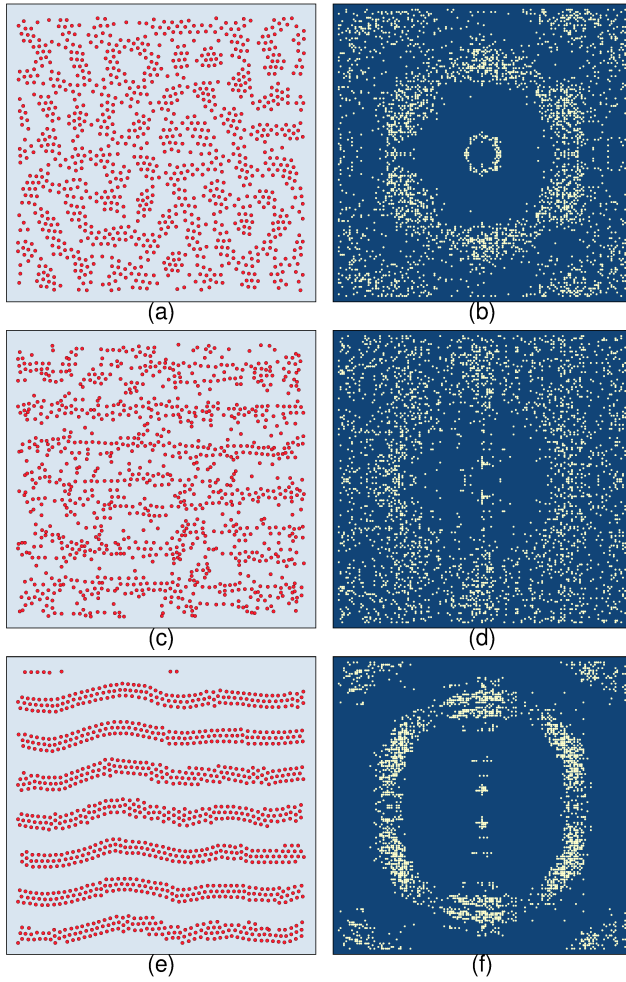


Figure 55. Simulations of a pattern-forming system in which the particles have a competing long-range repulsion and short-range attraction and are driven over a random pinning array. (a,c,e) The particle positions (dots) and (b,d,f) the corresponding structure factor $S(\mathbf{k})$. (a,b) In the pinned state the particles form disordered clumps. (c,d) Just above depinning, the structure is further disordered. (e,f) The dynamically reordered stripe phase at high drives. Adapted with permission from C. Reichhardt, C.J. Olson Reichhardt, I. Martin, and A.R. Bishop, Phys. Rev. Lett. **90**, 026401 (2003). Copyright 2003 by the American Physical Society.

stripe phase forms, and a void crystal appears at higher particle densities [279]. If weak pinning is added to the stripe phase, the stripe ordering can be preserved. In the presence of strong pinning, however, the stripes break up and the system forms an amorphous phase that still exhibits two length scales [9], as illustrated in figure 55(a). The corresponding structure factor $S(\mathbf{k})$ in figure 55(b) has two rings since disordered structures appear at the two characteristic length scales of the distance between particles within individual clumps and the average spacing between clumps. If a driving force is applied along the positive x direction, there is a finite depinning threshold. Just above depinning,

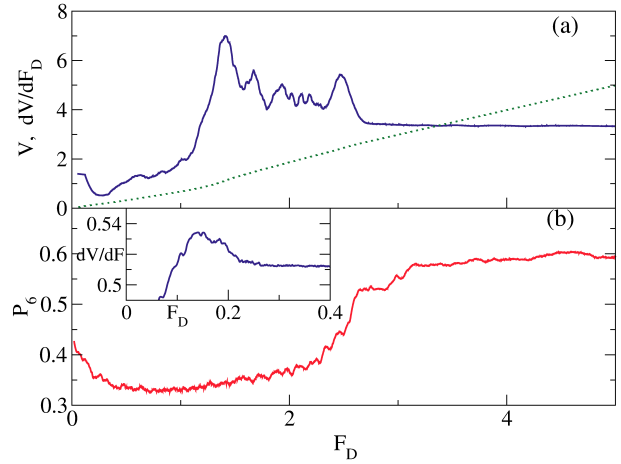


Figure 56. (a) Velocity-force curve (dashed line) for simulations of the stripe forming system in figure 55 and the corresponding dV/dF_D curve (solid line), which shows a two peak feature. (b) The corresponding fraction of six-fold particles P_6 vs F_D . Inset: dV/dF_D vs F_D for a sample with weak pinning has only a single peak. Adapted with permission from C. Reichhardt, C.J. Olson Reichhardt, I. Martin, and A.R. Bishop, Phys. Rev. Lett. **90**, 026401 (2003). Copyright 2003 by the American Physical Society.

the system becomes even more disordered as shown in figure 55(c), and some particles form 1D channels along the drive direction, producing faint smectic-like peaks in $S(\mathbf{k})$ in figure 55(d). At higher drives, the system dynamically orders into a moving stripe phase that resembles the static stripe state in a sample without disorder, except that the stripes are aligned with the driving direction as illustrated in figure 55(e,f).

Figure 56(a) shows the velocity-force curve for the stripe state on a strong random substrate along with dV/dF_D . There are two peaks in dV/dF_D rather than the single peak typically found for systems with purely repulsive particle-particle interactions. The double peak feature arises due to the two length scales in the system. At the first peak in dV/dF_D , there is a dynamical transition to clump ordering, while at the second peak in dV/dF_D , the system dynamically orders into the aligned stripe state illustrated in figure 55(e). A plot of the fraction of six-fold coordinated particles P_6 versus F_D in figure 56(b) shows that P_6 begins to increase at the first peak in dV/dF_D but remains at a low value since, even though clumps are beginning to form, the particles within each clump are still disordered. Near the second peak in dV/dF_D , there is a jump up in P_6 that occurs when the stripes form, since the particles within the stripes have a considerable amount of sixfold ordering, as illustrated in figure 55(e,f). The inset of figure 56(b) shows that when the pinning is weak, there is only one peak in dV/dF_D . At this weaker pinning, the stripes do not

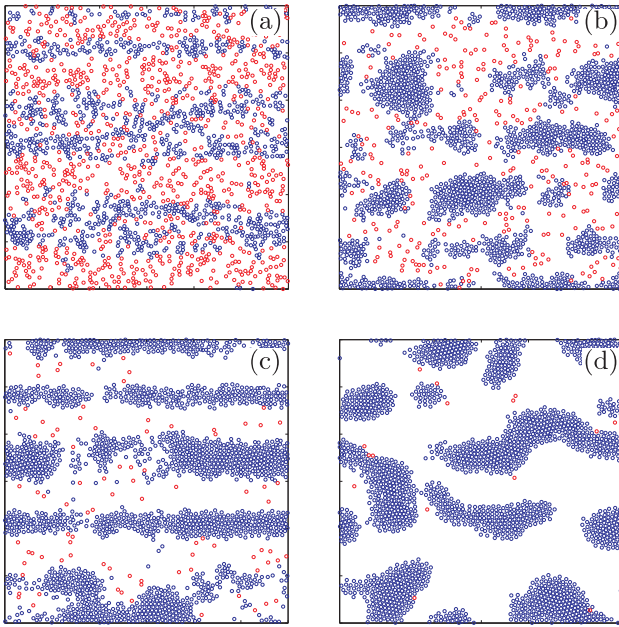


Figure 57. The particle positions for simulations of a system in which the particles interact with a short-range repulsion and a long-range attraction and are driven over a random pinning array. Red particles are pinned and blue particles are moving. The driving force increases from (a) to (d). (a) The disordered flow phase just above depinning. (b) Depinned clusters. (c) Moving stripes. (d) Cluster coarsening regime. Reprinted with permission from H.J. Zhao, V.R. Misko, and F.M. Peeters, *Phys. Rev. E* **88**, 022914 (2013). Copyright 2013 by the American Physical Society.

break up when placed on the disordered substrate; however, some plastic flow occurs within the stripes at drives above depinning, while at high enough drives the particles within the stripes order. These results show that in systems with multiple length scales, multiple dynamical ordering transitions can occur at well-separated drives.

Pattern forming systems exhibit strong hysteresis in the velocity-force curves, with the reordered stripe state persisting on the decreasing drive sweep down to drives that are much lower than the drive at which dynamical reordering into the stripe state occurs for an increasing drive sweep. Further studies show that hysteresis also occurs as a function of particle density for systems of driven clump crystals, stripes, and void crystals whenever two length scales come into play [280]. At very low densities where the particle-particle interactions are dominated by the long-range repulsive term, there is no hysteresis, and similarly at very high densities where the system forms a dense triangular lattice that is also dominated by the long-range repulsive term, there is no hysteresis. Simulations also show that anisotropic transport in the stripe phase appears only at low pinning strengths for which the stripes remain ordered above the depinning transition

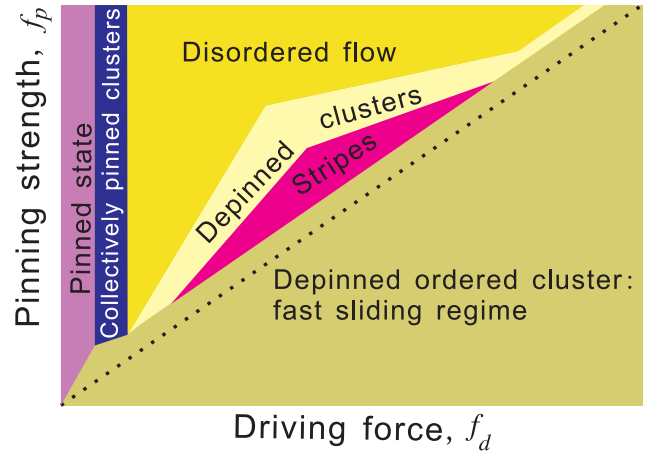


Figure 58. Schematic dynamic phase diagram for the pattern forming system in figure 57 as a function of pinning strength f_p vs driving force f_d showing a pinned phase, collectively pinned clusters, a disordered phase, depinned clusters, stripes, and a rapidly sliding cluster regime. Here f_p corresponds to the pinning strength F_p and f_d corresponds to the driving force F_D . Reprinted with permission from H.J. Zhao, V.R. Misko, and F.M. Peeters, *Phys. Rev. E* **88**, 022914 (2013). Copyright 2013 by the American Physical Society.

[281]. These results suggest that the appearance of hysteresis in the quantum Hall systems could be due to the formation of stripe or bubble states rather than Wigner crystals. Other simulations of colloidal systems with competing short range attraction and longer range repulsion show dynamical ordering transitions to aligned stripe phases [282]. Experiments on 2DEGs in regimes where stripes are believed to form show evidence of dynamical ordering of stripes along the direction of drive associated with a memory of the drive direction in the dynamically ordered stripe state [283].

Zhao *et al.* [284] studied the dynamical flow and ordering in pattern forming systems where the particles have a short range repulsion and a longer range attraction. In the absence of pinning, the system forms clump or labyrinth states. For strong disorder, a uniform disordered state appears as shown in figure 57(a). Under an applied drive, the particle flow just above depinning is plastic and occurs in a riverlike pattern. At higher drives, as illustrated in figure 57(b), there is a regime in which depinned clumps flow through a background of pinned particles, while at even higher drives, the clumps dynamically align into a stripe-like state as shown in figure 57(c). At the highest drives, these clumps coarsen as shown in figure 57(d). A schematic dynamic phase diagram for this system appears in figure 58 as a function of pinning force F_p versus applied drive F_D . The dashed line denotes the drive at which the clumps dynamically order. For weak pinning, the pinned clumps depin elastically into a moving clump phase; however, for stronger pinning, the system passes through a pinned

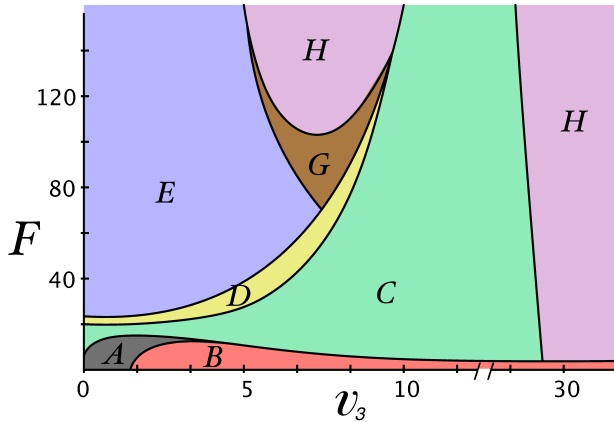


Figure 59. Schematic dynamic phase diagram as a function of driving force F vs the strength of the three-body interaction term v_3 for a system with a two-body repulsive force and a three-body interaction term that favors square ordering. A: pinned triangular lattice, B: pinned square lattice, C: plastic flow, D: anisotropic triangular lattice, E: moving triangular lattice, H: moving square lattice, G: coexistence between moving square and moving triangular lattice. Here F corresponds to the driving force F_D . Reprinted with permission from A. Sengupta, S. Sengupta, and G.I. Menon, *Phys. Rev. B* **81**, 144521 (2010). Copyright 2010 by the American Physical Society.

phase, a disordered plastic phase, a depinned cluster phase, a stripe phase, and finally a sliding phase as a function of increasing drive. The transport curves for this system have two peaks in dV/dF_D as well as hysteresis. Other studies of systems with long range attraction and short range repulsion also reveal a similar set of dynamical phases as well as the double peak feature in the dV/dF_D curves, and show that when periodic rather than random pinning is introduced, the stripe phases generally become more ordered [285]. These results underscore the fact that the double peak feature in dV/dF_D is associated with multiple ordering transitions. The appearance of hysteresis is also similar to that observed in 3D layered superconducting vortex systems, where the layering provides the additional length scale required to generate the hysteresis. Simulation studies of a 2D system with long-range repulsion and short range attractions also reveal a peak effect similar to that observed in the 3D vortex systems [286].

Stripes and other types of patterns can also form in systems with purely repulsive interactions provided that there are multiple length scales in the interaction potential. In general, such patterns occur whenever the Fourier transform of the particle-particle interaction potential has a negative peak in \mathbf{k} -space [287], so that even a simple two-step repulsive shoulder interaction potential can produce a remarkable number of patterned mesophases in 2D [288, 289]. There is also evidence that purely repulsive interactions with

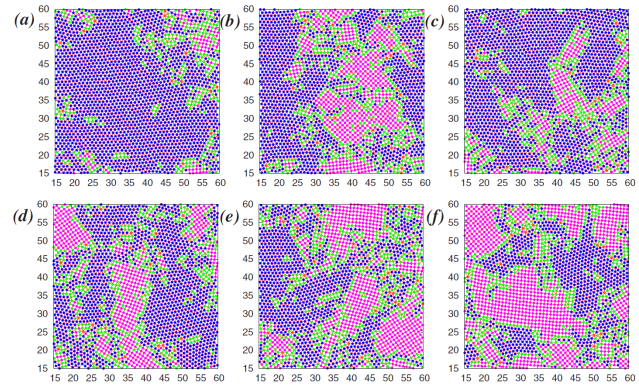


Figure 60. Snapshots of the dynamical evolution of the moving triangular lattice phase (phase E) into the coexistence regime (phase G) for the three-body competing interaction system in figure 59 for increasing driving forces of $F =$ (a) 90, (b) 95, (c) 100, (d) 105, (e) 110, and (f) 115. The particles are colored according to their coordination number z_i with $z_i = 4$ (magenta), 5 (green), 6 (blue) and 7 (orange). Here F corresponds to the driving force F_D . Reprinted with permission from A. Sengupta, S. Sengupta, and G.I. Menon, *Phys. Rev. B* **81**, 144521 (2010). Copyright 2010 by the American Physical Society.

two length scales can produce stripelike vortex patterns in certain types of superconductors [290]. Up until now, studies of pattern forming systems driven over random substrates have involved systems in which the competing repulsive and attractive interactions are explicit in the real space form of the particle-particle interaction potential. It would be interesting to study whether systems with purely repulsive interactions that have two or multiple length scales would also exhibit the same general dynamical ordering and hysteresis. The ordering and dynamics of pattern forming systems on periodic substrates, about which little is known, would be another interesting direction for future study.

11.2. Non-pairwise competing interactions

Non-pairwise interactions or three-body effects can also lead to the formation of patterns [291]. Interactions of this type can arise for particles coupled to a deformable substrate or particles that are hydrodynamically coupled. Sengupta *et al.* [292, 293] considered a system of repulsively interacting particles containing an additional three-body interaction term with fourfold symmetry that favors a square lattice ground state, so that a transition from a triangular lattice to a square lattice can occur as a function of the strength v_3 of the three-body term. A schematic dynamic phase diagram in figure 59 of this system in the presence of pinning as a function of driving force F_D versus v_3 shows that a rich variety of dynamical flow phases occur, including a pinned triangular lattice at small

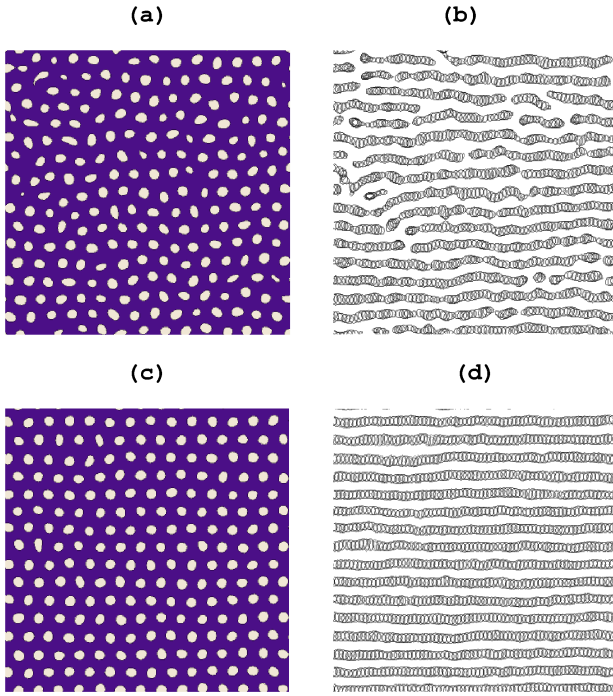


Figure 61. Phase field simulation studies of a system that forms a triangular lattice in the clean ground state driven over random disorder. (a,c) Snapshots of the phase field $\Psi(\mathbf{x})$ and (b,d) the trajectories of the peaks in $\Psi(\mathbf{x})$ in the moving state. (a,b) The moving liquidlike state at a drive of $f = 0.2$. (c,d) The moving smectic state at a drive of $f = 0.8$. Here f corresponds to the driving force F_D . Reprinted with permission from E. Granato, J.A.P. Ramos, C.V. Achim, J. Lehtikoinen, S.C. Ying, T. Ala-Nissila, and K.R. Elder, Phys. Rev. E **84**, 031102 (2011). Copyright 2011 by the American Physical Society.

v_3 , a pinned square lattice at higher v_3 , a plastic flow phase, an anisotropic hexatic phase, a moving triangular lattice, a coexistence regime, and a flowing square lattice regime. Figure 60 shows the evolution of the triangular lattice into a regime of coexisting square and triangular lattices as a function of increasing drive. The system is initially mostly triangular, but regions of square ordering form and grow as the drive increases.

11.3. Phase field models

Pattern forming systems can also be studied using phase field models [294], which describe the particle density $\Psi(\mathbf{x})$ on a diffuse time scale rather than a real microscopic time scale. Such methods are computationally efficient and have been used to study longitudinal and transverse depinning as well as the scaling of velocity-force curves for pattern forming systems on periodic substrates [295]. Granato *et al.* [296] used a phase field model to study a system that forms a triangular lattice in the clean ground state. Nonlinear velocity-force curves appear when the system is driven over random disorder, along with a

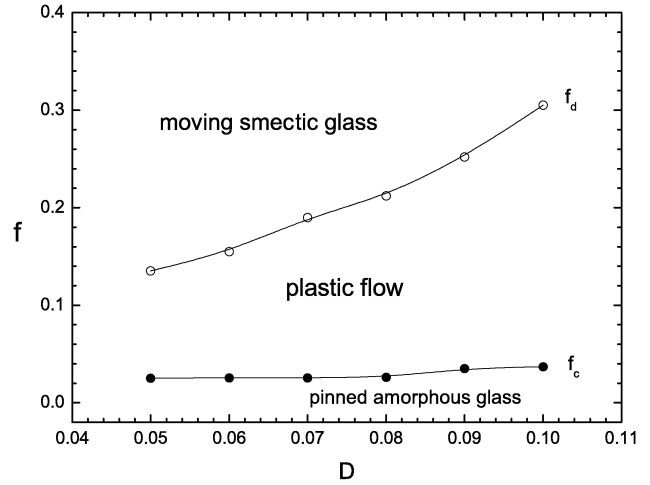


Figure 62. The simulated dynamic phase diagram for the phase field model from figure 61 as a function of external drive f versus disorder strength D showing a pinned phase, plastic flow phase, and moving smectic phase. Here f corresponds to the driving force F_D and D corresponds to the pinning strength F_p . Solid circles are the depinning threshold f_c which corresponds to F_c , while open circles indicate the dynamical reordering transition. Reprinted with permission from E. Granato, J.A.P. Ramos, C.V. Achim, J. Lehtikoinen, S.C. Ying, T. Ala-Nissila, and K.R. Elder, Phys. Rev. E **84**, 031102 (2011). Copyright 2011 by the American Physical Society.

transition from a pinned state to the plastic flow phase shown in figure 61(a,b) and a transition at higher drives to the smectic flow state illustrated in figure 61(c,d). The dynamical phase diagram in figure 62 highlights the different flow phases as a function of driving force F_D versus pinning strength F_p . Within the moving smectic phase Granato *et al.* observe a finite transverse depinning threshold; however, this threshold decreases with increasing system size, suggesting that it may vanish in the thermodynamic limit. It should be possible to use similar phase field models for systems in which the ground state consists of stripes or other patterns to study 2D and 3D pattern forming systems driven over periodic or random substrates.

11.4. Driven binary systems

In addition to systems with competing interactions, there are also examples of pattern forming binary systems that can demix over time. It would be interesting to study the dynamics of such systems when they are driven over random disorder. For example, in the case of binary colloidal systems, 2D simulations of Yukawa interacting particles that have different effective charges show that in the pinned state, the two species of particles are mixed and form a disordered structure, but that at higher drives, the system can order into a segregated state [297]. Figure 63(a) shows an example of the pinned mixed phase for this system,

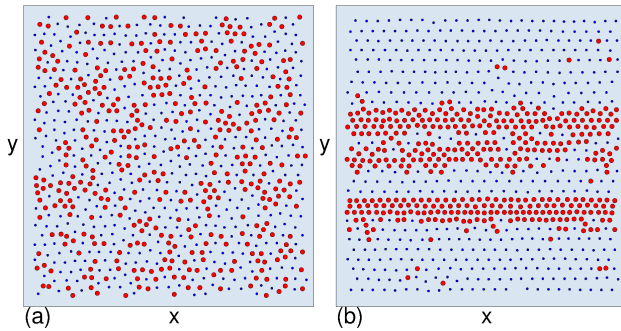


Figure 63. Simulation of a binary assembly of Yukawa interacting particles driven over random disorder. The two different particle species have different effective charges. The smaller red particles are more strongly charged and the larger blue particles are more weakly charged. (a) The pinned mixed phase. (b) The strongly driven dynamically ordered phase forms stripelike domains, with triangular ordering of the particles inside each domain. Adapted with permission from C. Reichhardt and C.J. Olson Reichhardt, *Phys. Rev. E* **75**, 040402(R) (2007). Copyright 2007 by the American Physical Society.

while in figure 63(b), for strong driving the system dynamically orders and phase separates into stripes of triangularly ordered particles.

12. Absorbing Phase Transitions and Reversibility At Depinning

The nature of plastic depinning is still an open question, and although there is considerable evidence to suggest that in many cases plastic depinning has critical properties, there is still a lack of knowledge of the associated universal exponents or even the identity of the proper order parameters [43]. A wide range of critical scaling exponents have been reported for elastic depinning, so it is not even clear whether there is a single unique behavior associated with the elastic regime [298]. Both elastic and plastic depinning have been characterized using the statistics of avalanches that occur near depinning, where critical behavior is associated with a power law distribution of avalanche sizes,

$$P(s) \propto s^{-\alpha}. \quad (11)$$

In many cases, however, it is difficult to identify the exact critical points or depinning thresholds, and experiments and simulations examining avalanche behavior at depinning have produced a wide variety of exponents, and, in some cases, no exponent at all when the avalanche sizes are not power-law distributed. The form of the avalanche size distribution depends strongly on the ratio of the number of pinning sites to the number of particles, the temperature, the dissipation mechanism, and how the system is driven [299, 300, 301, 302]. Other methods that have been

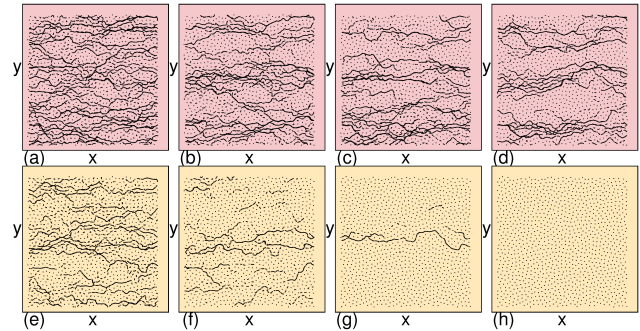


Figure 64. Colloid positions (dots) and trajectories (lines) for simulations of a system with random pinning subjected to the sudden application of a driving force of fixed direction and fixed magnitude F_D . (a-d) Time evolution of the particle trajectories as the system settles into a steady fluctuating state for a pinning force of $F_p/F_p^c = 0.93$, where F_p^c is the pinning force at the critical point. (e-h) The same for a sample with $F_p/F_p^c = 1.05$, which settles into a pinned state. Adapted with permission from C. Reichhardt and C.J. Olson Reichhardt, *Phys. Rev. Lett.* **103**, 168301 (2009). Copyright 2009 by the American Physical Society.

used to characterize the nature of plastic depinning include a Horton river structure analysis of the changes in the flow channel morphologies [303, 304] and changes in the fractal dimension of the system [305, 306].

Recently a new method to identify and characterize nonequilibrium phase transitions was developed in studies of periodically sheared dilute colloidal systems where thermal effects are negligible [307]. A stroboscopic technique reveals that as a function of shear amplitude or colloid density, there is a transition from a reversible flow where the particles return to the same position at the end of each shear cycle to an irreversible state where the particles no longer return to the same position and undergo anisotropic diffusion. Additional experiments and computational studies show that the system always begins in an irreversible state, but over time it settles into either a reversible state or a steadily fluctuating irreversible state. The time scale τ to reach either state diverges at the transition point as a power law with $\tau \propto |\sigma - \sigma_c|^{-\nu}$, where σ is the strain amplitude, $\nu = 1.33$ in 2D, and $\nu = 1.1$ in 3D [308]. The reversible state is termed a random organized state since the particle positions appear to be random even though the particles undergo no net diffusion. This system exhibits characteristics consistent with a nonequilibrium absorbing phase transition, in which a driven system becomes trapped or absorbed in a non-fluctuating or non-chaotic state [26].

In numerical examinations of the plastic depinning transition for colloids under an external drive in the presence of random pinning of varied strength F_p , Reichhardt *et al.* found that the sudden application of a driving force of fixed direction and fixed magnitude F_D produces plastic rearrangements of the colloids

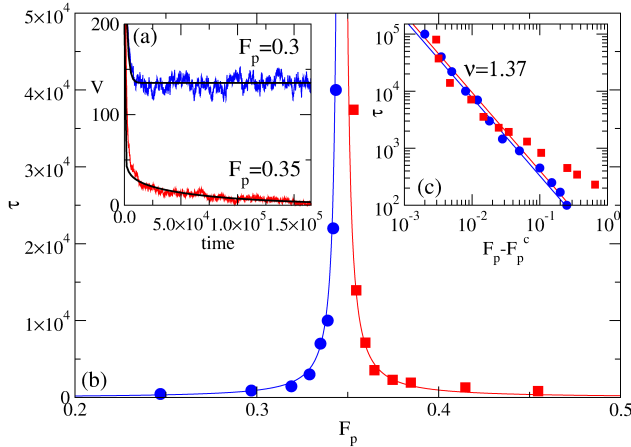


Figure 65. (a) The simulated colloid velocity V vs time for the system in figure 64 at $F_p/F_p^c = 0.86$ (blue) where the system settles into a steady fluctuating state and at $F_p/F_p^c = 1.008$ (red) where the system settles into a pinned state. (b) The time scale τ required to reach either state vs pinning force F_p . Here τ diverges at the critical point F_p^c . Blue dots are systems with $F_p/F_p^c < 1$ and red squares are systems with $F_p/F_p^c > 1$. (c) Power law fits of $\tau \propto |F_p - F_p^c|^{-\nu}$ with $\nu = 1.37 \pm 0.06$. Adapted with permission from C. Reichardt and C.J. Olson Reichardt, Phys. Rev. Lett. **103**, 168301 (2009). Copyright 2009 by the American Physical Society.

which subsequently settle into either a pinned state or a fluctuating flowing state [309]. The time scale τ required for the system to reach either of these states diverges near a critical pinning force F_p^c . Figure 64(a-d) shows the time evolution of the particle trajectories at $F_p/F_p^c = 0.93$, where the fixed drive F_D is larger than the depinning threshold of the system. The number of trajectories gradually decreases with time but settles eventually into a steady flowing state. In contrast, in figure 64(e-h) at $F_p/F_p^c = 1.05$, the fixed drive F_D is smaller than the depinning threshold and the number of trajectories continues to decrease until the system reaches a pinned state and can no longer evolve. In analogy with the reversible-irreversible transition, the pinned state corresponds to a reversible or absorbed state where the fluctuations are lost, while the fluctuating flowing state corresponds to the irreversible state. Figure 65(a) shows the colloid velocity V versus time in two samples: one with $F_p/F_p^c = 0.86$ which settles into a steady fluctuating state, and one with $F_p/F_p^c = 1.008$ which settles into a pinned state. The solid lines are fits to the time-dependent colloidal velocity of the form $V(t) = (V^0 - V^s) \exp(-t/\tau)/t^\alpha + V^s$, where V^0 is the initial velocity and V^s is the steady state velocity. At the critical point F_p^c , $V(t)$ has a power law form and $\tau \rightarrow \infty$. Based on this measure, τ can be identified on either side of the transition, as shown in figure 65(b), and used to determine the critical value of F_p at which τ diverges. In figure 65(c), a log-log plot of the time

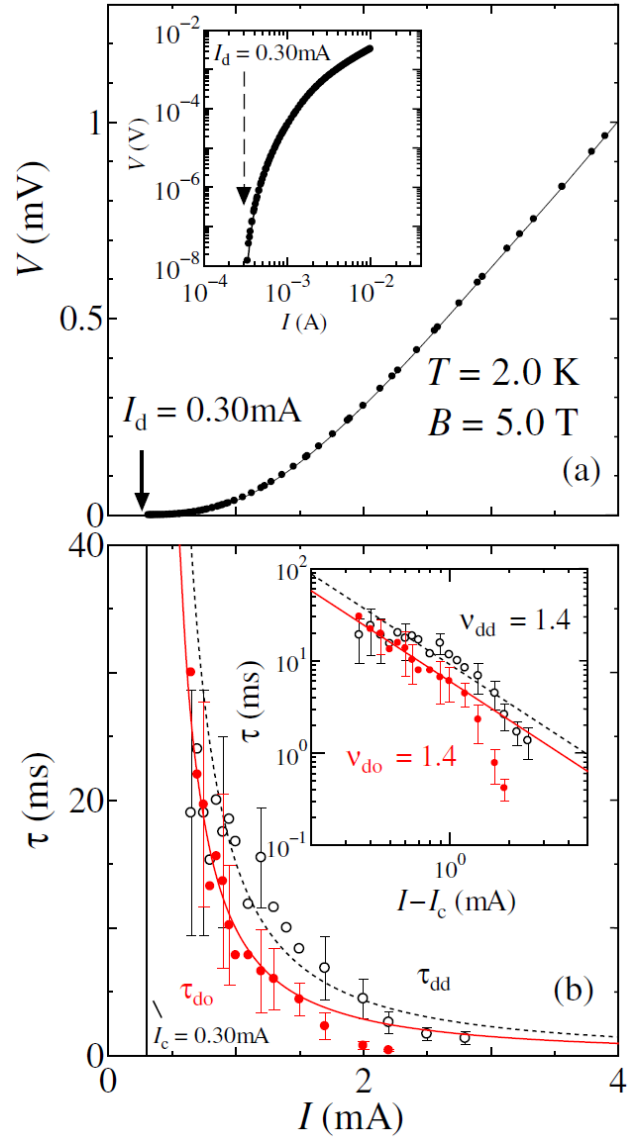


Figure 66. (a) Voltage V vs driving current I from experiments on superconducting vortices subjected to a suddenly applied current. The voltage V corresponds to the vortex velocity V , the driving current I corresponds to the driving force F_D , and the critical depinning current I_d corresponds to the critical depinning threshold F_c . Inset: The same data on a log-log scale. (b) The time scale τ required to reach a disordered state from an ordered initial condition (τ_{dd} , black) or an ordered state from a disordered initial condition (τ_{do} , red) vs driving current I . There is a power law divergence in τ near a critical drive I_c , which corresponds to a critical driving threshold F_D^c . Inset: τ vs $(I - I_c)$ can be fit to a power law with exponent $\nu = 1.4$. Reprinted with permission from S. Okuma and A. Motohashi, New J. Phys. **14**, 123021 (2012). Open Access (CC-BY) article, <http://creativecommons.org/licenses/by/3.0/>

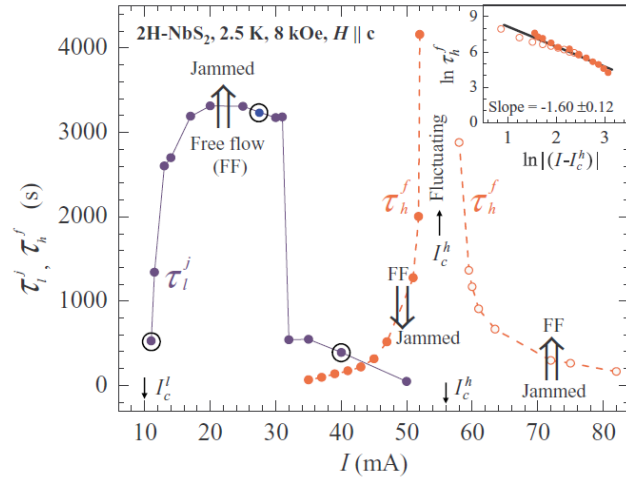


Figure 67. Experimental measurements of transient time scales τ vs driving current I for superconducting vortex states near a depinning threshold. Blue symbols: Vortices prepared in an ordered state depin above a critical current I_c^l and flow during a time scale τ_i^j before suddenly dropping into a disordered pinned state. Orange symbols: Vortices in the disordered pinned state exhibit a diverging transient time scale τ_h^f near the depinning current I_c^h ; for $I < I_c^h$ (filled circles), the steady state is a pinned phase, while for $I > I_c^h$ (open circles), the steady state is flowing. Here τ_h^f corresponds to the time scale τ measured near a depinning transition, the current I corresponds to the driving force F_D , and the critical current I_c^h corresponds to the critical driving threshold F_D^c . Inset: The divergence of τ can be fit to the form $\tau \propto |(F_D - F_D^c)|^{-\nu}$ with $\nu = 1.6$. Reprinted with permission from G. Shaw, P. Mandal, S.S. Banerjee, A. Niazi, A.K. Rastogi, A.K. Sood, S. Ramakrishnan, and A.K. Grover, *Phys. Rev. B* **85**, 174517 (2012). Copyright 2012 by the American Physical Society.

scale τ versus $F_p - F_p^c$ can be fit to a power law form with exponent $\nu = 1.37$, close to the value measured in the sheared colloidal system. At the critical point, the critical exponent for decay of the velocity is $\alpha = 0.5$. The exponents obtained in both the sheared colloidal system and the depinning system are close to the values predicted for conserved directed percolation (CDP), which are $\nu = 1.29$ in 2D and $\nu = 1.12$ in 3D. Ordinary directed percolation (DP) has exponents $\nu = 1.295$ in 2D and $\nu = 1.105$ in 3D [26]. Similarly, $\alpha = 0.5$ is close to the values $\alpha = 0.45$ in DP and $\alpha = 0.5$ in CDP. Experiments on nonequilibrium absorbing phase transitions between different turbulent states also give the value $\alpha = 1/2$ [28].

Okuma *et al.* [310] experimentally studied the plastic flow of superconducting vortices in a Corbino disk geometry under the sudden application of a dc driving current and measured the transient voltage response, which is proportional to the vortex velocity. Figure 66(a) shows the velocity-force curve for this system, indicating that there is a clearly defined finite depinning threshold F_c . After the vortices are prepared in an initially ordered or initially disordered

state, the time scale τ required to reach a steady state can be measured. Based on changes in τ it is possible to identify a critical driving threshold F_D^c at which τ diverges as a power law that can be fit with an exponent of $\nu = 1.4$, as shown in figure 66(b). For $F_D > F_D^c$, the flowing vortices become more ordered when the drive is applied, while for $F_D < F_D^c$, they become less ordered when the drive is applied. These results show that critical behavior in the form of a diverging time scale can occur near a dynamical ordering transition as well as near a depinning transition. Further studies of the same system at different magnetic fields where the ordering of the pinned state changes also show power law divergences in the transient time scale with exponents $\nu = 1.3$ to $\nu = 1$ [311]. Shaw *et al.* [312] experimentally examined the lifetimes of transient states near a superconducting vortex depinning threshold. When the system is prepared in an ordered state, there is a lower critical driving threshold above which the vortices flow transiently during a time scale τ_i^j before jumping abruptly to a pinned state. This sudden jump was argued to be a jamming phenomenon associated with the disordering of the vortex lattice. Figure 67 shows how the transient time scale τ_i^j changes as a function of driving force F_D . The disordered vortex system exhibits a higher critical driving threshold F_D^c near which there is another transient behavior associated with the time scale τ required for the system to settle into a pinned phase for $F_D < F_D^c$ or into a moving steady state for $F_D > F_D^c$, as shown in figure 67. The inset of figure 67 indicates that τ diverges as a power law at F_D^c according to $\tau \propto |F_D - F_D^c|^{-\nu}$ with $\nu = 1.6$.

The behavior of periodically driven superconducting vortex systems near depinning transitions has also been examined in numerical [313, 314, 315] and experimental [315, 316] studies. The experiments of Okuma *et al.* on a periodically sheared vortex system show diverging time scales for the system to settle into a reversible or irreversible state with $\nu = 1.3$ [317]. The consistency of the critical exponents in these different studies provides evidence that examining the transient time scales might be the most promising way to characterize nonequilibrium phase transitions in systems with pinning.

Criticality at reversible-irreversible transitions is currently an open topic with many new developments. For example, it was recently proposed that just at the transition, the spatial distribution of the particles is not truly random but is an example of a hyperuniform distribution [318]. Such a distribution has particular scaling features in $S(\mathbf{k})$, indicating that the large scale density fluctuations associated with a truly random distribution are lost [319]. Several studies of systems

of particles with contact interactions have produced evidence for hyperuniformity at the critical point [320, 321]. It would be interesting to determine whether hyperuniformity also arises near reversible-irreversible transitions in systems with longer range interactions, such as superconducting vortices, charge-stabilized colloids, or dislocations. It would also be interesting to apply the concepts of reversible-irreversible transitions to systems that undergo elastic depinning. In this case, although the system may always organize to a reversible state, there could be different types of reversible states, and there could still be a diverging time scale at transitions between these states. There is some work showing how avalanche statistics can be related to a diverging time scale near the reversible-irreversible transition in sheared materials [69], and it would be interesting to make a similar connection between avalanches and depinning transitions.

13. Other Systems and Future Directions

13.1. Single driven particles

It is possible to construct a velocity-force curve for a single probe particle driven through an assembly of other particles [322, 323, 324] or a combination of other particles and pinning sites [325, 326]. Such a system can exhibit a finite threshold for motion as well as nonlinear velocity-force curves with $V \propto (F_D - F_c)^\beta$. Simulations by Hastings *et al.* [322] for a colloid driven through a disordered assembly of other colloids showed both a finite depinning threshold and a power-law velocity-force curve with exponent $\beta = 1.5$ associated with plastic rearrangements of the particles surrounding the probe particle at the depinning transition. In experiments on a magnetic colloid driven through a 3D assembly of monodisperse colloids, Habdas *et al.* [323] found $\beta = 1.5$ below the 3D glass transition and $\beta = 2.5$ near the glass transition. It is not known whether the depinning process in this class of system is the same as that in collectively driven particle systems or whether it is possible for dynamical transitions to occur at higher drives. The local probe technique has been used in a variety of soft matter systems as a way to explore the rheological properties and is termed active microrheology; the interested reader is referred to a recent review on the topic [327].

13.2. Vortices in Bose-Einstein condensates

Particle-like vortices also occur in Bose-Einstein condensates (BECs) [328] and there have already been theoretical [329] and experimental [330] studies of BEC vortices in a co-rotating optical trap array showing commensurate and incommensurate pinning

transitions. The BEC vortices have much less damping in their dynamics and much stronger hydrodynamic interaction effects than superconducting vortices, making them ideal for studying new types of nonequilibrium dynamics, depinning, and dynamic phases that are not accessible using superconducting vortices. Experimentally it would be possible to introduce a co-rotating optical trap into the BEC and determine, by slowing the rotation of the optical trap, when the vortex lattice decouples from the optical traps and whether the lattice breaks up or forms coherent patterns. There has already been some computational work on dynamic phases of BEC vortices in optical trap arrays [331]. It is also possible to create binary BECs that can contain multiple species of vortices which form more complicated structures [332]. It is not known how such vortex systems would depin or what their dynamics would be. For example, if multiple vortex species enter a moving phase, it is possible that dynamical phase separation of the different vortex species could occur into moving bands, and such structure formation would be associated with hysteresis in a velocity-force curve.

13.3. Time dependent traps

The ability to pin BEC vortices, colloids, and even superconducting vortices with optical traps opens the possibility of studying the effect of a time-dependent substrate on the particle dynamics. For example, the pinning sites could be periodically flashed on and off or moved around in a correlated manner. Although it may seem that introducing time dependence to the pinning sites would only reduce the effectiveness of the pinning, it may be possible to introduce some type of dynamical feedback that could actually result in an increase in the pinning effectiveness. There has already been some work on colloids and vortices on time dependent substrates that shows interesting interference effects in the transport curves [333, 334]. In general, driven particle dynamics on a time dependent landscape is an open area of research that could be relevant to new nanoscale devices as well as to biological systems.

13.4. Flowing granular matter

In a simulation model of granular bed erosion in which particles with a short-range steric repulsive interaction are driven over a random substrate by a constant force representing a viscous fluid, Yan *et al.* [335] find that above a threshold drive F_c for motion, the plastic flow of the particles through channels is associated with a velocity scaling of $V \propto (F_D - F_c)^\beta$ with $\beta = 1.0$, an exponent considerably lower than that found for plastic depinning in other systems. In addition, near F_c the transient time scale τ required for the system to

settle into a steady state diverges as $\tau = |F_D - F_c|^{-\nu}$ with $\nu = 2.5$, which is considerably larger than the values of $\nu = 1.3$ to $\nu = 1.5$ observed in the colloidal and vortex depinning systems described in Section 12. These unusual exponents could be an indication of strong finite size effects, where systems of extremely large size would be required to obtain the correct exponent, they could arise since the flow in this model becomes effectively 1D rather than 2D, or they could indicate that plastic flow in granular systems with short-range steric repulsive interactions falls into a different universality class than that of particles that have much longer range repulsive interactions, such as vortices, charge-stabilized colloids, or Wigner crystals. It would be interesting to consider a system with short-range interactions and gradually increase the interaction range to determine how this modifies the scaling properties of the dynamics.

13.5. Active matter

In active matter systems, the particles are self-driven or self-propelled. Examples of active matter include swimming bacteria, pedestrian flow, vehicular traffic, molecular motors, flocks of birds, herds of animals, and crawling cells [336]. Recently, the creation of artificial swimmers such as self-driven colloids has attracted growing attention as a means for understanding collective nonequilibrium behaviors [337]. In most active matter studies, the particles move over a smooth substrate or interact with a fixed number of walls. In many real systems such as swimming bacteria, the active particles also interact with some type of disordered substrate, so the dynamics of active matter moving over random or periodic substrates will be a growing area of research. Although increasing the activity level of the particles might be expected to produce effects similar to increasing the temperature, it was shown that increased activity can produce new types of behaviors such as self-clustering [337, 338]. Studies of the mobility of active particles in disordered media under an external drive show that the mobility of the particles is nonmonotonic as a function of increasing activity, and that higher activity levels can cause the particles to become more strongly pinned [339]. Other studies of flocking models in disordered media indicate that there can be an optimal noise level that produces coherent flow [340]. It is also possible to create active solid systems [341], and it would be interesting to understand whether plastic or elastic depinning can occur in such systems, and if so, in what ways the depinning differs from the depinning of non-active systems.

13.6. Dusty plasmas

Dusty plasmas, which are composed of solid particles that become charged when they are placed in a plasma, can be modeled as repulsively interacting Yukawa particles that form a triangular lattice in the strongly coupled limit [342, 343]. The major difference between dusty plasma systems and colloidal systems is that in dusty plasmas the particle dynamics are underdamped. Due to the size scale, the speed of sound in a dusty plasma can be extremely low, making it possible to create shock waves, solitons, and other nonlinear wave phenomena with relatively small perturbations. In principle it should be possible to create dusty plasma systems in which the particles interact with some form of disordered or periodic landscape, and then to drive the particles across this landscape. Studies of this type could open a new class of depinning dynamics in which inertia plays a dominant role, and it would be interesting to see how the generation of shock waves might modify the depinning transition. It is also possible to create charged colloidal systems in air which obey underdamped dynamics, while a study of charged metal balls in air has demonstrated commensurate-incommensurate pinning transitions [344].

13.7. Nonequilibrium fluctuation relations

Over the last 30 years, various nonequilibrium fluctuation and work relations have been derived [345, 346], including those of Jarzynski [347] and Crooks [348], and these relations have been applied to a variety of systems including a colloid dragged through fluid [349] and biological systems [350]. It would be interesting to test whether there are any conditions under which such relations hold in the nonequilibrium flowing phases of systems with pinning. There has already been some initial work in this direction for colloids moving over random [351] and periodic [352] substrates.

13.8. Topological states

Topological states have been receiving growing attention in quantum systems [353], and similar ideas are beginning to be applied to the dynamics of classical systems as well, such as to the motion of solitons in classical mechanical insulators [354] and to edge mobility in coupled gyroscope arrays [355]. It is possible that some of these ideas could also be applied to systems that exhibit depinning phenomena. For example, the mobility at depinning could be limited to or enhanced along the edges of pinning array, or it may be possible to design pinning arrays in which only certain topologically restricted modes of motion can occur.

13.9. Curved geometries

In the systems described up to this point, depinning occurs on flat surfaces. There is, however, growing interest in studying particle dynamics and ordering in systems with curved geometries, such as dislocation patterns and motion on surfaces with positive or negative curvature [356, 357, 358]. It would be interesting to study elastic or plastic depinning phenomena on such curved geometries and compare them to the dynamics observed in flat geometries. In curved geometries, dynamically ordered states could correlate with certain types of pattern formation of moving topological defects.

13.10. Deformable substrates

In the studies described so far, the pinning sites or substrates remain fixed in space and only the particles can move. Another class of system that is wide open for study is one in which the pinning or substrate itself is deformable or can even exhibit plasticity. Such effects could come into play for particles moving over deformable membranes or elastic sheets, where the particle could create indentations in the surface that would introduce modified pairwise interactions between the particles. Another possibility is that near the depinning threshold, a wrinkling transition could occur in which the system could become strongly buckled into the third dimension, and that once the particles depin, the sheet could straighten again. It could also be possible to create systems in which the pinning sites can move past each other and exhibit plasticity. For example, the pinning sites could be modeled as obeying their own equation of motion with dynamics that differ from those of the driven particles. Effects of this type could occur for electron crystals pinned by charged doping sites, where the doping sites gradually electromigrate over time. It would also be possible to drive colloids through obstacle arrays in which the obstacles gradually change position. Such systems could exhibit strong memory effects that can change the transport over time, and may offer a new approach for creating novel memristor type devices [359].

13.11. Quantum effects

One of the major areas of condensed matter physics is focused on equilibrium quantum phase transitions that are driven by quantum fluctuations [360]. In principle there could also be nonequilibrium quantum phase transitions, in analogy with classical nonequilibrium phase transitions, and driven quantum systems that exhibit a depinning threshold or nonlinear transport at low temperatures could be ideal candidates in which to observe such effects. It might be expected that

adding dynamical fluctuations to quantum fluctuations would destroy the quantum effects; however, recent work shows that features of quantum critical states can survive in the presence of nonequilibrium noise [361]. It may also be possible that the application of a drive could in some cases suppress thermal noise or other dynamical noise while preserving the quantum fluctuations. Open issues include what the proper methods are to measure such nonequilibrium quantum transitions, how they would differ from their classical analogs, whether there are quantum analogs to dynamical ordering transitions, and whether new types of quantum phenomena exist only in the driven phase but not in the equilibrium state.

Acknowledgments

We thank the following people for discussions: Clemens Bechinger, Shobo Bhattacharya, Alan Bishop, Karen Dahmen, Roel Dullens, Thierry Giamarchi, John Goree, David Grier, Matt Hastings, Boldizar Jankó, Wai Kwok, Andras Libál, Shi-Zeng Lin, Andrea Liu, Cristina Marchetti, Jose Martín, Danielle McDermott, Victor Moshchalkov, Satoshi Okuma, David Pine, Dipanjan Ray, Ido Regev, Ivan Schuller, Alejandro Silhanek, Gabe Spalding, Pietro Tierno, Eric Weeks, and Zhili Xiao. This work was carried out under the auspices of the NNSA of the U.S. DoE at LANL under Contract No. DE-AC52-06NA25396.

References

- [1] Blatter G, Feigel'man M V, Geshkenbein V B, Larkin A I and Vinokur V M 1994 Vortices in high-temperature superconductors *Rev. Mod. Phys.* **66** 1125–388
- [2] Harada K, Kamimura O, Kasai H, Matsuda T, Tonomura A and Moshchalkov V V 1996 Direct observation of vortex dynamics in superconducting films with regular arrays of defects *Science* **274** 1167–70
- [3] Monceau P 2012 Electronic crystals: an experimental overview *Adv. Phys.* **61** 325–81
- [4] Grüner G 1988 The dynamics of charge-density waves *Rev. Mod. Phys.* **60** 1129–81
- [5] Middleton A A and Wingreen N S 1993 Collective transport in arrays of small metallic dots *Phys. Rev. Lett.* **71** 3198–201
- [6] Pertsinidis A and Ling X S 2008 Statics and dynamics of 2D colloidal crystals in a random pinning potential *Phys. Rev. Lett.* **100** 028303
- [7] Bohlein T, Mikhael J and Bechinger C 2012 Observation of kinks and antikinks in colloidal monolayers driven across ordered surfaces *Nature Mater.* **11** 126–30
- [8] Bohlein T and Bechinger C 2012 Experimental observation of directional locking and dynamical ordering of colloidal monolayers driven across quasiperiodic substrates *Phys. Rev. Lett.* **109** 058301
- [9] Reichhardt C, Reichhardt C J O, Martin I and Bishop A 2003 Dynamical ordering of driven stripe phases in quenched disorder *Phys. Rev. Lett.* **90** 026401
- [10] Vanossi A, Manini N, Urbakh M, Zapperi S and Tosatti E 2013 Modeling friction: From nanoscale to mesoscale *Rev. Mod. Phys.* **85** 529–52

- [11] Lemerle S, Ferré J, Chappert C, Mathet V, Giamarchi T and Le Doussal P 1998 Domain wall creep in an Ising ultrathin magnetic film *Phys. Rev. Lett.* **80** 849–52
- [12] Brazovskii S and Nattermann T 2004 Pinning and sliding of driven elastic systems: from domain walls to charge density waves *Adv. Phys.* **53** 177–252
- [13] Tang C, Feng S and Golubovic L 1994 Dynamics and noise spectra of a driven single flux line in superconductors *Phys. Rev. Lett.* **72** 1264–7
- [14] Ertas D and Kardar M 1994 Anisotropic scaling in depinning of a flux line *Phys. Rev. Lett.* **73**, 1703–6
- [15] Dong M, Marchetti M C, Middleton A A and Vinokur V 1993 Elastic string in a random potential *Phys. Rev. Lett.* **70** 662–5
- [16] Rosso A and Krauth W 2001 Origin of the roughness exponent in elastic strings at the depinning threshold *Phys. Rev. Lett.* **87** 187002
- [17] Chen Y J, Zapperi S and Sethna J P 2015 Crossover behavior in interface depinning *Phys. Rev. E* **92** 022146
- [18] Rolley E, Guthmann C, Gombrowicz R and Repain V 1998 Roughness of the contact line on a disordered substrate *Phys. Rev. Lett.* **80** 2865–8
- [19] Carlson J M and Langer L S 1989 Properties of earthquakes generated by fault dynamics *Phys. Rev. Lett.* **62** 2632–5
- [20] Reichhardt C and Olson C J 2002 Colloidal dynamics on disordered substrates *Phys. Rev. Lett.* **89** 078301
- [21] Bhattacharya S and Higgins M J 1993 Dynamics of a disordered flux line lattice *Phys. Rev. Lett.* **70** 2617–20
- [22] Persson B N J 2000 *Sliding Friction, Physical Properties and Applications* (Berlin: Springer)
- [23] Zykova-Timan T, Ceresoli D and Tosatti E 2007 Peak effect versus skating in high-temperature nanofriction *Nature Mater.* **6** 230–4
- [24] Sethna J P 2006 *Statistical Mechanics: Entropy, Order Parameters, and Complexity* (Oxford: Oxford Press)
- [25] Kardar, M 2007 *Statistical Physics of Particles* (Cambridge: Cambridge University Press)
- [26] Hinrichsen H 2000 Non-equilibrium critical phenomena and phase transitions into absorbing states *Adv. Phys.* **49** 815–958
- [27] Odor, G 2004 Universality classes in nonequilibrium lattice systems *Rev. Mod. Phys.* **76** 663–724
- [28] Takeuchi K A, Kuroda M, Chaté H and Sano M 2007 Directed percolation criticality in turbulent liquid crystals *Phys. Rev. Lett.* **99** 234503
- [29] Corte L, Chaikin P M, Gollub J P and Pine D J 2008 Random organization in periodically driven systems *Nature Phys.* **4** 420–4
- [30] Fisher D S 1985 Sliding charge-density waves as a dynamic critical phenomenon *Phys. Rev. B* **31** 1396–427
- [31] Myers C R and Sethna J P 1993 Collective dynamics in a model of sliding charge-density waves. I. Critical behavior *Phys. Rev. B* **47** 11171–93
- [32] Storm C, Pastore J J, MacKintosh F C, Lubensky T C and Janmey P A 2005 Nonlinear elasticity in biological gels *Nature* **435** 191–4
- [33] Lin Y C, Koenderink G H, MacKintosh F C and Weitz D A 2011 Control of non-linear elasticity in F-actin networks with microtubules *Soft Matter* **7** 902–6
- [34] King H, Schroll R D, Davidovitch B and Menon N 2012 Elastic sheet on a liquid drop reveals wrinkling and crumpling as distinct symmetry-breaking instabilities *Proc. Natl. Acad. Sci. (USA)* **109** 9716–20
- [35] Coppersmith S N 1990 Phase slips and the instability of the Fukuyama-Lee-Rice model of charge-density waves *Phys. Rev. Lett.* **65** 1044–7
- [36] Jensen H J, Brass A, Brechet Y and Berlinsky A J 1988 Current-voltage characteristics in a two-dimensional model for flux flow in type-II superconductors *Phys. Rev. B* **38** 9235–7
- [37] Domínguez D 1994 Critical dynamics and plastic flow in disordered Josephson junction arrays *Phys. Rev. Lett.* **72** 3096–9
- [38] Faleski M C, Marchetti M C and Middleton A A 1996 Vortex dynamics and defects in simulated flux flow *Phys. Rev. B* **54** 12427–36
- [39] Olson C J, Reichhardt C and Nori F 1998 Fractal networks, braiding channels, and voltage noise in intermittently flowing rivers of quantized magnetic flux *Phys. Rev. Lett.* **80** 2197–200
- [40] Cha M-C and Fertig H A 1994 Topological defects, orientational order, and depinning of the electron solid in a random potential *Phys. Rev. B* **50** 14368–80
- [41] Reichhardt C, Olson C J, Grønbech-Jensen N and Nori F 2001 Moving Wigner glasses and smectics: Dynamics of disordered Wigner crystals *Phys. Rev. Lett.* **86** 4354–7
- [42] Watson J and Fisher D S 1997 Dynamic critical phenomena in channel flow of driven particles in random media *Phys. Rev. B* **55** 14909–24
- [43] Fily Y, Olive E, Di Scala N and Soret J C 2010 Critical behavior of plastic depinning of vortex lattices in two dimensions: Molecular dynamics simulations *Phys. Rev. B* **82** 134519
- [44] Ammor L, Ruyter A, Shaidiuk V A, Hong N H and Plessis D 2010 Filamentary flow of vortices in a $\text{Bi}_2\text{Sr}_2\text{Ca}_1\text{Cu}_2\text{O}_{8+x}$ single crystal *Phys. Rev. B* **81** 094521
- [45] Miguel M C, Vespignani A, Zapperi S, Weiss J and Grasso J R 2001 Intermittent dislocation flow in viscoplastic deformation *Nature (London)* **410** 667–71
- [46] Dimiduk D M, Woodward C, LeSar R and Uchic M D 2006 Scale-free intermittent flow in crystal plasticity *Science* **312** 1188–90
- [47] Koshelev A E and Vinokur V M 1994 Dynamic melting of the vortex lattice *Phys. Rev. Lett.* **73** 3580–3
- [48] Chen J, Cao Y and Jiao Z 2004 Dynamics of two-dimensional colloids on a disordered substrate *Phys. Rev. E* **69** 041403
- [49] Tekic J, Braun O and Hu B 2005 Dynamic phases in the two-dimensional underdamped driven Frenkel-Kontorova model *Phys. Rev. E* **71** 026104
- [50] Reichhardt C, Ray D and Reichhardt C J O 2015 Collective transport properties of driven skyrmions with random disorder *Phys. Rev. Lett.* **114** 217202
- [51] Giamarchi T and Le Doussal P 1996 Moving glass phase of driven lattices *Phys. Rev. Lett.* **76** 3408–11
- [52] Moon K, Scalettar R T and Zimányi G T 1996 Dynamical phases of driven vortex systems *Phys. Rev. Lett.* **77** 2778–11
- [53] Balents L, Marchetti M C and Radzihovsky L 1997 Comment on Moving glass phase of driven lattices *Phys. Rev. Lett.* **78** 751
- [54] Balents L, Marchetti M C and Radzihovsky L 1998 Nonequilibrium steady states of driven periodic media *Phys. Rev. B* **57** 7705–39
- [55] Le Doussal P and Giamarchi T 1998 Moving glass theory of driven lattices with disorder *Phys. Rev. B* **57** 11356–403
- [56] Spencer S and Jensen H J 1997 Absence of translational ordering in driven vortex lattices *Phys. Rev. B* **55** 8473–81
- [57] Bak P 1982 Commensurate phases, incommensurate phases and the devil's staircase *Rep. Prog. Phys.* **45** 587–629
- [58] Baert M, Metlushko V V, Jonckheere R, Moshchalkov V V and Bruynseraede Y 1995 Composite flux-line lattices stabilized in superconducting films by a regular array of artificial defects *Phys. Rev. Lett.* **74** 3269–72
- [59] Reichhardt C, Olson C J and Nori F 1998 Commensurate and incommensurate vortex states in superconductors with periodic pinning arrays *Phys. Rev. B* **57** 7937–43
- [60] Vanossi A, Manini N and Tosatti E 2012 Static and dynamic friction in sliding colloidal monolayers *Proc. Natl. Acad.*

- Sci. (USA)* **109** 16429–33
- [61] Braun O M, Dauxois T, Paliy M V and Peyrard M 1997 Dynamical transitions in correlated driven diffusion in a periodic potential *Phys. Rev. Lett.* **78** 1295–98
- [62] Reichhardt C, Olson C J and Nori F 1997 Dynamic phases of vortices in superconductors with periodic pinning *Phys. Rev. Lett.* **78** 2648–51
- [63] Gutierrez J, Silhanek A V, Van de Vondel J, Gillijns W and Moshchalkov V V 2009 Transition from turbulent to nearly laminar vortex flow in superconductors with periodic pinning *Phys. Rev. B* **80** 140514(R)
- [64] McDermott D, Amelang J, Reichhardt C J O and Reichhardt C 2013 Dynamic regimes for driven colloidal particles on a periodic substrate at commensurate and incommensurate fillings *Phys. Rev. E* **88** 062301
- [65] Ott E 2002 *Chaos in Dynamical Systems* (Cambridge: Cambridge University Press)
- [66] Fiocco D, Foffi G and Sastry S 2013 Oscillatory athermal quasistatic deformation of a model glass *Phys. Rev. E* **88** 020301(R)
- [67] Regev I, Lookman T and Reichhardt C 2013 Onset of irreversibility and chaos in amorphous solids under periodic shear *Phys. Rev. E* **88** 062401
- [68] Nagamanasa K H, Gokhale S, Sood A K and Ganapathy R 2014 Experimental signatures of a nonequilibrium phase transition governing the yielding of a soft glass *Phys. Rev. E* **89** 062308
- [69] Regev I, Weber J, Reichhardt C, Dahmen K and Lookman T 2015 Reversibility and criticality in amorphous solids *Nature Commun.* **6** 8805
- [70] Ao P and Thouless D J 1993 Berrys phase and the Magnus force for a vortex line in a superconductor *Phys. Rev. Lett.* **70** 2158–61
- [71] Sonin E B 2013 Transverse forces on a vortex in lattice models of superfluids *Phys. Rev. B* **88** 214513
- [72] Pippard A B 1969 A possible mechanism for the peak effect in type II superconductors *Philos. Mag.* **19**, 217–20
- [73] Bhattacharya S and Higgins M J 1994 Peak effect and anomalous flow behavior of a flux-line lattice *Phys. Rev. B* **49** 10005–8
- [74] Marley A C, Higgins M J and Bhattacharya S 1995 Flux flow noise and dynamical transitions in a flux line lattice *Phys. Rev. Lett.* **74** 3029–32
- [75] Merithew R, Rabin M, Weissman M, Higgins M and Bhattacharya S 1996 Persistent metastable states in vortex flow at the peak effect in NbSe₂ *Phys. Rev. Lett.* **77** 3197–200
- [76] Higgins M J and Bhattacharya S 1996 Varieties of dynamics in a disordered flux-line lattice *Physica C* **257** 232–54
- [77] Cha M-C and Fertig H A 1998 Peak effect and the transition from elastic to plastic depinning *Phys. Rev. Lett.* **80** 3851–4
- [78] Reichhardt C, Moon K, Scalettar R and Zimányi G 1999 Comment on Peak effect and the transition from elastic to plastic depinning *Phys. Rev. Lett.* **83** 2282
- [79] Thorel P, Kahn R, Simon Y and Cribier D 1973 Fabrication et étude d'un monocristal de vortex dans le niobium supraconducteur *J. Phys. (Paris)* **34** 447–52
- [80] Shi A-C and Berlinsky A J 1991 Pinning and I-V characteristics of a two-dimensional defective flux-line lattice *Phys. Rev. Lett.* **67** 1926–9
- [81] Yaron U, Gammel P L, Huse D A, Kleiman R N, Oglesby C S, Bucher E, Batlogg B, Bishop D J, Mortensen K and Clausen K N 1995 Structural evidence for a two-step process in the depinning of the superconducting flux-line lattice *Nature (London)* **376** 753–5
- [82] Hellerqvist M C, Ephron D, White W R, Beasley M R and Kapitulnik A 1996 Vortex dynamics in two-dimensional amorphous Mo₇₇Ge₂₃ films *Phys. Rev. Lett.* **76** 4022–5
- [83] Ryu S, Hellerqvist M, Doniach S, Kapitulnik A and Stroud D 1996 Dynamical phase transition in a driven disordered vortex lattice *Phys. Rev. Lett.* **77** 5114–7
- [84] Fangohr H, Cox S and de Groot P 2001 Vortex dynamics in two-dimensional systems at high driving forces *Phys. Rev. B* **64** 064505
- [85] Aurenhammer F 1991 Voronoi diagrams - A survey of a fundamental geometric data structure *ACM Comput. Surveys* **23** 345–405
- [86] Rabin M W, Merithew R D, Weissman M B, Higgins M J and Bhattacharya S 1998 Noise probes of underlying static correlation lengths in the superconducting peak effect *Phys. Rev. B* **57** R720-3
- [87] Chandran M, Scalettar R and Zimányi G 2003 Dynamic transition in driven vortices across the peak effect in superconductors *Phys. Rev. B* **67** 052507
- [88] Li G, Andrei E, Xiao Z, Shuk P and Greenblatt M 2006 Onset of motion and dynamic reordering of a vortex lattice *Phys. Rev. Lett.* **96** 017009
- [89] Giamarchi T and Le Doussal P 1995 Elastic theory of flux lattices in the presence of weak disorder. *Phys. Rev. B* **52** 1242–70
- [90] Pardo F, de la Cruz F, Gammel P L, Bucher E and Bishop D J 1998 Observation of smectic and moving-Bragg-glass phases in flowing vortex lattices *Nature (London)* **396** 348–50
- [91] Troyanovski A M, Aarts J and Kes P H 1999 Collective and plastic vortex motion in superconductors at high flux densities *Nature (London)* **399** 665–8
- [92] Scheidl S and Vinokur V 1998 Driven dynamics of periodic elastic media in disorder *Phys. Rev. E* **57** 2574–93
- [93] Olson C J, Reichhardt C and Nori F 1998 Nonequilibrium dynamic phase diagram for vortex lattices *Phys. Rev. Lett.* **81** 3757–60
- [94] Domínguez D 1999 Dynamic transition in vortex flow in strongly disordered Josephson junction arrays and superconducting thin films *Phys. Rev. Lett.* **82** 181–4
- [95] Kolton A, Domínguez D and Grønbech-Jensen N 1999 Hall noise and transverse freezing in driven vortex lattices *Phys. Rev. Lett.* **83** 3061–4
- [96] Liu M, Liu X D, Wang J, Xing D Y and Lin H Q 2003 Dynamic phase diagram in a driven vortex lattice with random pinning and thermal fluctuations *Phys. Lett. A* **308** 149–56
- [97] Olson C J and Reichhardt C 2000 Transverse depinning in strongly driven vortex lattices with disorder *Phys. Rev. B* **61** R3811–4
- [98] Fangohr H, de Groot P and Cox S 2001 Critical transverse forces in weakly pinned driven vortex systems *Phys. Rev. B* **63** 064501
- [99] Lefebvre J, Hilke M and Altounian Z 2008 Transverse depinning in weakly pinned vortices driven by crossed ac and dc currents *Phys. Rev. B* **78** 134506
- [100] Okuma S, Shimamoto D and Kokubo N 2012 Velocity-induced reorientation of a fast driven Abrikosov lattice *Phys. Rev. B* **85** 064508
- [101] Olson C J, Reichhardt C and Bhattacharya S 2001 Critical depinning force and vortex lattice order in disordered superconductors *Phys. Rev. B* **64** 024518
- [102] Xu X B, Fangohr H, Xu X N, Gu M, Wang Z H, Ji S M, Ding S Y, Shi D Q and Dou S X 2008 Effect in the critical current of type II superconductors with strong magnetic vortex pinning *Phys. Rev. Lett.* **101** 147002
- [103] Paltiel Y, Zeldov E, Myasoedov N, Shtrikman H, Bhattacharya S, Higgins M J, Xiao Z L, Andrei E Y, Gammel P L and Bishop D J 2000 Dynamic instabilities and memory effects in vortex matter *Nature* **403** 398–401
- [104] Paltiel Y, Zeldov E, Myasoedov Y, Rappaport M, Jung G, Bhattacharya S, Higgins M, Xiao Z, Andrei E, Gammel P and Bishop D 2000 Instabilities and disorder-driven first-order transition of the vortex lattice *Phys. Rev. Lett.* **85**

- 3712–5
- [105] Wördenweber R, Kes P H and Tsuei C C 1986 Peak and history effects in two-dimensional collective flux pinning *Phys. Rev. B* **33** 3172–80
- [106] Henderson W, Andrei E Y, Higgins M J and Bhattacharya S 1996 Metastability and glassy behavior of a driven flux-line lattice *Phys. Rev. Lett.* **77** 2077–80
- [107] Dilley N, Herrmann J, Han S and Maple M 1997 Dynamic transition near the peak effect in CeRu₂ *Phys. Rev. B* **56** 2379–82
- [108] Henderson W, Andrei E and Higgins M 1998 Plastic motion of a vortex lattice driven by alternating current *Phys. Rev. Lett.* **81** 2352–5
- [109] Banerjee S S, Patil N G, Ramakrishnan S, Grover A K, Bhattacharya S, Mishra P K, Ravikumar G, Chandrasekhar Rao T V, Sahni V C, Higgins M J, Tomy C V, Balakrishnan G and Paul D M 1999 Disorder, metastability, and history dependence in transformations of a vortex lattice *Phys. Rev. B* **59** 6043–6
- [110] Xiao Z L, Andrei E Y and Higgins M J 1999 Flow induced organization and memory of a vortex lattice *Phys. Rev. Lett.* **83** 1664–7
- [111] Ling X S, Park S R, McClain B A, Choi S M, Dender D C and Lynn J W 2001 Superheating and supercooling of vortex matter in a Nb single crystal: Direct evidence for a phase transition at the peak effect from neutron diffraction *Phys. Rev. Lett.* **86** 712–715
- [112] Bermúdez M M, Eskildsen M R, Bartkowiak M, Nagy G, Bekkeris V and Pasquini G 2015 Dynamic reorganization of vortex matter into partially disordered lattices *Phys. Rev. Lett.* **115** 067001
- [113] Marchevsky M, Higgins M J and Bhattacharya S 2001 Two coexisting vortex phases in the peak effect regime in a superconductor *Nature* **409** 591–4
- [114] Zeldov E, Majer D, Konczykowski M, Geshkenbein V B, Vinokur V M and Shtrikman H 1995 Thermodynamic observation of first-order vortex lattice melting transition *Nature* **375** 373–6
- [115] Strandburg K J 1988 Two-dimensional melting *Rev. Mod. Phys.* **60** 161–207
- [116] Clem J R 1991 Two-dimensional vortices in a stack of thin superconducting films: A model for high-temperature superconducting multilayers *Phys. Rev. B* **43** 7837–46
- [117] Bullard T J, Das J, Daquila G L and Täuber U C 2008 Vortex washboard voltage noise in type-II superconductors *Eur. Phys. J. B* **65** 469–84
- [118] Täuber U C, Klongcheongsan T and Bullard T J 2010 Nonequilibrium steady states of driven magnetic flux lines in disordered type-II superconductors *Supercond. Sci. Technol.* **23** 025023
- [119] Olson C J, Reichhardt C and Vinokur V M 2001 Hysteretic depinning and dynamical melting for magnetically interacting vortices in disordered layered superconductors *Phys. Rev. B* **64** 140502
- [120] Olson C J, Zimányi G T, Kolton A B and Grønbech-Jensen N 2000 Static and dynamic coupling transitions of vortex lattices in disordered anisotropic superconductors *Phys. Rev. Lett.* **85** 5416–9
- [121] Kolton A B, Domínguez D, Olson C J and Grønbech-Jensen N 2000 Driven vortices in three-dimensional layered superconductors: Dynamical ordering along the c axis *Phys. Rev. B* **62** R14657–60
- [122] Zhao Z G, You Y X, Wang J and Liu M 2008 Two-step depinning and re-entrant behavior of three-dimensional flux line lattices *Europhys. Lett.* **82** 47003
- [123] Olson C J, Reichhardt C, Scalettar R, Zimányi G and Grønbech-Jensen N 2003 Metastability and transient effects in vortex matter near a decoupling transition *Phys. Rev. B* **67** 184523
- [124] Chen Q-H and Hu X 2003 Nonequilibrium phase transitions of vortex matter in three-dimensional layered superconductors *Phys. Rev. Lett.* **90** 117005
- [125] Hernández A D and Domínguez D 2004 Critical currents at the Bragg glass to vortex glass transition *Phys. Rev. Lett.* **92** 117002
- [126] Kolton A B, Domínguez D and Grønbech-Jensen N 2001 Mode locking in ac-driven vortex lattices with random pinning *Phys. Rev. Lett.* **86** 4112–5
- [127] Togawa Y, Abiru R, Iwaya K, Kitano H and Maeda A 2000 Direct observation of the washboard noise of a driven vortex lattice in a high-temperature superconductor, Bi₂Sr₂CaCu₂O_y *Phys. Rev. Lett.* **85** 3716–9
- [128] Togawa Y, Kitano H and Maeda A 2002 Ac-dc interference effects in the dynamic state of vortices in Bi₂Sr₂CaCu₂O_y *Physica C* **378–381** 448–52
- [129] Fiory A T 1971 Quantum interference effects of a moving vortex lattice in Al films *Phys. Rev. Lett.* **27** 501–3
- [130] Schmid A and Hauger W 1973 On the theory of vortex motion in an inhomogeneous superconducting film *J. Low Temp. Phys.* **11** 667–85
- [131] Harris J M, Ong N P, Gagnon R and Taillefer L 1995 Washboard frequency of the moving vortex lattice in YBa₂Cu₃O_{6.93} detected by ac-dc interference *Phys. Rev. Lett.* **74** 3684–7
- [132] Kokubo N, Kadowaki K and Takita K 2005 Peak effect and dynamic melting of vortex matter in NbSe₂ crystals *Phys. Rev. Lett.* **95** 177005
- [133] Okuma S, Inoue J and Kokubo N 2007 Suppression of broadband noise at mode locking in driven vortex matter *Phys. Rev. B* **76** 172503
- [134] Song K N, Wang H L, Ren J and Cao Y G 2015 Interference mode-locking of 2D magnetized colloids driven by dc and ac forces in periodic pinning arrays *Physica A* **417** 102–9
- [135] Higgins M J, Middleton A A and Bhattacharya S 1993 Scaling near mode locking in a charge density wave conductor *Phys. Rev. Lett.* **70** 3784–7
- [136] Kolton A B, Domínguez D and Grønbech-Jensen N 2002 Mode locking in driven vortex lattices with transverse ac drive and random pinning *Phys. Rev. B* **65** 184508
- [137] Candido L, Bernu B and Ceperley D M 2004 Magnetic ordering of the three-dimensional Wigner crystal *Phys. Rev. B* **70** 094413
- [138] Piot B A, Jiang Z, Dean C R, Engel L W, Gervais G, Pfeiffer L and West K W 2008 Wigner crystallization in a quasi-three-dimensional electronic system *Nature Phys.* **4** 936–9
- [139] Robbins M O, Kremer K and Grest G S 1988 Phase diagram and dynamics of Yukawa systems *J. Chem. Phys.* **88** 3286–3312
- [140] Hynninen A-P and Dijkstra M 2003 Phase diagrams of hard-core repulsive Yukawa particles *Phys. Rev. E* **68** 021407
- [141] Kanazawa N, Kim J-H, Inosov D S, White J S, Egetenmeyer N, Gavilano J L, Ishiwata S, Onose Y, Arima T, Keimer B and Tokura Y Possible skyrmion-lattice ground state in the B20 chiral-lattice magnet MnGe as seen via small-angle neutron scattering *Phys. Rev. B* **86** 134425
- [142] Tanigaki T, Shibata K, Kanazawa N, Yu X, Aizawa S, Onose Y, Park H S, Shindo D and Tokura Y Real-space observation of short-period cubic lattice of skyrmions in MnGe arXiv:1503.03945
- [143] Goldoni G and Peeters F M 1996 Stability, dynamical properties, and melting of a classical bilayer Wigner crystal *Phys. Rev. B* **53** 4591–603
- [144] Guillamón I, Córdoba R, Sesé J, De Teresa J M, Ibarra M R, Vieira S and Suderow H 2014 Enhancement of long-range correlations in a 2D vortex lattice by an incommensurate 1D disorder potential *Nature Phys.* **10**

- 851–6
- [145] Lemay S G, Thorne R E, Li Y and Brock J D 1999 Temporally ordered collective creep and dynamic transition in the charge-density-wave conductor NbSe₃ *Phys. Rev. Lett.* **83** 2793–6
- [146] Karttunen M, Haataja M, Elder K R and Grant M 1999 Defects, order, and hysteresis in driven charge-density waves *Phys. Rev. Lett.* **83** 3518–21
- [147] Vinokur V M and Nattermann T 1997 Hysteretic depinning of anisotropic charge density waves *Phys. Rev. Lett.* **79** 3471–4
- [148] Marchetti M C, Middleton A A, Saunders K and Schwarz J M 2003 Driven depinning of strongly disordered media and anisotropic mean-field limits *Phys. Rev. Lett.* **91** 107002
- [149] Saunders K, Schwarz J M, Marchetti M C and Middleton A A 2004 Mean-field theory of collective transport with phase slips *Phys. Rev. B* **70** 024205
- [150] Le Doussal P, Marchetti M C and Wiese K J 2008 Depinning in a two-layer model of plastic flow *Phys. Rev. B* **78** 224201
- [151] Besseling R, Kes P H, Dröse T and Vinokur V M 2005 Depinning and dynamics of vortices confined in mesoscopic flow channels *New J. Phys.* **7** 71
- [152] Deshpande V V and Bockrath M 2008 The one-dimensional Wigner crystal in carbon nanotubes *Nature Phys.* **4** 314–8
- [153] Galván-Moya J E, Lucena D, Ferreira W P and Peeters F M 2008 Magnetic particles confined in a modulated channel: Structural transitions tunable by tilting a magnetic field *Phys. Rev. E* **89** 032309
- [154] Liu B and Goree J 2005 Phonons in a one-dimensional Yukawa chain: Dusty plasma experiment and model *Phys. Rev. E* **71** 046410
- [155] del Campo A, De Chiara G, Morigi G, Plenio M B and Retzker A, 2010 Structural defects in ion chains by quenching the external potential: The inhomogeneous Kibble-Zurek mechanism *Phys. Rev. Lett.* **105** 075701
- [156] Reichhardt C and Reichhardt C J O 2011 Dynamically induced locking and unlocking transitions in driven layered systems with quenched disorder *Phys. Rev. B* **84** 174208
- [157] Schwarz J M and Fisher D S 2003 Depinning with dynamic stress overshoots: A hybrid of critical and pseudohysteretic behavior *Phys. Rev. E* **67** 021603
- [158] Li R-T, Duan W-S, Yang Y, Wang C-L and Chen J-M 2011 Hysteresis in the pinning-depinning transition in underdamped two-dimensional Frenkel-Kontorova model *EPL* **94** 56003
- [159] Binder K 1987 Theory of first-order phase transitions *Rep. Prog. Phys.* **50** 783–859
- [160] Klein W 1981 Percolation, droplet models, and spinodal points *Phys. Rev. Lett.* **47** 1569–72
- [161] Jones R A L, Norton L J, Kramer E J, Bates F S and Wiltzius P 1991 Surface-directed spinodal decomposition *Phys. Rev. Lett.* **66** 1326–9
- [162] Loscar E S, Ferreror E E, Grigera T S and Cannas S A 2009 Nonequilibrium characterization of spinodal points using short time dynamics *J. Chem. Phys.* **131** 024120
- [163] Martín J I, Vélez M, Nogués J and Schuller I K 1997 Flux pinning in a superconductor by an array of submicrometer magnetic dots *Phys. Rev. Lett.* **79** 1929–32
- [164] Grigorenko A N, Bending S J, Van Bael M J, Lange M, Moshchalkov V V, Fangohr H and de Groot A J 2003 Symmetry locking and commensurate vortex domain formation in periodic pinning arrays *Phys. Rev. Lett.* **90** 237001
- [165] Daldini O, Martinoli P, Olsen J L and Berner G 1974 Vortex-line pinning by thickness modulation of superconducting films *Phys. Rev. Lett.* **32** 218–21
- [166] Kemmler M, Gürlich C, Sterck A, Pöhler H, Neuhaus M, Siegel M, Kleiner R and Koelle D 2006 Commensurability effects in superconducting Nb films with quasiperiodic pinning arrays *Phys. Rev. Lett.* **97** 147003
- [167] Berdiyrov G, Milosevic M and Peeters F 2006 Novel commensurability effects in superconducting films with antidot arrays *Phys. Rev. Lett.* **96** 207001
- [168] Reichhardt C, Olson C J and Nori F 1998 Nonequilibrium dynamic phases and plastic flow of driven vortex lattices in superconductors with periodic arrays of pinning sites *Phys. Rev. B* **58** 6534–64
- [169] da Silva R M and de Souza Silva C C 2011 Vortex density waves and negative absolute resistance in patterned superconductors *Phys. Rev. B* **83** 184514
- [170] Reichhardt C, Zimányi G T and Grønbech-Jensen N 2001 Complex dynamical flow phases and pinning in superconductors with rectangular pinning arrays *Phys. Rev. B* **64**, 014501
- [171] Chen Q H, Teniers G, Jin B B and Moshchalkov V V 2006 Pinning properties and vortex dynamics in thin superconducting films with ferromagnetic and antiferromagnetic arrays of magnetic dots *Phys. Rev. B* **73** 014506
- [172] Reichhardt C and Reichhardt C J O 2008 Moving vortex phases, dynamical symmetry breaking, and jamming for vortices in honeycomb pinning arrays *Phys. Rev. B* **78** 224511
- [173] Chen Q H, Carballeira C, Nishio T, Zhu B Y and Moshchalkov V V 2008 Stress overshoot and configuration-induced hysteresis in type-II superconducting films with a periodic pinning array *Phys. Rev. B* **78** 172507
- [174] Ren Q.-B. and Luo M.-B. 2013 Dynamics of two-dimensional vortex system in a strong square pinning array at the second matching field *Phys. Lett. A* **377** 1966–9
- [175] Yetis H 2015 Transport properties of the multiple vortices in superconductors with square pinning arrays *Eur. Phys. J. B* **88** 80
- [176] Reichhardt C and Reichhardt C J O 2009 Transport anisotropy as a probe of the interstitial vortex state in superconductors with artificial pinning arrays *Phys. Rev. B* **79** 134501
- [177] Avci S, Xiao Z L, Hua J, Imre A, Divan R, Pearson J, Welp U, Kwok W K and Crabtree G W 2010 Matching effect and dynamic phases of vortex matter in Bi₂Sr₂CaCu₂O₈ nanoribbon with a periodic array of holes *Appl. Phys. Lett.* **97** 042511
- [178] Jiang Z, Dikin D A, Chandrasekhar V, Metlushko V V and Moshchalkov V V 2004 Pinning phenomena in a superconducting film with a square lattice of artificial pinning centers *Appl. Phys. Lett.* **84** 5371-3
- [179] Van Look L, Rosseel E, Van Bael M J, Temst K, Moshchalkov V V and Bruynseraede Y 1999 Shapiro steps in a superconducting film with an antidot lattice *Phys. Rev. B* **60** R6998–7000
- [180] Reichhardt C, Scalettar R T, Zimányi G T and Grønbech-Jensen N 2000 Phase-locking of vortex lattices interacting with periodic pinning *Phys. Rev. B* **61** R11914–17
- [181] Reichhardt C, Kolton A, Domínguez D and Grønbech-Jensen N 2001 Phase-locking of driven vortex lattices with transverse ac force and periodic pinning *Phys. Rev. B* **64** 134508
- [182] de Souza Silva C C, Van de Vondel J, Zhu B Y, Morelle M and Moshchalkov V V 2006 Vortex ratchet effects in films with a periodic array of antidots *Phys. Rev. B* **73** 014507
- [183] Löwen H 1994 Melting, freezing and colloidal suspensions

- Phys. Rep.* **237** 249–324
- [184] Murray C A and Grier D G 1995 Colloidal crystals - Solid particles suspended in fluid form ordered arrays with unusual and useful physical properties *Am. Sci.* **83** 238–45
- [185] Babic D, Schmitt C and Bechinger C 2005 Colloids as model systems for problems in statistical physics *Chaos* **15** 026114
- [186] Chowdhury A, Ackerson B J and Clark N A 1985 Laser-induced freezing *Phys. Rev. Lett.* **55** 833–6
- [187] Hu J and Westervelt R M 1997 Commensurate-incommensurate transitions in magnetic bubble arrays with periodic line pinning *Phys. Rev. B* **55** 771–4
- [188] Frey E, Nelson D and Radzihovsky L 1999 Light-induced melting of colloidal crystals in two dimensions *Phys. Rev. Lett.* **83** 2977–80
- [189] Bechinger C, Brunner M and Leiderer P 2001 Phase behavior of two-dimensional colloidal systems in the presence of periodic light fields *Phys. Rev. Lett.* **86** 930–3
- [190] Brunner M and Bechinger C 2002 Phase behavior of colloidal molecular crystals on triangular light lattices *Phys. Rev. Lett.* **88** 248302
- [191] Mangold K, Leiderer P and Bechinger C 2003 Phase transitions of colloidal monolayers in periodic pinning arrays *Phys. Rev. Lett.* **90** 158302
- [192] Reichhardt C and Reichhardt C J O 2005 Ordering and melting in colloidal molecular crystal mixtures *Phys. Rev. E* **71** 062403
- [193] El Shawish S, Trizac E and Dobnikar J 2012 Phase behaviour of colloidal assemblies on 2D corrugated substrates *J. Phys.: Condens. Matter* **24** 284118
- [194] McDermott D, Amelang J, Lopatina L M, Reichhardt C J O and Reichhardt C 2013 Domain and stripe formation between hexagonal and square ordered fillings of colloids on periodic pinning substrates *Soft Matter* **9** 4607–13
- [195] Korda P T, Taylor M B and Grier D G 2002 Kinetically locked-in colloidal transport in an array of optical tweezers *Phys. Rev. Lett.* **89** 128301
- [196] MacDonald M P, Spalding G C and Dholakia K 2003 Microfluidic sorting in an optical lattice *Nature* **426** 421–4
- [197] Ma X, Lai P-Y, Ackerson B J and Tong P 2015 Colloidal dynamics over a tilted periodic potential: Nonequilibrium steady-state distributions *Phys. Rev. E* **91** 042306
- [198] Lacasta A, Sancho J, Romero A and Lindenberg K 2005 Sorting on periodic surfaces *Phys. Rev. Lett.* **94** 160601
- [199] Speer D, Eichhorn R and Reimann P 2010 Exploiting lattice potentials for sorting chiral particles *Phys. Rev. Lett.* **105** 090602
- [200] Tahir M A, Gao L, Virgin L N and Yellen B B 2011 Transport of superparamagnetic beads through a two-dimensional potential energy landscape *Phys. Rev. E* **84** 011403
- [201] Risbud S R and Drazer G 2014 Directional locking in deterministic lateral-displacement microfluidic separation systems *Phys. Rev. E* **90** 012302
- [202] Vanossi A and Tosatti E 2012 Colloidal friction: Kinks in motion *Nature Mater.* **11** 97–8
- [203] Hasnain J, Jungblut S and Dellago C 2013 Dynamic phases of colloidal monolayers sliding on commensurate substrates *Soft Matter* **9** 5867–73
- [204] Mandelli D, Vanossi A, Invernizzi M, Paronuzzi S, Manini N and Tosatti E 2015 Superlubric-pinned transition in sliding incommensurate colloidal monolayers *Phys. Rev. B* **92** 134306
- [205] Juniper M P N, Straube A V, Besseling R, Aarts D G A L and Dullens R P A 2015 Microscopic dynamics of synchronization in driven colloids *Nature Commun.* **6** 7187
- [206] Ticco S V P, Fornasier G, Manini N, Santoro G E, Tosatti E and Vanossi A arXiv:1508.06201 Subharmonic Shapiro steps of sliding colloidal monolayers in optical lattices (unpublished)
- [207] Juniper M P N, Strauber A V, Aarts D G A L and Dullens R P A 2016 Colloidal particles driven across periodic optical-potential-energy landscapes *Phys. Rev. E* **93** 012608
- [208] Glotzer S C and Solomon M J 2007 Anisotropy of building blocks and their assembly into complex structures *Nature Mater.* **6** 557–62
- [209] Reichhardt C and Reichhardt C J O 2009 Nonequilibrium phases for driven particle systems with effective orientational degrees of freedom *Phys. Rev. E* **79** 061403
- [210] Reichhardt C and Reichhardt C J O 2012 Statics and dynamics of Yukawa cluster crystals on ordered substrates *Phys. Rev. E* **85** 051401
- [211] Speer D, Eichhorn R, Evstigneev M and Reimann P 2012 Dimer motion on a periodic substrate: Spontaneous symmetry breaking and absolute negative mobility *Phys. Rev. E* **85** 061132
- [212] Reichhardt C and Reichhardt C J O 2005 Pinning and dynamics of colloids on one-dimensional periodic potentials *Phys. Rev. E* **72** 032401
- [213] Tierno P 2012 Depinning and collective dynamics of magnetically driven colloidal monolayers *Phys. Rev. Lett.* **109** 198304
- [214] Kolton A B, Exartier R, Cugliandolo L F, Domínguez D and Grønbech-Jensen N 2002 Effective temperature in driven vortex lattices with random pinning *Phys. Rev. Lett.* **89** 227001
- [215] Shechtman D, Blech I, Gratias D and Cahn J W 1984 Metallic phase with long-range orientational order and no translational symmetry *Phys. Rev. Lett.* **53** 1951–3
- [216] Reichhardt C and Reichhardt C J O 2011 Dynamical ordering and directional locking for particles moving over quasicrystalline substrates *Phys. Rev. Lett.* **106** 060603
- [217] Reichhardt C J O and Reichhardt C 2012 Vortex dynamics and symmetry locking on quasiperiodic and periodic substrates *Physica C* **479** 45–8
- [218] Mikhael J, Roth J, Helden L and Bechinger C 2008 Archimedean-like tiling on decagonal quasicrystalline surfaces *Nature (London)* **454** 501–4
- [219] Schmiedeberg M and Stark H 2008 Colloidal ordering on a 2D quasicrystalline substrate *Phys. Rev. Lett.* **101** 218302
- [220] Thomas C K and Middleton A A 2007 Irrational mode locking in quasiperiodic systems *Phys. Rev. Lett.* **98** 148001
- [221] Schmiedeberg M and Stark H 2012 Comparing light-induced colloidal quasicrystals with different rotational symmetries *J. Phys.: Condens. Matter* **24** 284101
- [222] Kromer J A, Schmiedeberg M, Roth J and Stark H 2012 What phasons look like: Particle trajectories in a quasicrystalline potential *Phys. Rev. Lett.* **108** 218301
- [223] Williams F I B, Wright P A, Clark R G, Andrei E Y, Deville G, Glatl D C, Probst O, Etienne B, Dorin C, Foxon C T and Harris J J 1991 Conduction threshold and pinning frequency of magnetically induced Wigner solid *Phys. Rev. Lett.* **66**, 3285–8
- [224] Kukushkin I V, Pulsford N J, von Klitzing K, Ploog K, Haug R J, Koch S and Timofeev V B 1992 Magneto-optical evidence for depinning of the Wigner crystal by an electric field *Phys. Rev. B* **45** R4532–5
- [225] Shirahama K and Kono K 1995 Dynamical transition in the Wigner solid on a liquid helium surface *Phys. Rev. Lett.* **74** 781–4
- [226] Piacente G and Peeters F M 2005 Pinning and depinning of a classic quasi-one-dimensional Wigner crystal in the presence of a constriction *Phys. Rev. B* **72** 205208

- [227] Damasceno P F, DaSilva C J, Rino J P and Candido L 2010 Temperature and pinning effects on driving a 2D electron system on a helium film: A numerical study *J. Low Temp. Phys.* **160** 58–67
- [228] Cooper K B, Lilly M P, Eisenstein J P, Pfeiffer L N and West K W 1999 Insulating phases of two-dimensional electrons in high Landau levels: Observation of sharp thresholds to conduction *Phys. Rev. B* **60** R11285–8
- [229] Csathy G, Tsui D, Pfeiffer L and West K 2007 A stability and negative differential resistance of the Wigner solid *Phys. Rev. Lett.* **98** 066805
- [230] Zhu X, Littlewood P B and Millis A J 1994 Sliding motion of a two-dimensional Wigner crystal in a strong magnetic field *Phys. Rev. B* **50** 4600–21
- [231] Reichhardt C and Reichhardt C J O 2003 Charge transport transitions and scaling in disordered arrays of metallic dots *Phys. Rev. Lett.* **90** 046802
- [232] Kurdak C, Rimberg A J, Ho T R and Clarke J 1998 Activated transport and scaling behavior in the current-voltage characteristics and Coulomb-blockade oscillations of two-dimensional arrays of metallic islands *Phys. Rev. B* **57**, R6842–5
- [233] Duruöz C I, Clarke R M, Marcus C M and Harris J S 1995 Conduction threshold, switching, and hysteresis in quantum dot arrays *Phys. Rev. Lett.* **74** 3237–40
- [234] Parthasarathy R, Lin X-M and Jaeger H M 2001 Electronic transport in metal nanocrystal arrays: The effect of structural disorder on scaling behavior *Phys. Rev. Lett.* **87** 186807
- [235] Staley N E, Ray N, Kastner M A, Hanson M P and Gossard A C 2014 Electric-field-driven insulating-to-conducting transition in a mesoscopic quantum dot lattice *Phys. Rev. B* **90** 195443
- [236] Murray C B, Kagan C R and Bawendi M G 1995 Self-organization of CdSe nanocrystallites into three-dimensional quantum dot superlattices *Science* **270** 1335–8
- [237] Mühlbauer S, Binz B, Jonietz F, Pfleiderer C, Rosch A, Neubauer A, Georgii R and Böni P 2009 Skyrmion lattice in a chiral magnet *Science* **323** 915–9
- [238] Yu X Z, Onose Y, Kanazawa N, Park J H, Han J H, Matsui Y, Nagaosa N and Tokura Y 2010 Real-space observation of a two-dimensional skyrmion crystal *Nature (London)* **465** 901–4
- [239] Nagaosa N and Tokura Y 2013 Topological properties and dynamics of magnetic skyrmions *Nature Nanotechnol.* **8** 899–911
- [240] Jiang W, Upadhyaya P, Zhang W, Yu G, Jungfleisch M B, Fradin F Y, Pearson J E, Tserkovnyak Y, Wang K L, Heinonen O, te Velthuis S G E and Hoffmann A 2015 Blowing magnetic skyrmion bubbles *Science* **349** 283–6
- [241] Tokunaga Y, Yu X Z, White J S, Rønnow H M, Morikawa D, Taguchi Y and Tokura Y 2015 A new class of chiral materials hosting magnetic skyrmions beyond room temperature *Nature Commun.* **6** 7638
- [242] Woo S, Litzius K, Krüger B, Im M-Y, Caretta L, Richter K, Mann M, Krone A, Reeve R, Weigand M, Agrawal P, Fischer P, Kläui M and Beach G S D arXiv:1502.07376 Observation of room temperature magnetic skyrmions and their current-driven dynamics in ultrathin Co films (unpublished)
- [243] Fert A, Cros V and Sampaio J 2013 Skyrmions on the track *Nature Nanotech.* **8** 152–6
- [244] Lin S-Z, Reichhardt C, Batista C D and Saxena A 2013 Driven skyrmions and dynamical transitions in chiral magnets *Phys. Rev. Lett.* **110** 207202
- [245] Zang J, Mostovoy M, Han J H and Nagaosa N 2011 Dynamics of skyrmion crystals in metallic thin films *Phys. Rev. Lett.* **107** 136804
- [246] Schulz T, Rita R, Bauer A, Halder M, Wagner M, Franz C, Pfleiderer C, Everschor K, Garst M and Rosch A 2012 Emergent electrostatics of skyrmions in a chiral magnet *Nature Phys.* **8** 301–4
- [247] Yu X Z, Kanazawa N, Zhang W Z, Nagai T, Hara T, Kimoto K, Matsui Y, Onose Y and Tokura Y 2012 Skyrmion flow near room temperature in an ultralow current density *Nature Commun.* **3** 988
- [248] Iwasaki J, Mochizuki M and Nagaosa N 2013 Universal current-velocity relation of skyrmion motion in chiral magnets. *Nature Commun.* **4** 1463
- [249] Liang D, DeGrave J P, Stolt M J, Tokura Y and Jin S 2015 Current-driven dynamics of skyrmions stabilized in MnSi nanowires revealed by topological Hall effect *Nature Commun.* **6** 8217
- [250] Yu X Z, Tokunaga Y, Kaneko Y, Zhang W Z, Kimoto K, Matsui Y, Taguchi Y and Tokura Y 2014 Biskyrmion states and their current-driven motion in a layered manganite *Nature Commun.* **5** 3198
- [251] Lin S-Z, Reichhardt C, Batista C D and Saxena A 2013 Particle model for skyrmions in metallic chiral magnets: Dynamics, pinning, and creep *Phys. Rev. B* **87** 214419
- [252] Müller J and Rosch A 2015 Capturing of a magnetic skyrmion with a hole *Phys. Rev. B* **91** 054410
- [253] Thiele A A 1973 Steady-state motion of magnetic domains *Phys. Rev. Lett.* **30** 230–
- [254] Liu Y-H and Li Y-Q 2013 A mechanism to pin skyrmions in chiral magnets *J. Phys.: Condens. Matter* **25** 076005
- [255] Büttner F, Moutafis C, Schneider M, Krüger B, Günther C M, Geilhufe J, Schmising C v K, Mohanty J, Pfau B, Schaffert S, Bisig A, Forester M, Schulz T, Vaz C A F, Franken J H, Swagten H J M, Kläui M and Eisebitt S 2015 Dynamics and inertia of skyrmionic spin structures *Nature Phys.* **11** 225–8
- [256] Reichhardt C, Ray D and Reichhardt C J O 2015 Quantized transport for a skyrmion moving on a two-dimensional periodic substrate *Phys. Rev. B* **91** 104426
- [257] Reichhardt C and Reichhardt C J O 2015 Shapiro steps for skyrmion motion on a washboard potential with longitudinal and transverse ac drives *Phys. Rev. B* **92** 224432
- [258] Troncoso R E and Núñez A S 2014 Thermally assisted current-driven skyrmion motion *Phys. Rev. B* **89** 224403
- [259] Liu A J and Nagel S R 1998 Nonlinear dynamics: Jamming is not just cool any more *Nature (London)* **396** 21–22
- [260] O’Hern C S, Silbert L E, Liu A J and Nagel S R 2003 Jamming at zero temperature and zero applied stress: The epitome of disorder *Phys. Rev. E* **68** 011306
- [261] Liu A J and Nagel S R 2010 The jamming transition and the marginally jammed solid *Annu. Rev. Condens. Matter Phys.* **1** 347–69
- [262] Reichhardt C and Reichhardt C J O 2014 Aspects of jamming in two-dimensional athermal frictionless systems *Soft Matter* **10** 2932–44
- [263] Reichhardt C J O, Groopman E, Nussinov Z and Reichhardt C 2012 Jamming in systems with quenched disorder *Phys. Rev. E* **86** 061301
- [264] Graves A L, Nashed S, Padgett E, Goodrich C P, Liu A J and Sethna J P arXiv:1509.00806 Pinning susceptibility: The effect of dilute, quenched disorder on jamming (unpublished)
- [265] Seul M and Andelman D 1995 Domain shapes and patterns: the phenomenology of modulated phases. *Science* **267** 476–83
- [266] Fogler M M, Koulakov A A and Shklovskii B I 1996 Ground state of a two-dimensional electron liquid in a weak magnetic field *Phys. Rev. B* **54** 1853–71
- [267] Emery V J, Kivelson S A and Zachar O 1997 Spin-gap proximity effect mechanism of high-temperature superconductivity *Phys. Rev. B* **56** 6120–47
- [268] Reichhardt C J O, Reichhardt C and Bishop A R 2004

- Fibrillar templates and soft phases in systems with short-range dipolar and long-range interactions *Phys. Rev. Lett.* **92** 016801
- [269] Kabanov V V, Mertelj T and Mihailovic D 2006 Coulomb frustrated JahnTeller phase transition in 2D *J. Phys. Chem. Solids* **67** 2041–5
- [270] Kozhevnikov V, Wijngaarden R J, de Wit J and Van Haesendonck C 2014 Magnetic flux density and the critical field in the intermediate state of type-I superconductors *Phys. Rev. B* **89** 100503(R)
- [271] Babaev E and Speight M 2005 Semi-Meissner state and neither type-I nor type-II superconductivity in multicomponent superconductors *Phys. Rev. B* **72** 180502(R)
- [272] Moshchalkov V V, Menghini M, Nishio T, Chen Q, Silhanek A V, Dao V, Chibotaru L, Zhigadlo N and Karpinski J 2009 Type-1.5 superconductivity *Phys. Rev. Lett.* **102** 117001
- [273] Garaud J, Agterberg D F and Babaev E 2012 Vortex coalescence and type-1.5 superconductivity in Sr_2RuO_4 *Phys. Rev. B* **86** 060513(R)
- [274] Varney C N, Sellin K A H, Wang Q-Z, Fangohr H and Babaev E 2013 Hierarchical structure formation in layered superconducting systems with multi-scale inter-vortex interactions *J. Phys.: Condens. Matter* **25** 415702
- [275] Komendova L, Milosevic M V and Peeters F M 2013 Soft vortex matter in a type-I/type-II superconducting bilayer *Phys. Rev. B* **88** 094515
- [276] Lilly M P, Cooper K B, Eisenstein J P, Pfeiffer L N and West K W 1999 Evidence for an anisotropic state of two-dimensional electrons in high Landau levels *Phys. Rev. Lett.* **82** 394–7
- [277] Cooper K B, Eisenstein J P, Pfeiffer L N and West K W 2003 Observation of narrow-band noise accompanying the breakdown of insulating states in high Landau levels *Phys. Rev. Lett.* **90** 226803
- [278] Cooper K B, Lilly M P, Eisenstein J P, Pfeiffer L N and West K W 1999 Insulating phases of two-dimensional electrons in high Landau levels: Observation of sharp thresholds to conduction *Phys. Rev. B* **60** R11285
- [279] Reichhardt C J O, Reichhardt C and Bishop A R 2010 Structural transitions, melting, and intermediate phases for stripe- and clump-forming systems *Phys. Rev. E* **82** 041502
- [280] Reichhardt C, Reichhardt C J O and Bishop A R 2005 Hysteresis and noise in stripe- and clump-forming systems *Europhys. Lett.* **72** 444–50
- [281] Reichhardt C J O, Reichhardt C and Bishop A R 2011 Anisotropic sliding dynamics, peak effect, and metastability in stripe systems *Phys. Rev. E* **83** 041501
- [282] Chen J-X, Mao J-W, Thakur S, Xu J-R and Liu F 2011 Dynamical phase of driven colloidal systems with short-range attraction and long-range repulsion *J. Chem. Phys.* **135** 094504
- [283] Göres J, Gamez G, Smet J H, Pfeiffer L, West K, Yacoby A, Umansky V and von Klitzing K 2007 Current-induced anisotropy and reordering of the electron liquid-crystal phases in a two-dimensional electron system *Phys. Rev. Lett.* **99** 246402
- [284] Zhao H J, Misko V R and Peeters F M 2013 Dynamics of self-organized driven particles with competing range interaction *Phys. Rev. E* **88** 022914
- [285] Drocco J A, Reichhardt C J O, Reichhardt C and Bishop A R 2013 Static and dynamic phases for magnetic vortex matter with attractive and repulsive interactions *J. Phys.: Condens. Matter* **25** 345703
- [286] Reichhardt C J O, Reichhardt C and Bishop A R 2011 Anisotropic sliding dynamics, peak effect, and metastability in stripe systems *Phys. Rev. E* **83** 041501
- [287] Edlund E and Jacobi M N 2010 Universality of striped morphologies *Phys. Rev. Lett.* **105** 137203
- [288] Malescio G and Pellicane G 2003 Stripe phases from isotropic repulsive interactions *Nature Mater.* **2** 97–100
- [289] Glaser M A, Grason G M, Kamien R D, Kosmrlj A, Santangelo C D and Zihlerl P 2007 Soft spheres make more mesophases *EPL* **78** 46004
- [290] Curran P J, Desoky W M, Milosevic M V, Chaves A, Laloë J-B, Moodera J S and Bending S J 2015 Spontaneous symmetry breaking in vortex systems with two repulsive length scales *Sci. Rep.* **5** 15569
- [291] Sellin K A H and Babaev E 2013 Stripe, gossamer, and glassy phases in systems with strong nonpairwise interactions *Phys. Rev. E* **88** 042305
- [292] Sengupta A, Sengupta S and Menon G I 2007 Driven disordered periodic media with an underlying structural phase transition *Phys. Rev. B* **75** 180201(R)
- [293] Sengupta A, Sengupta S and Menon G I 2010 Driven disordered polymorphic solids: Phases and phase transitions, dynamical coexistence and peak effect anomalies *Phys. Rev. B* **81** 144521
- [294] Elder K R, Katakowski M, Haataja M and Grant M 2002 Modeling Elasticity in Crystal Growth *Phys. Rev. Lett.* **88** 245701
- [295] Ramos J A P, Granato E, Ying S C, Achim C V, Elder K R and Ala-Nissila T 2010 Dynamical transitions and sliding friction of the phase-field-crystal model with pinning *Phys. Rev. E* **81** 011121
- [296] Granato E, Ramos J A P, Achim C V, Lehikoinen J, Ying S C, Ala-Nissila T and Elder K R 2011 Glassy phases and driven response of the phase-field-crystal model with random pinning *Phys. Rev. E* **84** 031102
- [297] Reichhardt C and Reichhardt C J O 2007 Stripes, clusters, and nonequilibrium ordering for bidisperse colloids with repulsive interactions *Phys. Rev. E* **75** 040402(R)
- [298] Di Scala N, Olive E, Lansac Y, Fily Y and Soret J C 2012 The elastic depinning transition of vortex lattices in two dimensions *New J. Phys.* **14** 123027
- [299] Field S, Witt J, Nori F and Ling X S 1995 Superconducting vortex avalanches *Phys. Rev. Lett.* **74** 1206–9
- [300] Olson C J, Reichhardt C and Nori F 1997 Superconducting vortex avalanches, voltage bursts, and vortex plastic flow: Effect of the microscopic pinning landscape on the macroscopic properties *Phys. Rev. B* **56** 6175–94
- [301] Bassler K E and Paczuski M 1998 Simple model of superconducting vortex avalanches *Phys. Rev. Lett.* **81** 3761–4
- [302] Altshuler E 2004 Colloquium: Experiments in vortex avalanches *Rev. Mod. Phys.* **76** 471–87
- [303] Mehta M P, Reichhardt C, Olson C J and Nori F 1999 Topological invariants in microscopic transport on rough landscapes: Morphology, hierarchical structure, and Horton analysis of riverlike networks of vortices *Phys. Rev. Lett.* **82** 3641–4
- [304] Bassler K, Paczuski M and Reiter G 1999 Braided rivers and superconducting vortex avalanches *Phys. Rev. Lett.* **83** 3956–9
- [305] Olson C J, Reichhardt C and Nori F 1998 Fractal networks, braiding channels, and voltage noise in intermittently flowing rivers of quantized magnetic flux *Phys. Rev. Lett.* **80** 2197–200
- [306] Zapperi S, Moreira A and Andrade J 2001 Flux front penetration in disordered superconductors *Phys. Rev. Lett.* **86** 3622–5
- [307] Pine D, Gollub J, Brady J and Leshansky A 2005 Chaos and threshold for irreversibility in sheared suspensions, *Nature (London)* **438** 997–1000
- [308] Corte L, Chaikin P M, Gollub J P and Pine D J 2008 Random organization in periodically driven systems *Nature Phys.* **4** 420–4
- [309] Reichhardt C and Reichhardt C J O 2009 Random

- organization and plastic depinning *Phys. Rev. Lett.* **103** 168301
- [310] Okuma S and Motohashi A 2012 Critical behavior associated with transient dynamics near the depinning transition *New J. Phys.* **14** 123021
- [311] Okuma S, Motohashi A and Kawamura Y 2013 Critical dynamics associated with dynamic disordering near the depinning transition in different vortex phases *Phys. Lett. A* **377** 2990–4
- [312] Shaw G, Mandal P, Banerjee S S, Niazi A, Rastogi A K, Sood A K, Ramakrishnan S and Grover A K 2012 Critical behavior at depinning of driven disordered vortex matter in 2H-NbS₂ *Phys. Rev. B* **85** 174517
- [313] Mangan N, Reichhardt C and Reichhardt C J O 2008 Reversible to irreversible flow transition in periodically driven vortices *Phys. Rev. Lett.* **100** 187002
- [314] Zhang W, Zhou W and Luo M 2010 Irreversibility of two-dimensional vortex systems with random pinning *Phys. Lett. A* **374** 3666–70
- [315] Daroca D P, Pasquini G, Lozano G S and Bekeris V 2011 Dynamics of superconducting vortices driven by oscillatory forces in the plastic-flow regime *Phys. Rev. B* **84** 012508
- [316] Bermúdez M M, Eskildsen M R, Bartkowiak M, Nagy G, Bekeris V and Pasquini G 2015 Dynamic reorganization of vortex matter into partially disordered lattices *Phys. Rev. Lett.* **115** 067001
- [317] Okuma S, Tsugawa Y and Motohashi A 2011 Transition from reversible to irreversible flow: Absorbing and depinning transitions in a sheared-vortex system *Phys. Rev. B* **83** 012503
- [318] Hexner D and Levine D 2015 Hyperuniformity of critical absorbing states *Phys. Rev. Lett.* **114** 110602
- [319] Torquato S and Stillinger F H 2003 Local density fluctuations, hyperuniformity, and order metrics *Phys. Rev. E* **68** 041113
- [320] Tjhung E and Berthier L 2015 Hyperuniform density fluctuations and diverging dynamic correlations in periodically driven colloidal suspensions *Phys. Rev. Lett.* **114** 148301
- [321] Weijs J H, Jeanneret R, Dreyfus R and Bartolo D 2015 Emergent hyperuniformity in periodically driven emulsions *Phys. Rev. Lett.* **115** 108301
- [322] Hastings M B, Reichhardt C J O and Reichhardt C 2003 Depinning by fracture in a glassy background *Phys. Rev. Lett.* **90** 098302
- [323] Habdas P, Schaar D, Levitt A C and Weeks E R 2004 Forced motion of a probe particle near the colloidal glass transition *Europhys. Lett.* **67** 477–83
- [324] Dullens R P A and Bechinger C 2011 Shear thinning and local melting of colloidal crystals *Phys. Rev. Lett.* **107** 138301
- [325] Reichhardt C J O and Reichhardt C 2008 Viscous decoupling transitions for individually dragged particles in systems with quenched disorder *Phys. Rev. E* **78** 011402
- [326] Auslaender O M, Luan L, Straver E W J, Hoffman J E, Koshnick N C, Zeldov E, Bonn D A, Liang R, Hardy W N and Moler K A 2009 Mechanics of individual isolated vortices in a cuprate superconductor *Nature Phys.* **5** 35–9
- [327] Voightmann Th and Fuchs M 2013 Force-driven micro-rheology Th. Voightmann and M. Fuchs *Eur. Phys. J. Spec. Top.* **222** 2819–33
- [328] Madison K W, Chevy F, Wohlleben W and Dalibard J 2000 Vortex formation in a stirred Bose-Einstein condensate *Phys. Rev. Lett.* **84** 806–9
- [329] Pu H, Baksmaty L O, Yi S and Bigelow N P 2005 Structural phase transitions of vortex matter in an optical lattice *Phys. Rev. Lett.* **94** 190401
- [330] Tung S, Schweikhard V and Cornell E A 2006 Observation of vortex pinning in Bose-Einstein condensates *Phys. Rev. Lett.* **97** 240402
- [331] Kasamatsu K and Tsubota M 2006 Dynamical vortex phases in a Bose-Einstein condensate driven by a rotating optical lattice *Phys. Rev. Lett.* **97** 240404
- [332] Kasamatsu K, Tsubota M and Ueda M 2005 Vortices in multicomponent Bose-Einstein condensates *Int. J. Mod. Phys. B* **19** 1835–1904
- [333] Libál A, Reichhardt C, Jankó B and Reichhardt C J O 2006 Dynamics, rectification, and fractionation for colloids on flashing substrates *Phys. Rev. Lett.* **96** 188301
- [334] Jelić Z L, Milosević M V, Van de Vondel J and Silhanek A V 2015 Stroboscopic phenomena in superconductors with dynamic pinning landscape *Sci. Rep.* **5** 14604
- [335] Yan L, Barizien A and Wyart M 2016 Model for the erosion onset of a granular bed sheared by a viscous fluid *Phys. Rev. E* **93** 012903
- [336] Marchetti M C, Joanny J F, Ramaswamy S, Liverpool T B, Prost J, Rao M and Simha R A 2013 Hydrodynamics of soft active matter *Rev. Mod. Phys.* **85** 1143–89
- [337] Buttinoni I, Bialké J, Kümmel F, Löwen H, Bechinger C and Speck T 2013 Dynamical clustering and phase separation in suspensions of self-propelled colloidal particles *Phys. Rev. Lett.* **110** 238301
- [338] Fily Y and Marchetti M C 2012 Athermal phase separation of self-propelled particles with no alignment *Phys. Rev. Lett.* **108** 235702
- [339] Reichhardt C and Reichhardt C J O 2014 Active matter transport and jamming on disordered landscapes *Phys. Rev. E* **90** 012701
- [340] Chepizhko O, Altmann E G and Peruani F 2013 Optimal noise maximizes collective motion in heterogeneous media *Phys. Rev. Lett.* **110** 238101
- [341] Shen H, Tan P and Xu L 2016 Probing the role of mobility in the collective motion of nonequilibrium systems *Phys. Rev. Lett.* **116** 048302
- [342] Chu J H and I L 1994 Direct observation of Coulomb crystals and liquids in strongly coupled rf dusty plasmas *Phys. Rev. Lett.* **72** 4009–12
- [343] Thomas H, Morfill G E, Demmel V, Goree J, Feuerbacher B and Möhlmann D 1994 Plasma crystal: Coulomb crystallization in a dusty plasma *Phys. Rev. Lett.* **73** 652–5
- [344] Coupier G, Saint Jean M and Guthmann C 2007 Enhancement of mobilities in a pinned multidomain crystal *Phys. Rev. B* **75** 224103
- [345] Gallavotti G and Cohen E G D 1995 Dynamical ensembles in nonequilibrium statistical mechanics *Phys. Rev. Lett.* **74** 2694–7
- [346] Seifert U 2012 Stochastic thermodynamics, fluctuation theorems and molecular machines *Rep. Prog. Phys.* **75** 126001
- [347] Jarzynski C 1997 Nonequilibrium equality for free energy differences *Phys. Rev. Lett.* **78** 2690–3
- [348] Crooks G E 1999 Entropy production fluctuation theorem and the nonequilibrium work relation for free energy differences *Phys. Rev. E* **60** 2721–6
- [349] Wang G M, Sevick E M, Mittag E, Searles D J and Evans D J 2002 Experimental demonstration of violations of the second law of thermodynamics for small systems and short time scales *Phys. Rev. Lett.* **89** 050601
- [350] Liphardt J, Dumont S, Smith S B, Tinoco I and Bustamante C 2002 Equilibrium information from nonequilibrium measurements in an experimental test of Jarzynski's equality *Science* **296** 1832–5
- [351] Drocco J A, Reichhardt C J O and Reichhardt C 2011 Characterizing plastic depinning dynamics with the fluctuation theorem *Eur. Phys. J. E* **34** 117
- [352] Gomez-Solano J R, July C, Mehl J and Bechinger C 2015 Non-equilibrium work distribution for interacting

- colloidal particles under friction *New J. Phys.* **17** 045026
- [353] Hasan M Z and Kane C L 2010 Colloquium: Topological insulators *Rev. Mod. Phys.* **82** 3045–67
- [354] Chen B G, Upadhyaya N and Vitelli V 2014 Nonlinear conduction via solitons in a topological mechanical insulator *Proc. Natl. Acad. Sci. (USA)* **111** 13004–9
- [355] Nash L M, Kleckner D, Read A, Vitelli V, Turner A M and Irvine W T M 2015 Topological mechanics of gyroscopic metamaterials *Proc. Natl. Acad. Sci. (USA)* **112** 14495–500
- [356] Vitelli V, Lucks J B and Nelson D R 2006 Crystallography on curved surfaces *Proc. Natl. Acad. Sci. (USA)* **103** 12323–8
- [357] Irvine W T M, Vitelli V and Chaikin P M 2010 Pleats in crystals on curved surfaces *Nature* **468** 947–51
- [358] Irvine W T M, Bowick M J and Chaikin P M 2012 Fractionalization of interstitials in curved colloidal crystals *Nature Mater.* **11** 948
- [359] Strukov D B, Snider G S, Stewart D R and Williams S R 2008 The missing memristor found *Nature* **453** 80–83
- [360] Sachdev S 1999 *Quantum Phase Transitions* (Cambridge: Cambridge Univ. Press)
- [361] Dalla Torre E G, Demler E, Giamarchi T and Altman E 2010 Quantum critical states and phase transitions in the presence of non-equilibrium noise *Nature Phys.* **6** 806–810